



GROUP NUMBER: 20

AVAILABILITY:

Department of Civil Engineering and Energy Technology Phone: 67 23 50 00
Mailing address: PB 4. St. Olavs plass, 0130 Oslo www.hioa.no
Address for visitors: Pilestredet 35, Oslo

MASTER'S THESIS

| | |
|---|---|
| TITLE: Improving the ventilation in passive house swimming pool: a case study of Åfjord swimming pool | DATE: 22.05.2019 |
| | NUMBER OF PAGES/ATTACHMENTS: 86/10 |
| AUTHOR: Mohamed Josef Addas | SUPERVISORS: Arnab Chaudhuri-OsloMet Wolfgang Kampel-Multiconsult |

| | |
|--|---------------------------------|
| DONE IN COLLABORATION WITH: Multiconsult og OsloMet | CONTACT: Mohamed Josef Addas |
|--|---------------------------------|

ABSTRACT

The importance of satisfactory air quality and thermal comfort are continuous scientific research regarding energy efficiency and health in swimming pool. This study aims to improve the ventilation efficiency in passive house swimming pools with respect to the air quality for swimmers and thermal comfort. Numerical simulations are performed with computational fluid dynamics CFD methodology for this. The CFD model in this work is based on the swimming pool under construction (Åfjord swimming pool) located in central Norway.

Multicomponent compressible Navier-Stokes system of equations together with turbulence models are solved for this. The evaporation of water from the pool surface are modelled based on the ASHRAE Shah phenomenological model. The multi-component gas mixture consists of water vapour, chlorine and air. Surface to surface radiation models are also considered to include the effects of radiation inside the swimming pool. Five different ventilation strategies are investigated e.g., mixing ventilation (MV), mixing ventilation-displacement ventilation (MV-DV), and three more displacement ventilation (DV4, DV5 and DV7) cases with different air change per hour (ACH). These three cases are considered as conventional DV strategies in swimming pool.

The results confirm that the MV case can be a highly recommended option to use in Åfjord swimming pool. For this case, due to the indicator for air quality with local mean age of air (LMA) there are no stagnant air regions inside the swimming pool. Also, due to the air exchange efficiency indicator (ACE) this system exchange the air similar to "piston mode" ventilation. Furthermore, the air quality in the swimming pool is clearly improved and there is no sign observed for condensation risk. The thermal comfort is considered as accepted. Worthy reduction in operation expenses is strongly expected for this system. The analysis of MV-DV case reveals that, it is highly recommended to use especially during the winter time when the heat demand is high. This system shows the best performance in order to reduce the chlorine concentration near and above the water bath. This system exchange the air with intermediate efficiency similar to "fully mixing" ventilation according to the ACE measurements. It also shows good thermal comfort due to stable air temperature, low air velocity and good air humidity level. In case of DV, we found a poor performance to reduce the chlorine concentration swimming breathing zone. Furthermore, It can also be concluded that, the chlorine concentration reduction is negligible with the increase in ACH for DV cases with conventional strategies.

3 keywords:

Swimming pool

Ventilation

CFD

Project Description

The importance of satisfactory air quality and thermal comfort are continuous scientific research regarding energy efficiency and health in swimming pool. The number of air change per hour ACH is a rule of thumb that is widely used to provide information on the intensity of the ventilation in swimming pools. This rule of thumb is usually used with the conventional ventilation where high volume of air flows along the windows in the exterior facades to avoid condensation and to reduce the contaminant especially the chlorine by-products in the swimming bath. ACH does not provide information on the quality of fresh air distribution and contaminant concentration.

Åfjord Swimming pool is a passive house swimming pool which is still under construction and it is located in Åfjord city, Trøndelag County, Central Norway. Passive house swimming pool provides the opportunity to use other ventilation strategy than the conventional ventilation. Multiconsult Norway AS is interested in testing diverse ventilation strategies in Åfjord swimming pool in order to provide a healthy air quality for the swimmers and to achieve more energy reduction benefits.

In this research, different ventilation cases e.g. mixed, displacement or combination of both should be considered for Åfjord swimming pool with the use of numerical analysis in order to explore:

- The air exchange efficiency in the pool area.
- The relationship between the ventilation strategy and chlorine concentration in the water bath.
- The impact of ACH with conventional ventilation due to the air quality in the water bath and ventilation efficiency.
- The condensation risk on external windows and glazed facade.
- The thermal comfort in terms of measuring air temperature, air velocity and relative humidity in the breathing zone.

Acknowledgements

I would like to thank Multiconsult, for giving me the opportunity to work on this master thesis. And I would like also to thank my mentor Dr. Ing. Wolfgang Kampel at Multiconsult, and I appreciate for highlighting this problem and for providing me the necessary resources throughout the research period.

Special thanks to my supervisor Arnab Caudhuri, associate Professor at Oslo-Met, without his amazing support and guidance throughout this research, it would not be realised.

I would also like to thank Dimitrios Kraniotis, associate Professor at Oslo-Met, Peter G. Schild, professor at Oslo-Met and Habtamu Bayera Madessa, associate Professor at Oslo-Met for their academically discussion and suggestions.

Last, but not least, I would like to thank my family, friends and my classmates for moral support and good discussion.

Abstract

The importance of satisfactory air quality and thermal comfort are continuous scientific research regarding energy efficiency and health in swimming pool. This study aims to improve the ventilation efficiency in passive house swimming pools with respect to the air quality for swimmers and thermal comfort. Numerical simulations are performed with computational fluid dynamics CFD methodology for this. The CFD model in this work is based on the swimming pool under construction (Åfjord swimming pool) located in central Norway. Multi-component compressible Navier-Stokes system of equations together with turbulence models are solved for this. The evaporation of water from the pool surface are modelled based on the ASHRAE Shah phenomenological model. The multi-component gas mixture consists of water vapour, chlorine and air. Surface to surface radiation models are also considered to include the effects of radiation inside the swimming pool. Five different ventilation strategies are investigated e.g., mixing ventilation (MV), mixing ventilation-displacement ventilation (MV-DV), and three more displacement ventilation (DV4, DV5 and DV7) cases with different air change per hour (ACH). These three cases are considered as conventional DV strategies in swimming pool.

The results confirm that the MV case can be a highly recommended option to use in Åfjord swimming pool. For this case, due to the indicator for air quality with local mean age of air (LMA) there are no stagnant air regions inside the swimming pool. Also, due to the air exchange efficiency indicator (ACE) this system exchange the air similar to "piston mode" ventilation. Furthermore, the air quality in the swimming pool is clearly improved and there is no sign observed for condensation risk. The thermal comfort is considered as accepted. Worthy reduction in operation expenses is strongly expected for this system.

The analysis of MV-DV case reveals that, it is highly recommended to use especially during the winter time when the heat demand is high. This system shows the best performance in order to reduce the chlorine concentration near and above the water bath. This system exchange the air with intermediate efficiency similar to "fully mixing" ventilation according to the ACE measurements. It also shows good thermal comfort due to stable air temperature, low air velocity and good air humidity level.

In case of DV, we found a poor performance to reduce the chlorine concentration swimming breathing zone. Furthermore, It can also be concluded that, the chlorine concentration reduction is negligible with the increase in ACH for DV cases with conventional strategies.

Contents

| | | |
|----------|--|-----------|
| 1 | Introduction | 6 |
| 1.1 | Passive house swimming pools | 9 |
| 1.2 | Purpose of the study | 10 |
| 1.3 | Literature study | 10 |
| 1.4 | Åfjord swimming pool | 12 |
| 2 | Theory | 13 |
| 2.1 | Byggforsk’s recommendation | 13 |
| 2.2 | CIBSE’s recommendation | 14 |
| 2.3 | ASHRAE’s recommendation | 15 |
| 2.4 | Computational Fluid Dynamics | 18 |
| 2.4.1 | Pre-processor | 19 |
| 2.4.2 | Solver | 19 |
| 2.4.3 | Post-processor | 20 |
| 2.4.4 | Governing equations | 21 |
| 2.5 | Governing equations of radiative heat transfer | 24 |
| 2.6 | Transport equations for gas species | 24 |
| 2.7 | Turbulence models in CFD | 25 |
| 2.8 | Reynolds-averaged Navier-Stokes Models RANS | 25 |
| 2.8.1 | RANS Two-Equation model: Standard $k - \epsilon$ | 25 |
| 2.8.2 | RANS Two-Equation: Standard $k - \omega$, and SST $k - \omega$ | 26 |
| 3 | Method | 27 |
| 3.1 | Geometry and design model | 27 |
| 3.2 | Mesh | 28 |
| 3.3 | Physics setup and solvers | 30 |
| 3.3.1 | SST(Menter) K-Omega, All $y+$ wall treatment | 33 |
| 3.4 | Passive scalar of local mean age of air LMA and air exchange efficiency ACE | 37 |
| 3.4.1 | The local mean age of air | 37 |
| 3.4.2 | Air exchange efficiency | 38 |
| 3.4.3 | Validation | 39 |
| 3.5 | Boundary conditions and different test cases of swimming hall (DV, MV-DV, DV4, 5, 7 ACH) | 42 |
| 3.5.1 | Mixing ventilation (MV) case: | 44 |
| 3.5.2 | Mixing ventilation-displacement ventilation (MV-DV) case | 49 |
| 3.5.3 | Displacement ventilation (DV4, 5 and 7 ACH) | 50 |

| | | |
|----------|---|-----------|
| 4 | Results and discussion | 50 |
| 4.1 | Mixing ventilation (MV) case | 53 |
| 4.1.1 | Swimming breathing zone | 53 |
| 4.1.2 | People around | 57 |
| 4.2 | Mixing ventilation-displacement ventilation (MV-DV) case | 61 |
| 4.2.1 | Swimming breathing zone | 61 |
| 4.2.2 | People around | 65 |
| 4.3 | Displacement ventilation (DV4 ACH) case | 69 |
| 4.3.1 | Swimming breathing zone | 69 |
| 4.3.2 | People around | 72 |
| 4.4 | Displacement ventilation (DV5 ACH) case | 75 |
| 4.4.1 | Swimming breathing zone | 75 |
| 4.4.2 | People around | 78 |
| 4.5 | Displacement ventilation (DV7 ACH) case | 80 |
| 4.5.1 | Swimming breathing zone | 80 |
| 4.5.2 | People around | 83 |
| 5 | Conclusion | 84 |
| 5.1 | Future work | 85 |
| 6 | References | 87 |
| A | ASHRAE Shah's density difference table | 91 |
| B | Plan view | 91 |
| C | Section view | 92 |
| D | Facades | 93 |
| E | Ventilation pipes and exhaust plan | 95 |
| F | Residual plots | 95 |
| G | Textile duct specification | 97 |
| H | The surface average of molar chlorine concentration in the swimming breathing zone | 99 |

1 Introduction

Norway ranks number one when it comes to the number of swimming pool per population, with approximately 1000 swimming pools distributed throughout the country [1]. Energy efficiency of buildings in the recent years has become increasingly important in Norway, and many buildings continuously meet more strict requirements such as TEK 17 and passive house standard. Well insulated buildings with better U-values reduces the heat loss from building significantly.

Enova published statistics on energy consumption in various types of buildings. A building category that consumes a significant amount of energy are sports facilities. Within this category, swimming pools and ice rinks constitute the highest energy consumption (see figure 1).

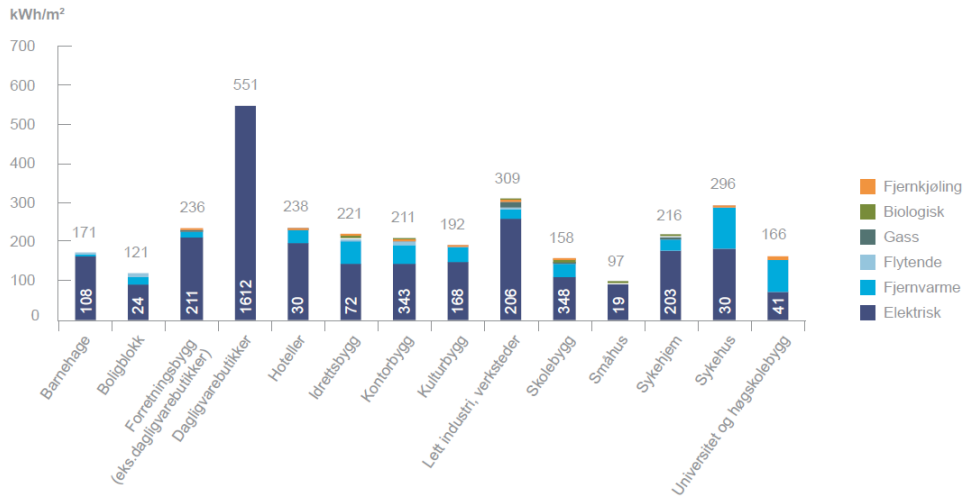


Figure 1: Energy consumption in different building categories [2]

It is predicted that in the coming years a large number of public swimming pools need to undergo considerable renovations. Swimming pools have a high consumption of energy for ventilation and water treatment in order to obtain good indoor climate and high water quality [3].

It is well reported in a research work done for approximately 850 swimming facilities in Norway that the delivered energy (DE) for all Norwegian swimming facilities is approximately $883 \frac{GWh}{year}$ [3]. The DE varies from one swimming facility to another with approximately from $1\ 000 \frac{kWh}{m^2_{WS}}$ to $11\ 000 \frac{kWh}{m^2_{WS}}$, according to their water surface [WS] size and building year (see figure 2 and 3). Interesting fact is

that the oldest building have the highest DE, while buildings built over the next decade had a considerably lower DE.

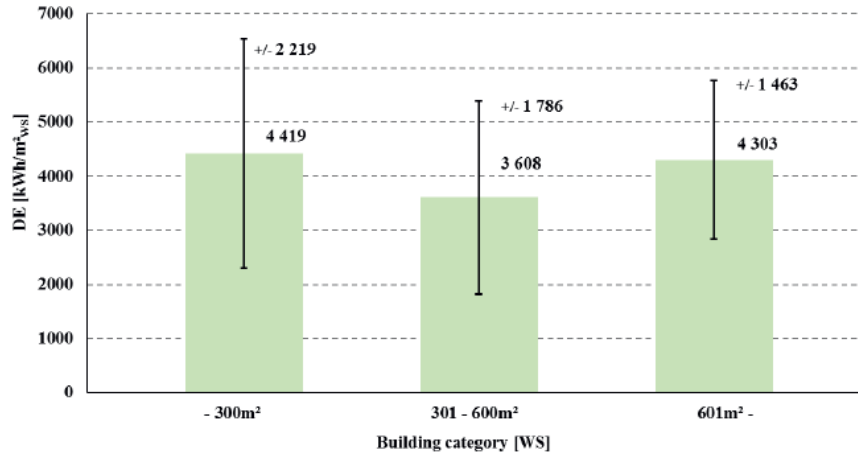


Figure 2: Average DE for each swimming pool category with standard deviation [3]

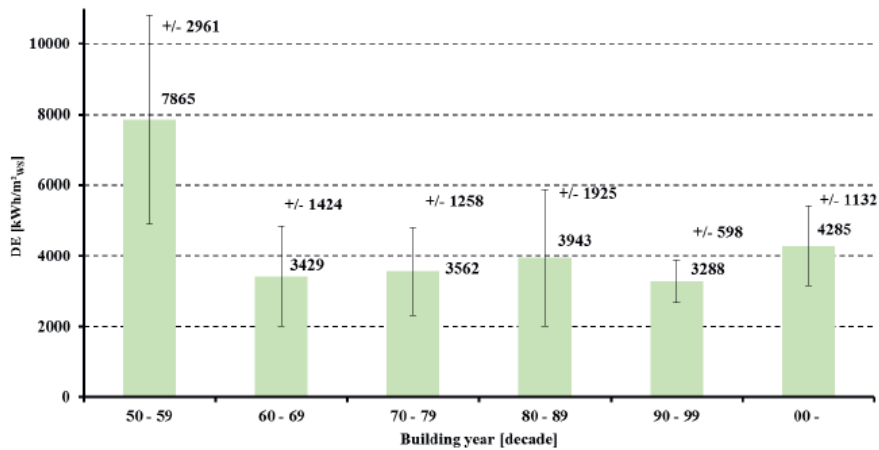


Figure 3: Average DE according to the building year in decades with standard deviation [3]

In an interesting research work reported by *Kampel et al.* [3], about the energy usage in swimming pool based on four different other studies. It is concluded with the fact that the ventilation has the largest energy usage in the swimming facilities as shown in figure 4

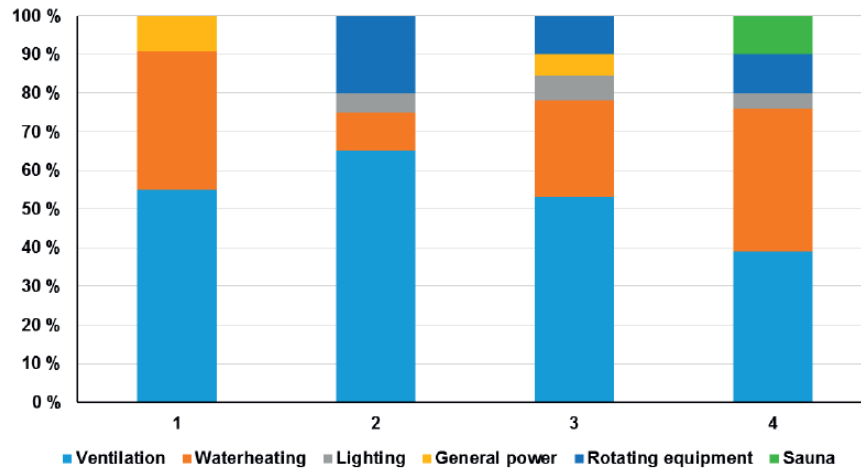


Figure 4: Energy usage for ventilation is greatest in swimming facilities and vary between 40-66% presented from various publications [3]

The ventilation system in swimming pools maintains the design temperature, relative humidity, and secures acceptable air quality within the pool hall. Swimming pools conventionally are ventilated by blowing up hot air, typically fresh air and recirculated air along the windows in the exterior facades to avoid condensation on the cold surfaces. This method requires large volume of airflow to dehumidify the air to the desired design humidity level and also to ensure an acceptable mixing of the air in the ventilated room (see figure 5).

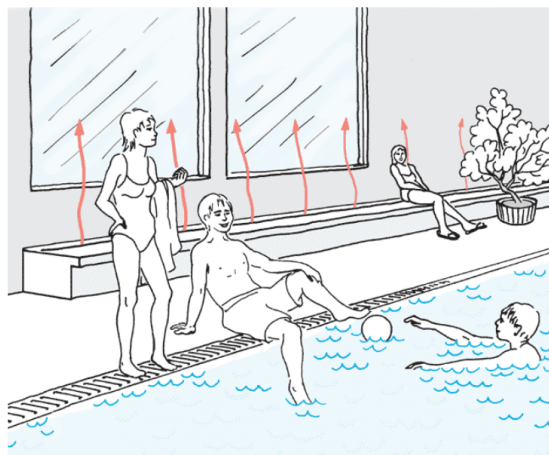


Figure 5: Conventional ventilation in swimming pool

1.1 Passive house swimming pools

The passive house swimming pools are energy efficient and have become widely popular, which is likely the case study of Ålfjord swimming pool in this work. The concept of the passive house focuses on enhancing both the building's design and installations to reduce the heating and cooling energy. Several studies reported analysis and methods to achieve energy savings in passive house swimming pools. High ability of insulation and air tightness in passive house building shows opportunities to think better compared to the conventional ventilation (see figure 6).

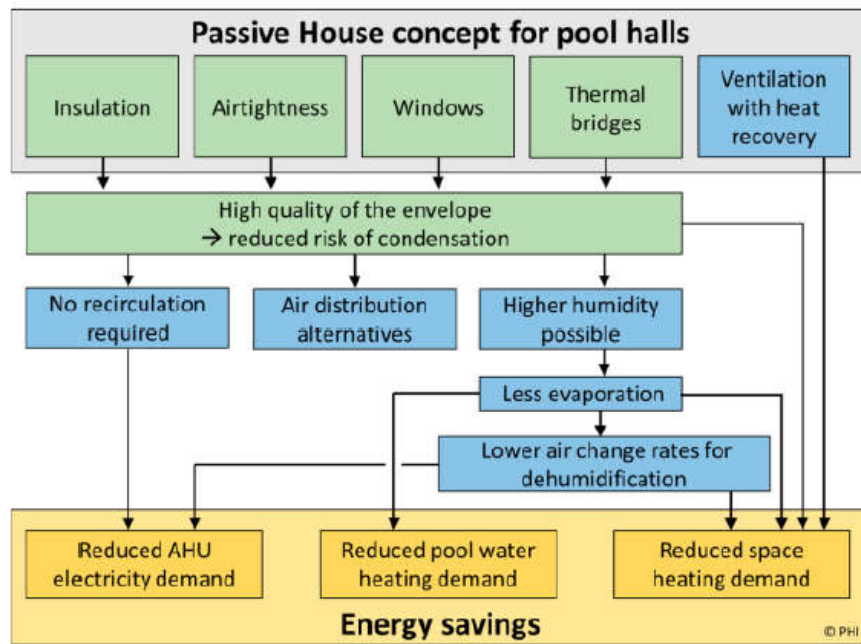


Figure 6: Energy savings opportunities in passive house swimming pools [4]

Conventional ventilation is no longer necessary thanks to high temperature surfaces of well insulated building envelope. This gives the opportunity to investigate new ventilation concepts that take into account the athletes in the pool when they are swimming and breathing the most polluted air in the entire room especially in the present of chlorine by-products. Chlorine by-products like trichloramine NCL_3 and trihalomethans THM_s are to be found in gaseous form in the swimming pool air and they can cause eye irritation and respiratory symptoms [5][6].

1.2 Purpose of the study

As part of the energy savings for passive house swimming pools, it is suggested to operate ventilation in pool halls with lower air circulation, which could result in energy efficiency. This work describes the method and result of a study using computational fluid dynamics CFD in order to assess different ventilation strategies in swimming pools in terms of their ventilation efficiency. The CFD model in this work is based on the swimming pool under construction (Åfjord swimming pool) and results may contribute for energy efficiency. Furthermore the airflow inlet should be located in consideration for air quality and thermal comfort for the visitors.

The objectives of this study are therefore to address the points mentioned in the project description with respect to the ventilation strategy towards the air quality for swimmers, thermal comfort and energy usage.

1.3 Literature study

Previous studies using CFD technique to evaluate indoor air quality and the thermal comfort of occupants in swimming pools generally concluded with poor air quality and thermal discomfort in swimming pools.

A study was conducted for the semi-Olympic pool of Bishop's University (Sherbrooke, Quebec, Canada) [7], where the airflow inlet and exhaust are positioned on the ceiling of the swimming pool (see figure 7). Both the numerical results and experimental measurements in the swimming pool show positive outcome, furthermore the study states that CFD studies of the conditions in large enclosed spaces with HVAC system can be performed at low cost [8].

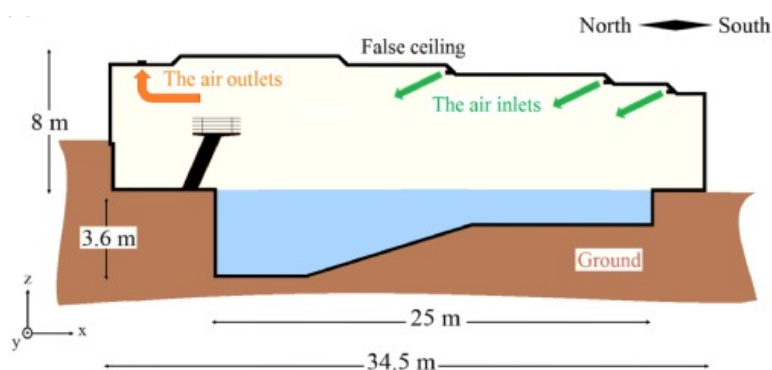


Figure 7: Airflow inlet and outlet in the semi-Olympic pool of Bishop's University [8]

Another investigated case regarding a swimming pool was at school in Byton, Poland [9], where the inlet airflow is positioned along the windows and exhaust on the ceiling (figure 8). This is the most common air distribution method that operates in the swimming pools in Norway, which this study clearly states for further improvements.

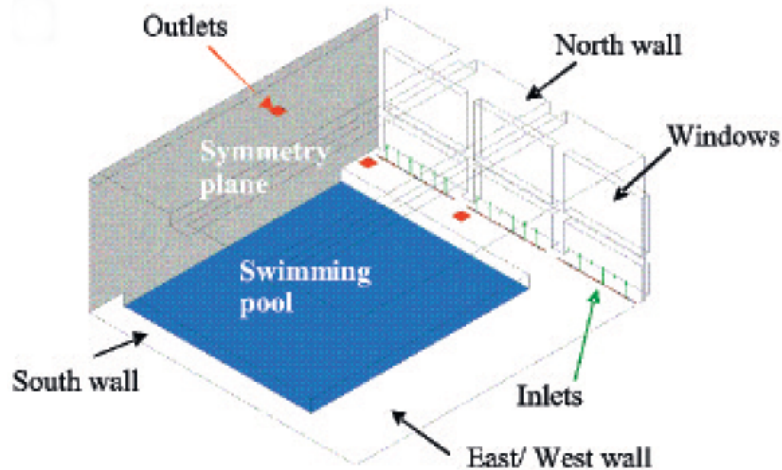


Figure 8: Airflow inlet and Outlet at the school swimming pool in Byton [9]

Several studies have used the CFD methods in order to estimate the evaporation rate from the swimming pool. Li and Heiselberg conducted a study about the influence of the evaporation on indoor air conditions in swimming pool by using a CFD model [10]. The study concluded that the two water evaporation models for the member ASHRAE - Shah correlation for unoccupied pool [11] and Shah empirical correlation for occupied pool [12] are quite good to calculate the water evaporation from water pools. An improved version of Shah's evaporation models for unoccupied and occupied were latest reported in the year 2018 [13].

There are two big challenges when simulating ventilation/swimming pool situation in CFD. The prediction of the jet inlet airflow and the importance of correct turbulence model. In order to describe the jet inlet airflow from supply diffuser, ASHRAE Srebric and Chen have suggested two methods. These are known as the box method or the momentum method [14].

Li and Nielsen reported in their study, the importance of using the correct turbulent model in CFD simulations to obtain realistic airflow in room [15], and how this depends on inlet airflow and corresponding Reynolds number in the turbulent flow.

1.4 Åfjord swimming pool

Åfjord Swimming facility is located in Årnest also called Åfjord city, Trøndelag County, central Norway. The local municipality decided on 16th June 2016, to build new swimming facility as a part of the new larger activity and cultural building for the local population. Construction work started on the first quarter of the year 2019 and it is expected to take up to two year to complete the project. However, it is still not announced an official date for the pool opening (see figure 9).



Figure 9: Åfjord swimming pool [16]

Åfjord swimming facility satisfies the passive house standard and it is potentially expected to have much lower air leakage infiltration than the requirement of the passive house. The gross floor area of the facility is around 1314 m² accommodating two particular pools and various area services. The investigated swimming pool is a 25 metre pool with 6 swimming lanes, jumping boards and water slide and it has the water temperature of 28 °C (figure 10). The other one is a therapy pool and expected to have the water temperature of 34 °C. The two swimming pools are separated from each other with glass facade.

Table 1: Investigated swimming pool volume and area

| Property | Examined hall | Pool [water surface area] | Floor area |
|--------------------------|---------------|---------------------------|------------|
| Area [m ²] | 732.9 | 387.5 | 345.4 |
| Volume [m ³] | 5142 | - | - |



Figure 10: Invistgated swimming pool [16]

2 Theory

2.1 Byggforsk's recommendation

The Norwegian Building Quality Directorate DiBK recommends using SINTEF Byggforsk Building Research Design Guides as a documentations for the technical solutions in buildings.

Byggforsk series 552.315 recommends to ventilate the swimming pools with approximately 4-7 ACH airflow in order to achieve an acceptable indoor climate [17].

Table 2: Airflow for åfjord swimming pool due to the rule of thumb ACH

| ACH | Airflow $\frac{m^3}{hour}$ |
|-----|----------------------------|
| 4 | 20568 |
| 5 | 25710 |
| 6 | 30852 |
| 7 | 35994 |

Tabel 2 above shows huge required airflow due to the conventional ventilation strategy in swimming pool. A pure supply of outdoor fresh air would bring an unacceptable huge energy consumption.

Good hygiene and low pollution level in the hall makes recirculation of the air quite safety. The required amount of outdoor fresh air must be able to ensure good air quality. This depends on dehumidification technique in the facility.

Byggforsk series 552.315 recommends to use the highest fresh outdoor airflow from one of the two values in table 3

Table 3: Minimum outdoor fresh air Byggforsk series 552.315

| Area type | SI value |
|---------------------------------|---------------------------------|
| Water surface area + floor area | $Area(m^2) \times 1.4(L/s.m^2)$ |
| Water surface | $Area(m^2) \times 2.8(L/s.m^2)$ |

- $1.4 \frac{L}{s.m^2} = 5.04 \frac{m^3}{h.m^2}$ (water surface area + floor area).
- $2.8 \frac{L}{s.m^2} = 10.08 \frac{m^3}{h.m^2}$ (water surface area).

Evaporation occurs on the water surface of the pool and also from the unclothed bodies of the swimmers as result of the heat lost. In order to minimise this evaporation rate and consequently reducing the risk for moisture and moulds. The air temperature should be two or three degrees above the temperature of the pool of the water during operation hours [10] [17]. For a water temperature of 28 °C, the air temperature should be 30 °C. Furthermore, Byggforsk recommends the rule of thumb ($0.25 \frac{kg}{h.m^2}$ (water surface area)) to estimate the evaporation rate.

2.2 CIBSE's recommendation

The Chartered Institution of Building Services Engineers CIBSE makes standards and is the authority on building services engineering and it is consulted by the government in the UK. It is also well represented in the EU and worldwide.

CIBSE reports about several guides that could be used in order to calculate the airflow in swimming pools (see table 4). Those guides show large variations in their results as reported for 4-10 ACH . The reason for this variation is that the swimming pools vary in the design of the building and conditions.

Table 4: CIBSE reported guides for airflow calculation in swimming pool

| Legislation | Guide |
|--|--|
| Sport England HSE Managing Health Safety in Swimming Pools. Pool Water Treatment Advisory Group Building Regulations Approved Document F CIBSE Guide B2005 | Swimming Pools Updated Guidance for 2013 Published 2003 (Revised 2013) Treatment and Quality Standard for Pools and Spas Table 6.3 refers to CIBSE Section 2.3.21 (Table 2.27) - Sports Centre Ventilation Guide |

CIBSE recommends 30 % minimum fresh outdoor air for the circulation purpose [18]. This is higher than the Byggforsk recommendation for outdoor fresh air.

CIBSE reports that based on their experiences and experiments with evaporation rate in swimming pool, the empirical equation of Biasin & Krumme (1974) is the most reliable model to calculate evaporation rate. Using the Biasin & Krumme (1974) empirical correlation in equation 1 for occupied swimming pool, the evaporation rate becomes $0.26 \frac{kg}{hm^2}$. The evaporation rate is similar to the recommended one from the Byggforsk. However, Byggforsk does not specify any information for this empirical correlation.

$$E = 0.118 + 0.01995(0.4823(p_w - p_r)) \quad (1)$$

Where:

- E is the evaporation rate for occupied pool.
- r = at room temperature and humidity.
- w = saturated at water surface temperature.
- p is the partial pressure of water vapour in air, Pa.
- $p_r = 2268.6 \text{ pa}$ @ air temperature = 28 °C and RH= 60%.
- $p_w = 3784 \text{ pa}$ @ water surface temperature = 28 °C and RH= 60%.
- 0.118 is an empirical factor applied for the random shape of disturbed water.
- 0.01995 is a factor applied relating to heat convection.
- 0.4823 is an activity factor for public swimming pool.

2.3 ASHRAE's recommendation

American Society of Heating and Air-Conditioning Engineers ASHRAE is known as the World's largest institute for making standards in providing well advanced sustainable technology for the built environment and industry.

(ASHRAE,1999) Applications Handbook recommends the following air changing rate for swimming pools :

- 4 to 6 ACH for pools with no spectator area.
- 6 to 8 ACH for pools with spectator areas
- 4 to 6 ACH for therapeutic pools

ASHRAE Standard 62.1 recommends the following minimum values for outdoor fresh airflow (see table 5).

Table 5: ASHRAE Standard 62.1: Minimum outdoor fresh air rate

| Area type | SI |
|----------------------------|---|
| Pool & wet deck | Area (m ²) \times 2.4(L/s.m ²) |
| Remaining floor (dry area) | Remaining Area (m ²) \times 0.30(L/s.m ²) |
| Spectator & Bleacher | Spectator area (m ²) \times 0.30(L/s.m ²) + <i>number of spectators</i> \times 3.8(L/s) |

ASHRAE Shah has developed two methods in order to calculate the evaporation rate form occupied swimming pools. The first one is an empirical correlation, which it is obtained by regression curve to Shah's tested data. It is known as Shah empirical correlation as equation 2 below.

$$E = 0.113 - \frac{0.000079}{U} + 0.000059(p_w - p_r) \quad (2)$$

where:

- $U = 4.5N^* = 4.5 \times 0.20 = 0.91$ is the pool utilisation factor .
- $N^* = \frac{N}{A} = \frac{78 \text{ persons}}{387.9 \text{ m}^2} = 0.20 \frac{\text{person}}{\text{m}^2}$ is the occupant's density.
- N is the number of occupant.
- A is the pool surface area.
- p is the partial pressure of water vapour in air, Pa.
- $p_r = 2268.6 \text{ pa}$ @ air temperature = 28 °C, and RH= 60%.
- $p_w = 3784 \text{ pa}$ @ water surface temperature = 28, °C, and RH= 60%.
- r = at room temperature and humidity.
- w = saturated at water surface. temperature.

Computing the design data for the Åfjord swimming pool in the previous correlation, it provides evaporation rate of $0.20 \frac{\text{kg}}{\text{m}^2 \cdot \text{h}}$.

The second method for the evaporation rate calculation considers physical phenomena in the pool. It is called Shah phenomenological model, and it is based on experiments that notes that the evaporation increases proportional to the increasing in water surface area caused by the number of occupants [13].

$$\frac{E}{E_0} = 3.3U + 1 \text{ for } U < 0.1 \quad (3)$$

$$\frac{E}{E_0} = 1.3U + 1.2 \text{ for } 0.1 \leq U \leq 1 \quad (4)$$

$$\frac{E}{E_0} = 2.5 \text{ for } U > 1 \quad (5)$$

Where:

- E is the rate of evaporation from occupied swimming pool, $\frac{kg}{m^2.h}$
- E_0 is the rate of evaporation from unoccupied swimming pool, $\frac{kg}{m^2.h}$

The rate of evaporation from unoccupied swimming pool $E_0 \frac{kg}{m^2.h}$ can be obtained by using the larger evaporation rate of equation 6 and 7 or from Shah's developed table 6 for the unoccupied pool evaporation rate.

$$E_0 = C \rho_w (\rho_r - \rho_w)^{\frac{1}{3}} (W_w - W_r) \quad (6)$$

$$E_0 = b(p_w - p_r) \quad (7)$$

where:

- $C = 35$ in SI units.
- $b = 0.00005$ in SI units.
- ρ is density of air, mass of dry air per unit volume of moist air, kg/m³ (This is the density in psychometric charts and tables).
- $\rho_r - \rho_w$ can be obtained from Shah's developed table for the air density differences at swimming pool appendix A.
- W is specific humidity of air, kg of moisture/kg of air (psychometric chart).

Table 6: Shah formulas SI unit: Evaporation from unoccupied indoor swimming pools

| Water Temp., °C | Evaporation from Unoccupied Pool (E_0), Space Air Temperature, and Relative Humidity | | | | | | | | | | | |
|-----------------|--|--------|--------|--------|--------|--------|--------|--------|--------|--------|--------|--------|
| | 25°C | | 26°C | | 27°C | | 28°C | | 29°C | | 30°C | |
| | 50% | 60% | 50% | 60% | 50% | 60% | 50% | 60% | 50% | 60% | 50% | 60% |
| 25 | 0.1085 | 0.0809 | 0.0917 | 0.0636 | 0.0732 | 0.0515 | 0.0639 | 0.0450 | 0.0583 | 0.0382 | 0.0523 | 0.0311 |
| 26 | 0.1333 | 0.1042 | 0.1171 | 0.0872 | 0.0997 | 0.0693 | 0.0806 | 0.0547 | 0.0679 | 0.0479 | 0.0620 | 0.0408 |
| 27 | 0.1597 | 0.1289 | 0.1433 | 0.1118 | 0.1262 | 0.0941 | 0.1081 | 0.0753 | 0.0885 | 0.0582 | 0.0723 | 0.0510 |
| 28 | 0.1877 | 0.1556 | 0.1711 | 0.1380 | 0.1539 | 0.1200 | 0.1360 | 0.1014 | 0.1171 | 0.0818 | 0.0968 | 0.0618 |
| 29 | 0.2174 | 0.1841 | 0.2006 | 0.1661 | 0.1831 | 0.1477 | 0.1651 | 0.1287 | 0.1463 | 0.1092 | 0.1268 | 0.0888 |
| 30 | 0.2491 | 0.2146 | 0.2319 | 0.1962 | 0.2142 | 0.1773 | 0.1959 | 0.1579 | 0.1771 | 0.1380 | 0.1575 | 0.1176 |

Using the design condition for Åfjord swimming pool in table 6 will result in a evaporation rate of $E_0 = 0.0618 \frac{kg}{m^2h}$ when the pool is unoccupied. Furthermore, the evaporation rate for occupied pool E , using equation 5 becomes as following:

$$E = 3.3 \times 0.91 \times 0.0618 = 1.19 \frac{kg}{hm^2} \quad (8)$$

2.4 Computational Fluid Dynamics

CFD stands for Computational Fluid Dynamics, it is a technique that allow us to simulate fluid flow using computer simulations. We solve primary equations called the Navier Stokes Equations, and then to get more information out of the simulation, it is needed to solve more additional equations. This is typically the case for engineering applications.

Flow analysis are governed by partial dierential equations that represent the conservation of mass, momentum and energy. However the physical processes are modelled using simplified mathematical equations for saving computational efficiency, these models interact with the fundamental governing equations, then numerical analysis is used to solve this governing equations on a computational mesh, and finally an engineering quantities can be obtained as output. Star CCM+ is the simulation software used in this study. In details it contains three main elements[19]:

1. Pre-processor.
2. Solver.
3. Post-processor.

2.4.1 Pre-processor

Pre-processing is the input data made by the user for a flow problem. These data is normally transformed in a suitable form for the solver. This includes:

- Geometry definition called the computational domain.
- Grid generation into smaller mesh for control volumes.
- Fluid properties.
- Boundary conditions and interfaces

Star CCM+ resolve velocity, pressure, temperature and mass flow in each cells and any other properties should be computed. Pre-processing large number of cells, increase the accuracy of the solution, but on the other hand calculation time increases dramatically which can be a time issue. Modelling a situation involving swimming pool is challenging. Very large number of cells require a suitable super computer. To reduce the computational cost the mesh generation can be controlled. Star CCM+ offers the volumetric control to refine the mesh in the areas where large variation occurs and coarse mesh in areas with little changes.

2.4.2 Solver

Star CCM+ operates finite volume method. The numerical algorithm consists of the following steps:

- Integration of the governing equations of fluid flow over all the finite control volumes of the domain.
- Discretisation converse the integral governing equations into a system of algebraic equations.
- Solution of the algebraic equations by an iterative method.

The control volume integration in the first step is one of the biggest advantages of the finite volume method. The practical conversion of integral equations into algebraic equations, and then solving it for each cell by iterative method, considered as a clear relation between the numerical algorithm and physical conservation principle, and make it easy to understand by many engineers.

The conservation of general flow variable ϕ within a finite control volume is shown figure 11.

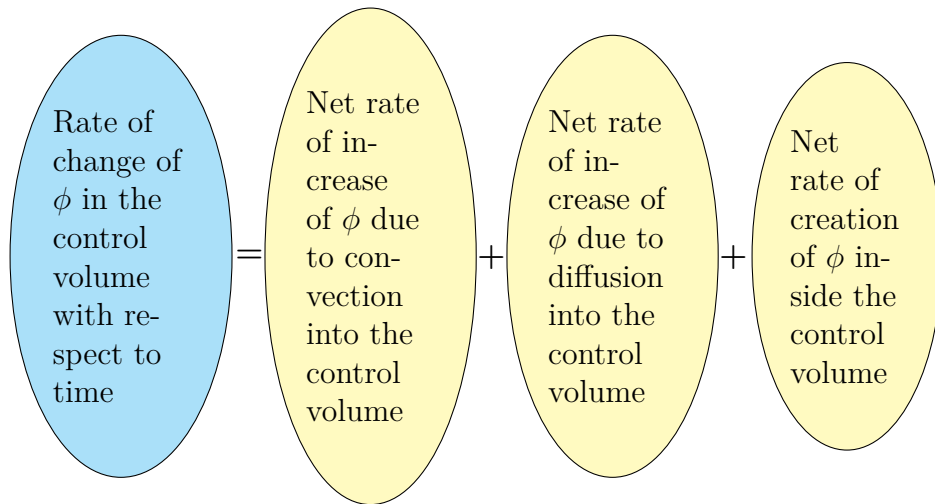


Figure 11: General conservation of flow in finite volume method

The discretization step in CFD process the transport phenomena with respect to time due to the:

- Convection is the physical process that occurs in a flow which some property of the fluid is transported by fluid motion usually due to the temperature differences.
- Diffusion is the physical process that occurs in a flow which some property of the fluid is transported by random motion of fluid molecules usually due to the concentration differences.
- Source terms: the creation or destruction of ϕ .

2.4.3 Post-processor

The Post-processor presents and visualizes the results in clearly and friendly way. The Star CCM+ software is equipped with versatile data visualisation tools. These includes:

- Geometry and grid display.
- Scalar plot.
- vector plot.
- Contour plot.

- view options(Translation, rotation, scaling).
- Colour Postscript output.

2.4.4 Governing equations

Historically only the momentum equations was referred to as the Navier Stokes Equations, but these days this definition is no longer used in a very strong sense. Many engineers refer to this entire set of equations in figure 12 as Navier Stokes Equations [20].

These equations describe how the flow takes place without taking into account the application, so the way these equations are able to understand that the flow is actually taking place in a swimming pool ventilation is from the boundary conditions.

So, in order to use CFD effectively, it needed to have a full understanding of each of these terms. Figure 12 shows four boxes that divide the equations for explaining reason. The red box called the time derivative terms, they represents how the quantity inside the time derivative changes as a function of time. The blue box called as a convective terms, this term is a special derivatives and they are present in all equations. The orange box called as pressure drop terms. This term is responsible for capturing the effect of pressure. Finally the black box called as diffusion terms. Diffusion is related to the shear tensor which help in taking into account the wall effect and describing the boundary layer flows. The stress tensor τ is the cross product of multiplying two velocity vectors. The stress tensor has nine velocity components, and each component of the stress tensor is the second derivatives of the velocity component. In the CFD the stress tensor are often approximated by turbulence model.

There are four independent variables \mathbf{x} , \mathbf{y} , \mathbf{z} and time \mathbf{t} . and six dependent variables, which are three velocity components (\mathbf{u} , \mathbf{v} and \mathbf{w}) in the direction of x, y and z respectively, pressure \mathbf{p} , and temperature \mathbf{T} . Noticed the energy equation contains all the six dependent variables.

Three-dimensional turbulence flow, is based on the solution of the governing equations for the six dependent variables, which are functions of all four independent variables.

| | | |
|--|---|---|
| Coordinates: (x,y,z) Velocity Components: (u,v,w) | Time : t Pressure: p Density: ρ Stress: τ Total Energy: Et | Heat Flux: q Reynolds Number: Re Prandtl Number: Pr |
| Continuity: | $\frac{\partial \rho}{\partial t} + \frac{\partial(\rho u)}{\partial x} + \frac{\partial(\rho v)}{\partial y} + \frac{\partial(\rho w)}{\partial z} = 0$ | |
| X – Momentum: | $\frac{\partial(\rho u)}{\partial t} + \frac{\partial(\rho u^2)}{\partial x} + \frac{\partial(\rho uv)}{\partial y} + \frac{\partial(\rho uw)}{\partial z} = -\frac{\partial p}{\partial x} + \frac{1}{Re_r} \left[\frac{\partial \tau_{xx}}{\partial x} + \frac{\partial \tau_{xy}}{\partial y} + \frac{\partial \tau_{xz}}{\partial z} \right]$ | |
| Y – Momentum: | $\frac{\partial(\rho v)}{\partial t} + \frac{\partial(\rho uv)}{\partial x} + \frac{\partial(\rho v^2)}{\partial y} + \frac{\partial(\rho vw)}{\partial z} = -\frac{\partial p}{\partial y} + \frac{1}{Re_r} \left[\frac{\partial \tau_{xy}}{\partial x} + \frac{\partial \tau_{yy}}{\partial y} + \frac{\partial \tau_{yz}}{\partial z} \right]$ | |
| Z – Momentum | $\frac{\partial(\rho w)}{\partial t} + \frac{\partial(\rho uw)}{\partial x} + \frac{\partial(\rho vw)}{\partial y} + \frac{\partial(\rho w^2)}{\partial z} = -\frac{\partial p}{\partial z} + \frac{1}{Re_r} \left[\frac{\partial \tau_{xz}}{\partial x} + \frac{\partial \tau_{yz}}{\partial y} + \frac{\partial \tau_{zz}}{\partial z} \right]$ | |
| Energy: | $\frac{\partial(E_T)}{\partial t} + \frac{\partial(uE_T)}{\partial x} + \frac{\partial(vE_T)}{\partial y} + \frac{\partial(wE_T)}{\partial z} = -\frac{\partial(up)}{\partial x} - \frac{\partial(vp)}{\partial y} - \frac{\partial(wp)}{\partial z} - \frac{1}{Re_r Pr_r} \left[\frac{\partial q_x}{\partial x} + \frac{\partial q_y}{\partial y} + \frac{\partial q_z}{\partial z} \right] + \frac{1}{Re_r} \left[\frac{\partial}{\partial x}(u \tau_{xx} + v \tau_{xy} + w \tau_{xz}) + \frac{\partial}{\partial y}(u \tau_{xy} + v \tau_{yy} + w \tau_{yz}) + \frac{\partial}{\partial z}(u \tau_{xz} + v \tau_{yz} + w \tau_{zz}) \right]$ | |

Figure 12: Navier-Stokes Equations 3-dimensional-unsteady [20]

The demonstrated equations were derived independently by G.G. Stokes in England, and M. Navier in France, in the early 1800's. The equations are expansion of Euler equations, and include the impact of viscosity on the flow [20].

Re Reynolds number. It is a dimensionless number that express the ratio between inertial forces and viscous forces ($Re = \frac{\rho \times V \times L}{\mu}$). Laminar flow occurs at low Re, when the viscous forces dominates and its characterisation as smooth fluid motion. The turbulent flows occurs at high Re, when the inertial forces dominates and its characterisation as chaotic fluctuating flow.

Pr Prandtl number. It is a dimensionless number that express the ratio between the kinematic viscosity to the thermal diffusivity.

Usually, the value for Prandtl number is approximated to be around 0.7-1.0 for gasses and round 1-10 for water [21].

The following equations are the governing equation expressed in the dimensional form for turbulent flow.

Continuity equation:

$$\frac{\partial \rho}{\partial t} + \frac{\partial}{\partial x_i}(\rho U_i) = 0 \quad (9)$$

where:

- ρ is the the density of the fluid [$\frac{kg}{m^3}$].
- t is the time [s].
- U_i is mean velocity component corresponding to the i direction [$\frac{m}{s}$].
- x_i is the coordinate direction i [m].

Energy equation: the conservative energy form is expressed in the following general transport equation.

$$\frac{\partial}{\partial t}(\rho T) + \rho U_j \frac{\partial T}{\partial x_j} = \frac{\partial}{\partial x_j}(\gamma \frac{\partial T}{\partial x_j} - \rho u'_j T') + S_T \quad (10)$$

Where:

- T is the time-mean temperature of the fluid [$^{\circ}C$].
- γ is the diffusion coefficient.
- T' is the fluctuating temperature [$^{\circ}C$].
- U_j is the mean velocity component corresponding to the j. direction [$\frac{m}{s}$].
- x_j is the coordinate direction j [m].
- u'_j is the fluctuating velocity component in the j direction [$\frac{m}{s}$].
- S_T is the source term [$\frac{W}{m^3}$].

Momentum equations (Navier-Stokes equations)

$$\frac{\partial}{\partial t}(\rho U_j) \frac{\partial U_i}{\partial x_j} = -\frac{\partial P}{\partial x_i} + \frac{\partial}{\partial x_j}(\mu \frac{\partial U_i}{\partial x_j} - \rho u'_i u'_j) + \rho g_i \quad (11)$$

Where:

- P is pressure [Pa]
- μ is laminar dynamic viscosity [$\frac{kg}{ms}$]
- g_i is gravitational acceleration in the i direction [$\frac{m^2}{s}$]

2.5 Governing equations of radiative heat transfer

Thermal radiation is the emission of electromagnetic waves from all matter that has a temperature greater than absolute zero, and represents a conversion of thermal energy into electromagnetic energy. The radiative transfer equation (RTE) governs this process. This equation can be written in terms of radiant intensity for a specific wavelength λ :

$$\frac{dI_\lambda}{ds} = -\beta_\lambda I_\lambda + k_{a\lambda} I_{b\lambda} + \frac{k_{s\lambda}}{4\pi} \int_{4\pi} I_\lambda \Omega d\Omega + k_{pa\lambda} I_{pb\lambda} + \frac{k_{ps\lambda}}{4\pi} \int_{4\pi} I_\lambda \Omega d\Omega \quad (12)$$

Where:

- I_λ : radiative intensity at wavelength λ [$\frac{W}{m^2 sr m^{-1}}$].
- $I_{b\lambda}$: black body intensity at wavelength λ .
- $I_{pb\lambda}$: particle black body intensity at wavelength λ and current particle temperature.
- s : distance in the direction.
- β_λ : extinction coefficient.
- $k_{a\lambda}$: absorption coefficient at wavelength λ (m^{-1}).
- $k_{s\lambda}$ scattering coefficient at wavelength λ (m^{-1}).
- $k_{pa\lambda}$ particle absorption coefficient at wavelength λ (m^{-1}).
- $k_{ps\lambda}$ particle scattering coefficient at wavelength λ (m^{-1}).
- Ω solid angle.

2.6 Transport equations for gas species

Gases like water vapour and chlorine are usual to be found in the swimming pool environment. Therefore, additional differential equations for the multicomponent gases in the swimming pool need to be solved by additional equations given by:

The transport equation for species (k) is shown in equation 13.

$$\frac{\partial}{\partial t}(\rho Y_k) + \frac{\partial}{\partial x_i}(\rho u_i Y_k) = \frac{\partial}{\partial x_i}(\rho D_k \frac{\partial Y_k}{\partial x_i}) \quad (13)$$

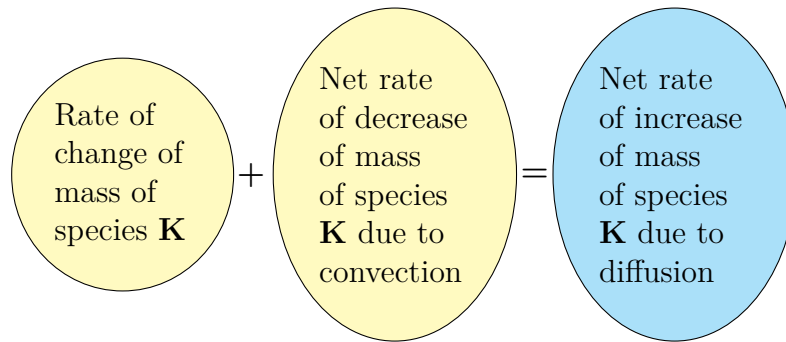


Figure 13: Description of the gas species transport equation

2.7 Turbulence models in CFD

Several turbulent models have been developed in order to fit the various application systems. It is important to understand turbulent model's definition, its strength and weakness, when it comes to choose the most accurate one. The closure of the Navier Stokes equations to their stress term in the equation, describes the turbulence model.

2.8 Reynolds-averaged Navier-Stokes Models RANS

Reynolds-averaged Navier-Stokes Models RANS is the most common used model in the field of turbulence flow. The models attempts to close the turbulence equation using the viscosity term and the kinetic energy per unit mass of turbulent fluctuations variable k .

2.8.1 RANS Two-Equation model: Standard $k - \epsilon$

The **advantages** of this model can be assumed as following:

- Simple turbulence model requires just boundary and initial conditions.
- Good performance for several industrially flows.
- The most widely validated and established model.

The reported **disadvantages** of this model:

- Poor performance in some important case like swirling flow, rotating flows, and fully turbulent developed flow in a non circular form.

The $k - \epsilon$ model is based on the transport equations 14 and 15 for k and ϵ respectively [19]:

$$\frac{\partial(\rho k)}{\partial t} + \text{div}(\rho k U) = \text{div}\left(\frac{\mu_t}{\sigma_k} \text{grad}.k\right) + 2\mu_t S_{ij} S_{ij} - \rho \epsilon \quad (14)$$

$$\frac{\partial(\rho \epsilon)}{\partial t} + \text{div}(\rho \epsilon U) = \text{div}\left(\frac{\mu_t}{\sigma_\epsilon} \text{grad}.\epsilon\right) + C_{1\epsilon} \frac{\epsilon}{k} 2\mu_t S_{ij} S_{ij} - C_{2\epsilon} \rho \frac{\epsilon^2}{k} \quad (15)$$

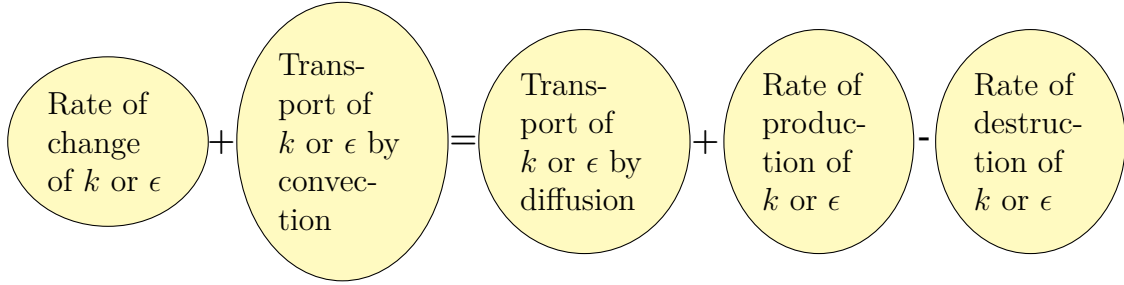


Figure 14: Description of k and ϵ transport equation

2.8.2 RANS Two-Equation: Standard $k - \omega$, and SST $k - \omega$

This model shows good performance in complex geometry and phenomena at different length scales induced by the geometry which considered as a huge advantage. The disadvantages of this model is that this model showing problems in free stream flow. ω is based on the transport model shown in equation 16.

$$\frac{\partial(\rho \omega)}{\partial t} + \text{div}(\rho \omega U) = \text{div}\left(\mu + \frac{\mu_t}{\sigma_\omega} \text{grad}.\omega\right) + \gamma_1 (1\rho S_{ij} \cdot S_{ij} - \frac{2}{3}\rho \omega \frac{\partial U_i}{\partial x_j} \delta_{ij}) - \beta_1 \rho \omega^2 \quad (16)$$

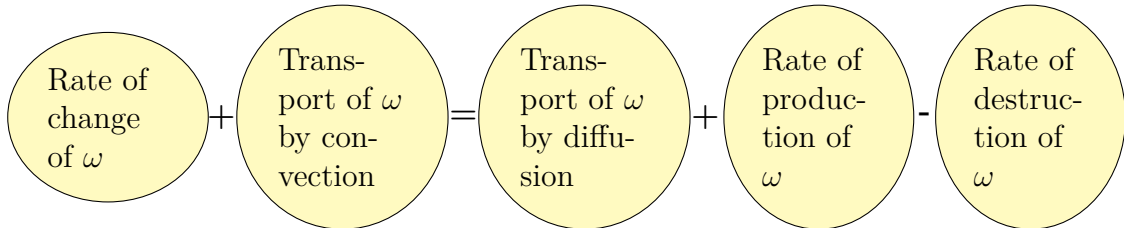


Figure 15: Description of ω transport equation

1. **Standard $k - \omega$ model** : this is a popular two equation model where the turbulent kinetic energy k and the specific dissipation rate ω equations governing the turbulence of the flow. The main aim of this model is to simulate flow near wall regions more accurately than $k - \epsilon$, however the model has problems with free stream flow.
2. **SST $k - \omega$ model**: is more like a hybrid model. The model has better reattachment and separation an ability compared with both $k - \omega$ and $k - \epsilon$ models. In other words, working like $k - \epsilon$ far from the wall and like $k - \omega$ near from the wall.

3 Method

The present study is accomplished using two steps: pre-processing the investigated swimming pool and studying the air quality indicators like local mean age of air LMA and air exchange efficiency ACE.

3.1 Geometry and design model

The investigated swimming hall has the geometry shape of a right trapezoid appendix [B] and its ceiling has two different heights to fits the jumping boards and water slide shown in appendix [C]. The water pool has the dimensions of 15.5×25 metre, and the 15.5 meters pool's width is divided into 6 lanes with a width of 2.50 metres for each lane appendix [B]. According to the specifications and regulations of swimming pool which are published by the Norwegian swimming federation, this basin is certified as a short pool for non competition purpose [22].

The main purpose of creating the geometry, is to generate computation of cells to solve the the governing equations. The pre-processing starts using Star CCM+ implemented 3D cad user interface tools. Creating 2D and 3D sketches is often the first step in creating a body. These sketched is used as basis for 3D operations like extrude, revolve, sweep, loft and sheet from sketch. Then when parts is created, the Boolean operations (like unite, intersect, and subtract) is used to combine multiple body to create a single body or to create a single body from multiple body.

The facade's features like external walls, floor, ceiling and external windows are pre-processed based on the 2D drawing of swimming pool see appendix [C]. The ventilation pipes are drawn in the design model to operate like a mixing ventilation

(MV) and it is located on the ceiling, and the exhaust is positioned according to the building shaft plan shown in the appendix [E]. It is considered in the simulation setup displacement ventilation (DV) diffusers under the external windows .

Figure 16 shows all bodies and surfaces for the swimming pools like the water bath, external walls and windows, MV, DV and exhaust.

The 3D coordinate system that is used in modelling near the bottom surface see figure 16. The negative Z- direction is pointing to the north while the positive Z direction is pointing to the south. The positive X- direction is pointing to the east while the negative X-direction pointing to the west. The top and the bottom of the model is pointing to the positive and negative Y-direction respectively.

In more detailed words we have external walls, windows and DV diffusers in the west and south facade. The MV is in the top while the water bath is in the bottom. The exhaust is located in the north facade.

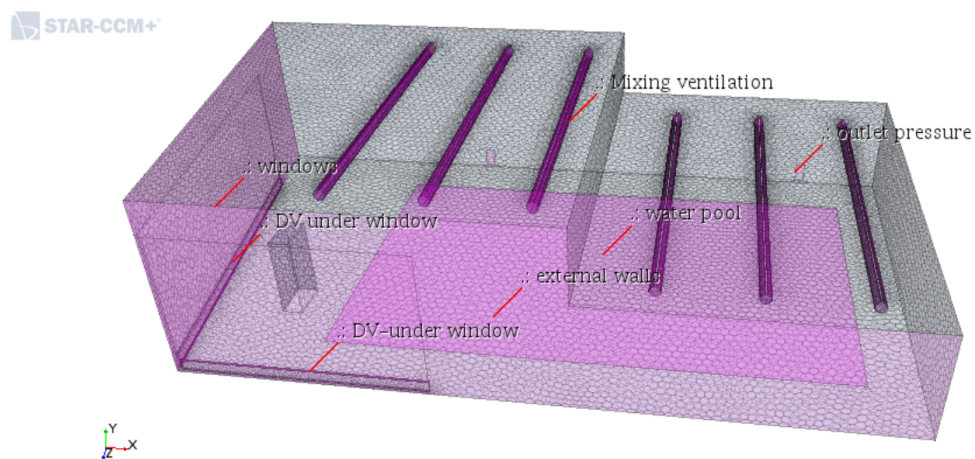


Figure 16: Åfjord model: positive Z-axis direction is pointing to south, negative Z-axis direction is pointing to north, positive X-axis direction is pointing to east and negative X-axis direction is pointing to west

3.2 Mesh

Star CCM+ is powerful to generate mesh of very good quality even with complex geometries. Still, mesh quality always needs to be checked as the mesh specifications could sometimes not fit with what is required by the complexity of the model's geometry.

It is used the **polyhedral mesh** mesh for this study. The polyhedral volume mesher is a good balance between speed and efficiency and creates a high-quality mesh. The mesher starts by building a tetrahedral mesh, then combines cells to generate the poly mesh with a lower number of cells, though each is slightly larger. This mesher is the most common core volume mesher and used most often in internal flows.

A representative mesh distribution is shown in figure 17. Generating fine meshes in areas where it is expected to have the greatest change in e.g. pressure, energy, or velocity. The mesh is then refined with the **volumetric control** function in areas such inlet flow, pressure outlet, water pool, and near the relevant breathing area.

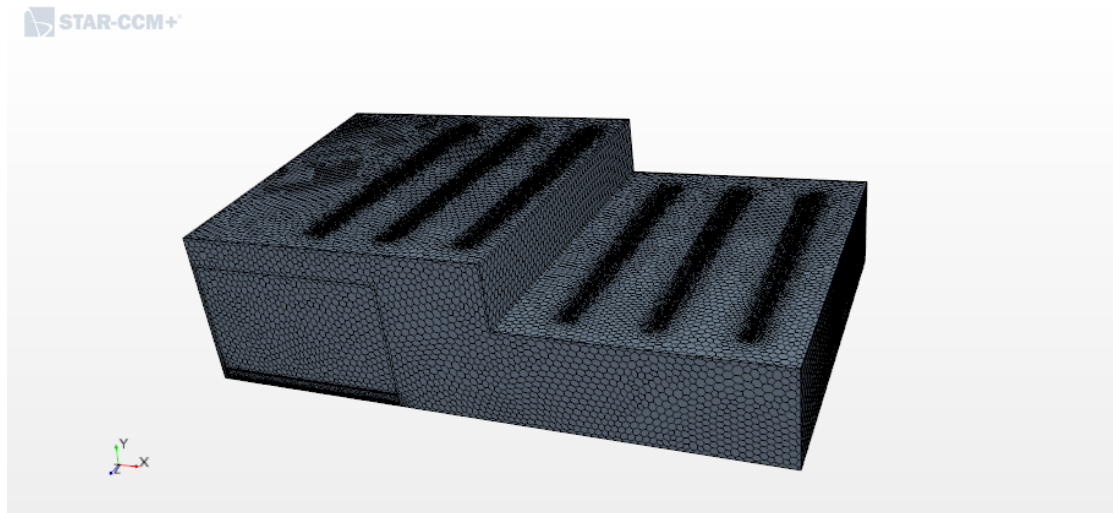


Figure 17: mesh

The polyhedral mesh is combined with a highly recommended optional boundary mesher called the **prism layer mesher**. This helps to obtain an accurate solution as it will ensure capture of the boundary layer and accounts turbulence modelling. It creates prismatic cells on the walls in the simulation. This capture boundary layer effects like friction and flow separation.

For turbulent flows a wall treatment is applied. Depending on this it is needed to choose the number of prism layers required to resolve the boundary layer adequately while maintaining the height of the first cell near the wall within the acceptable y^+ values. In this study the All y^+ wall treatment is used and at least 2-3 prism layers should be used according to Star CCM+ guideline. Here 4 prism

layers were chosen see figure (18). Furthermore, based on the size of the model and number of prism layers, a value between 1.1-1.5 is recommended for the **stretch factor**, here the value 1.5 is chosen.

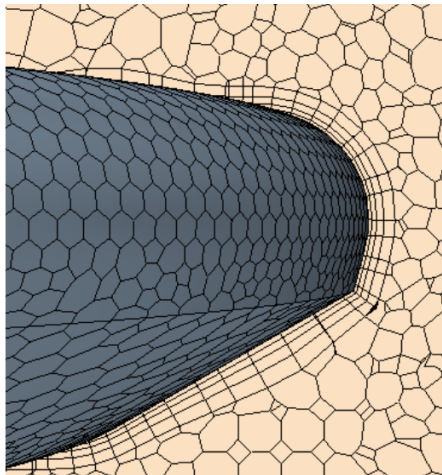


Figure 18: Prism layer near MV distributor

Once the polyhedral volume mesh has been generated, its validity and quality have been checked. The mesh may generate and when visualized appear to capture the geometry, but it is important to ensure that the cells are of high quality and not invalid (no negative volume cells, for example). The face validity of the cells is around 99.9% and the volume change equal to one is around 99.8%.

Table 7: Mesh's specifications

| Properties | Value |
|------------------------|----------------------------------|
| Mesh type | PSP |
| Base size | 0.4 m |
| Prisme layer thickness | 33% |
| Number of layers | 4.0 |
| Prims layer stretching | 1.5 |
| Number of cells | 420,000 |
| Volumetric control | 50% of base size and prims layer |

3.3 Physics setup and solvers

Now as the volume polyhedral mesh is defined, it is needed to define what the various sections are made of. These sections in swimming pool will be fluid. Con-

tinua in Star CCM+ presents various physic models to specify for the design model condition.

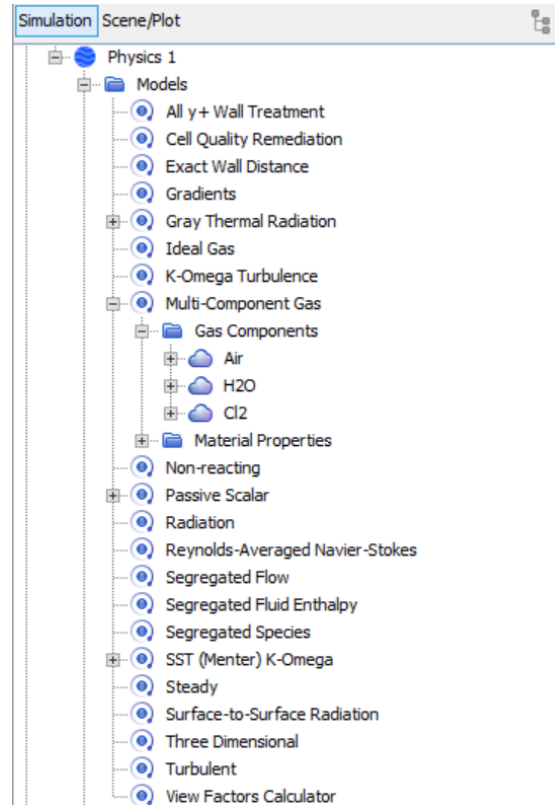


Figure 19: Physics models

Figure 19 shows the physics models that have been used for all five cases simulated in this study. The applied physics models presents a realistic scenario of heat transfer and thermodynamic of water evaporation and air that occur in a swimming pool. The physic continua is selected as following:

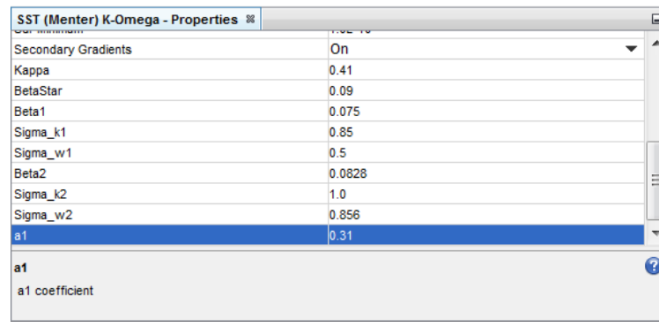
- The spatial dimensions for simulation is set as three dimensional and therefore a 3d volumetric mesh is created.
- The time is set as a **steady** simulation.
- Specifying the material whether the part is solid, liquid gas or some combination of the three. A **multi component-gas** means have different materials of the same state. Air, water and chlorine is selected. **Gradient** and **Ideal gas** is also selected here.

- Once the material is selected, the flow solvers options will appear. **Segregated flow** solver is selected. The Segregated Flow model solves the flow equations (one for each component of velocity and one for pressure) in a segregated or uncoupled manner. The linkage between the momentum and continuity equations is achieved with a predictor-corrector approach. It is capable of handling compressible flows and low Rayleigh number natural convection, and uses less memory than the coupled flow solver. The **segregated species** is an additional segregated solver that solves for multi component gas materials.
- With a flow solver selected, an equation of state will appear to define the flow. A **Segregated fluid enthalpy** is selected.
- When defining the viscous regime in swimming pool, flow viscosity and turbulence cannot be neglected. One the viscous model **Turbulent** is selected, there will be several options for turbulence modelling. **K-Omega Turbulence**, **SST(Menter) K-Omega** and **All y+ wall treatment** are then selected.
- Optional model like **surface to surface radiation** is activated. This model define the overall solution method for the governing radioactive transfer equation (RTE). The **view factors calculator model** enables solvers for generating radiation patches and calculating view factors. The **Gray Thermal Radiation** option models is then selected, which purely depends on surface temperatures, material properties, transmission media, and topology of the geometry.

The optional model **Cell quality redemption** is also activated. This model define the overall solution method for the governing radioactive transfer equation (RTE). This tool is ideal for detecting and correcting for poor cells in the model. It attempts to identify poor-quality cells, based on a set of predefined criteria, such as Skewness Angle, that exceed a certain threshold. Once these cells and their neighbors have been identified, the computed gradients in these cells are modified in such a way as to improve the robustness of the solution. **Passive scalar** model is selected. Its called passive because they do not affect the physical properties of the simulation. Passive scalars are user-defined variables, which are assigned to fluid phases or individual particles. They are used in this study because of the interest in tracing a fluid flow.

3.3.1 SST(Menter) K-Omega, All y+ wall treatment

The Menter SST K-Omega model is one of the most commonly used Reynolds-Averaged Navier-Stokes (RANS) turbulence models. The **K-Omega Turbulence models** allows to compute the **turbulent kinetic energy k** and the **specific dissipation rate ω** to provide closure to the Reynolds-Averaged Navier-Stokes equations. In this turbulence model, the shear stress limiter, commonly referred to as the **a1 coefficient** figure 20, can have a significant impact on solution accuracy. The shear stress limiter prevents turbulent shear stress from exceeding the **a1 coefficient** multiplied by the turbulent kinetic energy in the inner part of the boundary layer.



| Parameter | Value |
|---------------------|-------------|
| Secondary Gradients | On |
| Kappa | 0.41 |
| BetaStar | 0.09 |
| Beta1 | 0.075 |
| Sigma_k1 | 0.85 |
| Sigma_w1 | 0.5 |
| Beta2 | 0.0828 |
| Sigma_k2 | 1.0 |
| Sigma_w2 | 0.856 |
| a1 | 0.31 |

a1
a1 coefficient

Figure 20: Value of a1 coefficient used in the simulations

The following turbulence model and physical quantities is used in this study in order to estimate the turbulent properties at the inlets of a CFD simulation.

The turbulent kinetic energy k is the measure of how much energy is contained in the fluctuations of the turbulent flow. K is equal to:

$$k = \frac{3}{2}(Iv)^2 \left[\frac{m^2}{s^2} \right] \quad (17)$$

where:

- I is the turbulence intensity.
- v is the local velocity magnitude.

The Turbulent dissipation rate ϵ is the measure of the rate at which turbulent kinetic energy is dissipated, it means destructed and converted into thermal energy. ϵ is equal to:

$$\epsilon = \frac{C_\mu^{\frac{3}{4}} k^{\frac{3}{2}}}{L} \left[\frac{m^2}{s^3} \right] \quad (18)$$

Where:

- C_μ is a model coefficient and it is equal to 0.9
- k is the turbulent kinetic energy.
- L is the turbulent length scale

The specific turbulence dissipation rate ω is the rate of converting the turbulence kinetic energy into thermal energy.

$$\omega = \left[\frac{\sqrt{k}}{L\beta^{\frac{1}{4}}} \right] \left[\frac{1}{s} \right] \quad (19)$$

Where:

- β is a model coefficient and its equal to 0.9.

The turbulent length scale L is the measure of how big the eddies in a turbulent flow. Simulating a fully developed turbulent flow in CFD, the length scale become as following:

$$L = 0.07d_h \quad (20)$$

Where:

- d_h is the hydraulic diameter

Hydraulic diameter d_h is a useful quantity for the calculation of the Reynolds number in non-circular tubes. It can also be used to estimate the turbulent length scale for setting inlet boundary conditions. For a circular tube the hydraulic diameter corresponds to the actual geometric diameter. For rectangular tube or channel geometry is defined as following:

$$d_h = 2 \frac{ab}{a+b} [m] \quad (21)$$

Where:

- a and b are the width and the height of the hydraulic diameter.

The conservative law of mass flow rate of fluids passes through a pipes, is used in this study in order to determine the relation between the mass flow and inlet velocity of air.

$$Q = vA \left[\frac{m^3}{h} \right] \quad (22)$$

Where:

- v is the mean velocity of fluid in $\left[\frac{m}{s} \right]$.
- A is the cross section area in $[m^2]$.

Furthermore:

$$\rho = \frac{m}{V} \left[\frac{kg}{m^3} \right] \quad (23)$$

Where:

- ρ is the fluid's density $\left[\frac{kg}{m^3} \right]$.
- m is the fluid's mass $[kg]$.
- V is fluid's volume $[m^3]$.

The Wall treatment in STAR-CCM+ is the set of assumptions for modelling near-wall turbulence quantities such as wall shear stress, turbulent production and turbulent dissipation. Traditionally, the two basic types of wall treatment are available:

1. High $y+$ wall treatment is the classic wall-function approach, where wall shear stress, turbulent production and turbulent dissipation are all derived from equilibrium turbulent boundary layer theory. It is assumed that the near-wall cell lies within the logarithmic region of the boundary layer, therefore the centroid of the cell attached to the wall should have $y+ > 30$.
2. The low- $y+$ wall treatment assumes that the viscous sublayer is well resolved by the mesh, and thus wall laws are not needed. It should only be used if the entire mesh is fine enough for $y+$ to be approximately 1 or less.

The all **$y+$ wall treatment** is an additional hybrid wall treatment that attempts to combine the high $y+$ wall treatment for coarse meshes and the low $y+$ wall treatment for fine meshes. It is designed to give results similar to the low- $y+$ treatment as $y+ < 1$ and to the high- $y+$ treatment for $y+ > 30$. It is also formulated to produce reasonable answers for meshes of intermediate resolution,

when the wall-cell centroid falls within the buffer region of the boundary layer, i.e. when $1 < y^+ < 30$.

y^+ is The non-dimensional wall distance and u^+ is the non-dimensional velocity. The inner region of the boundary layer can be split up into three sublayers. In each of them the flow has different characteristics and can be modelled using different empirical approaches:

- Viscous sublayer: The fluid layer in contact with the wall is dominated by viscous effects and is almost laminar. The mean flow velocity only depends on the fluid density, viscosity, distance from the wall, and the wall shear stress.
- Log-law layer : The turbulent log-law layer is dominated equally by viscous and turbulent effects.
- Buffer layer: The buffer layer is a transitional layer between the viscous sublayer and the log-law layer.

Figure 21 below shows the regions of applicability of the wall treatments:

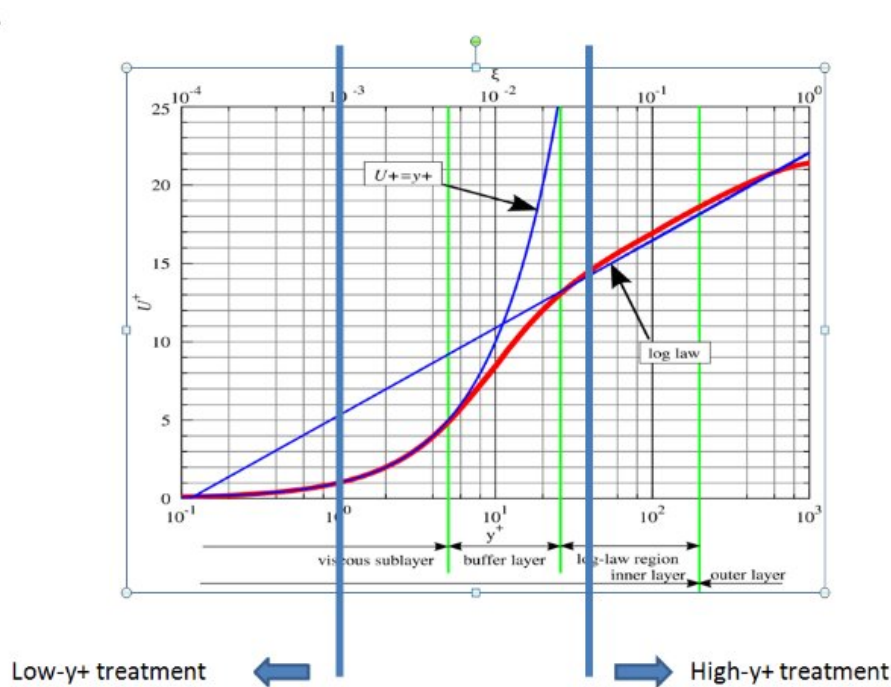


Figure 21: Y^+ wall treatment

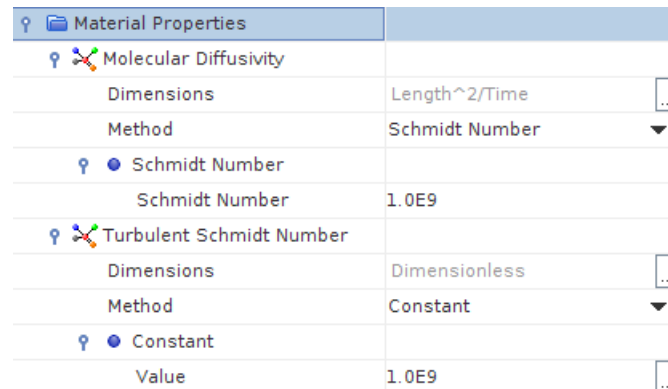
3.4 Passive scalar of local mean age of air LMA and air exchange efficiency ACE

3.4.1 The local mean age of air

Considering the air flow as particles motion, the average time needed for air to reach a point P in the room, since It entered the room, called the local mean age of air. LMA increases from zero at the entrance to the nominal time at the exit [23].

LMA is considered as an important parameter to remove the contaminant from the room or ventilated spaces, the longer times spend the air's particle at a point, the more it will be contaminated by the pollutant . LMA has low value in short circuited zone and high value in stagnate zone [24]. Using separate differential equation of passive scalar, can one estimate the LMA in CFD calculations. This defined passive scalar will act like attaching a clock to each volume element of air. These virtual clocks can be used to measure the residence time of the air in position in room.

One way to make the passive scalar in Star CCM+ tracking the fluid particles, is to modify the scalars diffusivity properties, setting both Schmidt numbers to very high values figure 22, setting the Passive Scalar Source Option to Scalar flux with inferred density, and set the Passive Scalar Source Density Inferred to $[\frac{1}{s}]$ figure 23. This allows advection to dominate the transport of the time scalar where there is motion in the flow, whilst allowing diffusion to work on the scalar where there is little to no advection.



| | |
|--------------------------|----------------|
| Material Properties | |
| Molecular Diffusivity | |
| Dimensions | Length^2/Time |
| Method | Schmidt Number |
| Schmidt Number | |
| Schmidt Number | 1.0E9 |
| Turbulent Schmidt Number | |
| Dimensions | Dimensionless |
| Method | Constant |
| Constant | |
| Value | 1.0E9 |

Figure 22: Schmidt number properties

| | | |
|---|---|-------------------------------------|
| ☑ | Physics Conditions | |
| ☞ | Energy Source Option | |
| ☞ | Initial Condition Option | |
| ☞ | Mass Source Option | |
| ☞ | Momentum Source Option | |
| ☑ | Passive Scalar Source Option | |
| | Source Definition | Scalar flux with inferred density ▼ |
| ☞ | Turbulence Source Option | |
| ☑ | Physics Values | |
| ☞ | Axis | |
| ☞ | Motion Specification | |
| ☑ | Passive Scalar Source Density Inferred | |
| | Method | Constant ▼ |
| | Value | [1.0] /s ... |
| | Dimensions | /Time ... |
| ☞ | Passive Scalar Source Derivative Density Inferred | |

Figure 23: Passive scalar source option

Without the high Schmidt numbers, diffusion in boundary layers keeps the mean age near-zero at the wall, which is incorrect. The suggested values accounts for the turbulent diffusion of "young" air into the mixing sublayer of the boundary layer, while keeping the age of air in viscous sublayer relatively undiffused.

3.4.2 Air exchange efficiency

It is an air quality indicator. understand the air quality indicator that express the efficiency of air distribution in the room. It represents the ratio between shortest time required to replace the air in the room τ_n and the average time for air exchanges τ_{exe} [25]. It is given by:

$$\eta_a = \frac{\tau_n}{\tau_{exe}} \quad (24)$$

Where:

- η_m has an efficiency, having values between $0 < \eta_m \leq 1$.
- $\tau_n = \frac{V}{q}$ is the ratio between the room's volume and its supplied fresh air.
- τ_{exe} is equal twice the local mean age of air LMA.

The ventilation modes with the typical flow pattern and air exchange efficiency are described in figure 24.

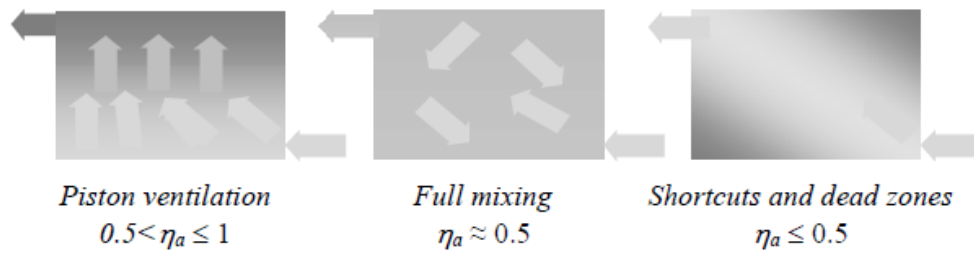


Figure 24: Air exchange efficiency [26]

There are defined user field functions for the several investigated ventilation cases in this study. These functions depend on the particular of both local mean age of air LMA and supplied fresh air q .

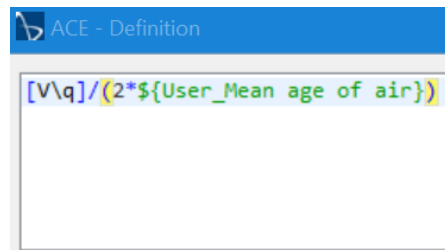


Figure 25: Air exchange efficiency user field function

3.4.3 Validation

In this validation, a CFD simulation of ventilated room was performed in order to measure the mean age of air and then to validate the defined passive scalar function for LMA in STAR-CCM+.

In a reported experimental and numerical study of local mean age of air [24], the test room was simulated using ANSYS software with the $k-\epsilon$ turbulent model figure 26. The room is supplied with an air flow of $363 \frac{m^3}{h}$, an inlet air velocity of $1.68 \frac{m}{s}$, an air temperature of $23 \text{ }^\circ\text{C}$, and 14% turbulent intensity.

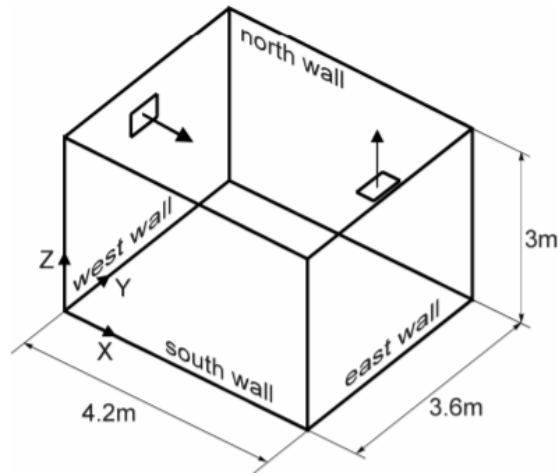


Figure 26: Test room

The validation case started with pre-processing the test room, and a segregated solver was assigned with the applied physics figure as shown in 27.

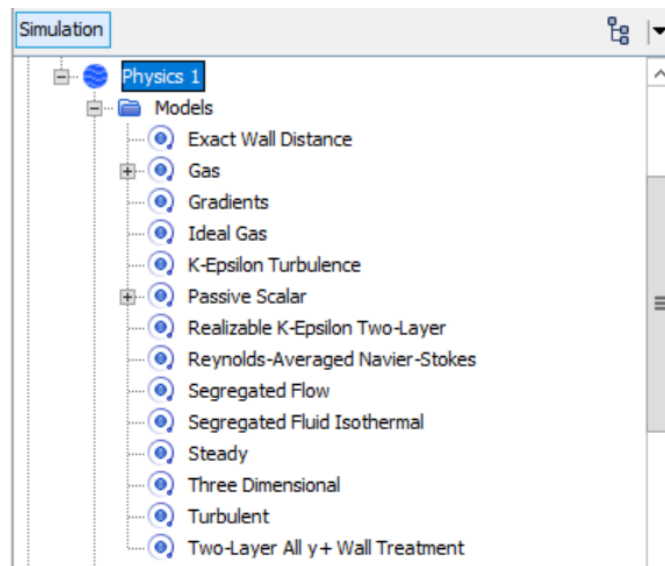


Figure 27: physics model

Post-processing the validation case for the LMA shows clearly low LMA values nearly the inlet along the jet and reaching high LMA values in recirculation zone.

A value of 1.1 to 1.3 LMA is everywhere presented in the room at the height of 1.1 m which is considered as breathing zone for a sitting person.

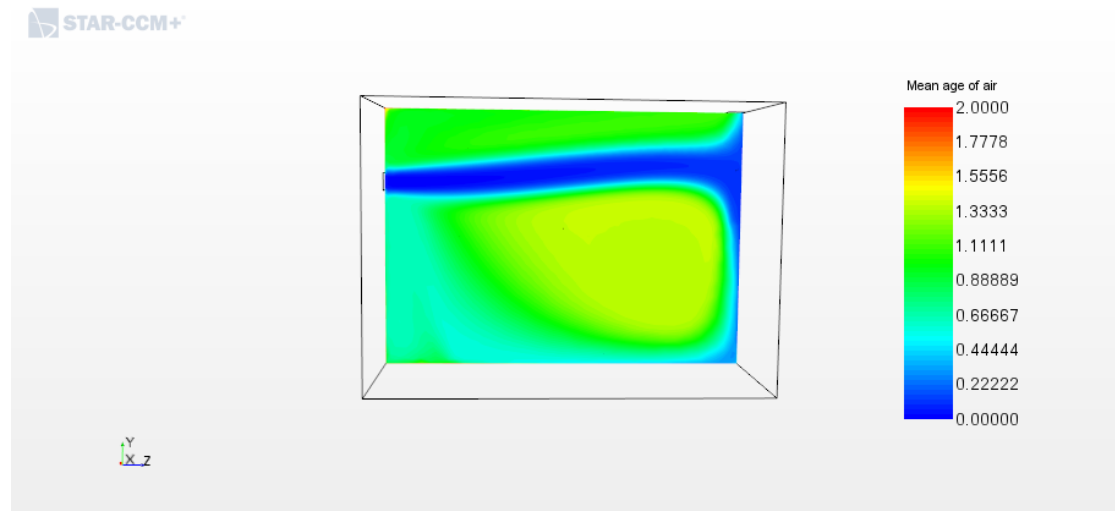


Figure 28: LMA-validated case

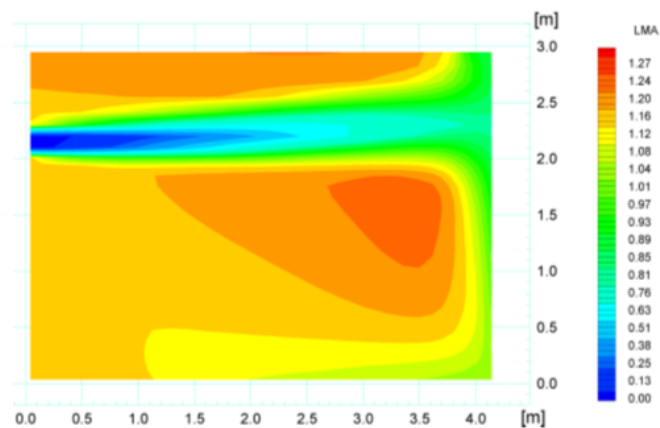


Figure 29: LMA-reported case [24]

In CFD, the residual measures the convergence or divergence of a simulation, and it tends to decrease for convergence. For this validation case a residual level of $10^{-5} - 10^{-7}$ is achieved (see figure 30).

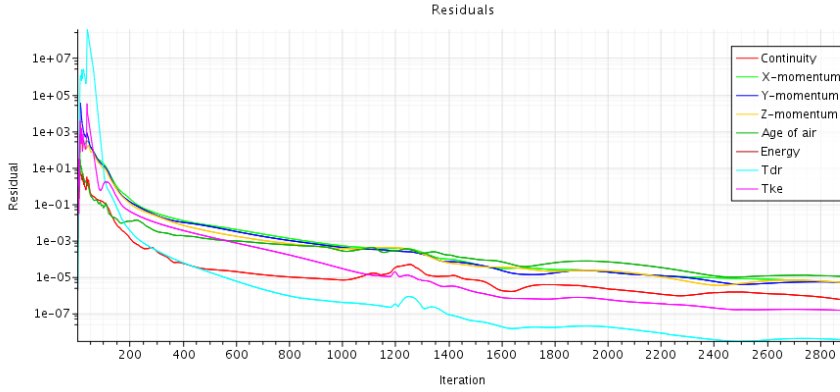


Figure 30: The validation case residual

3.5 Boundary conditions and different test cases of swimming hall (DV, MV-DV, DV4, 5, 7 ACH)

The Åfjord swimming pool satisfies the passive house standard NS 3701 [27], having the u-values for constructions and components described in table 8.

Table 8: U-values for passive house

| Property | Value [$\frac{W}{m^2k}$] |
|-----------------|----------------------------|
| window and door | 0.8 |
| external walls | 0.12 |
| ceiling | 0.09 |
| floor | 0.08 |

The outside designing temperature in Åfjord municipality is around -21.4°C [28], and computing the u-values for external walls and windows in equation 25 , produces surface temperatures of 26.9°C and 22.9°C receptively [29].

$$\theta_{si} = \theta_i - UR_{si}(\theta_i - \theta_e) \text{ [}^{\circ}\text{C]} \quad (25)$$

Where:

- θ_{si} is surface temperature.
- θ_i is the room air temperature
- R_{si} is the internal thermal transition resistance and it is equal to $0.13 \text{ [}\frac{m^2k}{W}\text{]}$

- U is the u-value of component or part.

Internal walls, floor and ceiling are in contacts with neighbour zones and therefore heat lost is considered as negligible. The exhaust valves are defined as a **gradient pressure outlet**.

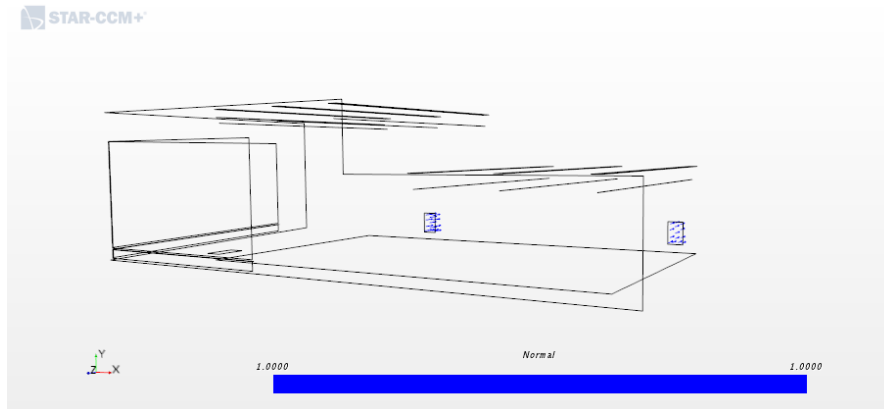


Figure 31: Pressure outlet

The water bath boundary conditions is defined as **mass flow inlet** with a thermal temperature of 28°C . The rate of mass flow evaporation is based on Shah ASHRAE phenomenological model equation 8, which gives a total evaporation rate of equal $0.124 \frac{\text{kg}}{\text{s}}$.

The minimum guideline value for free active chlorine in the swimming pool water range between $0.4\text{-}1.0 \text{ mg } \frac{\text{Cl}_2}{\text{L}}$ [30]. The Åfjord swimming pool contains approximately 866.10^3 litre water. A $1.0e^{-6} \frac{\text{kg}}{\text{s}}$ mass fraction of the evaporation rate is represented as a chlorine evaporation in this study (see figure 32).

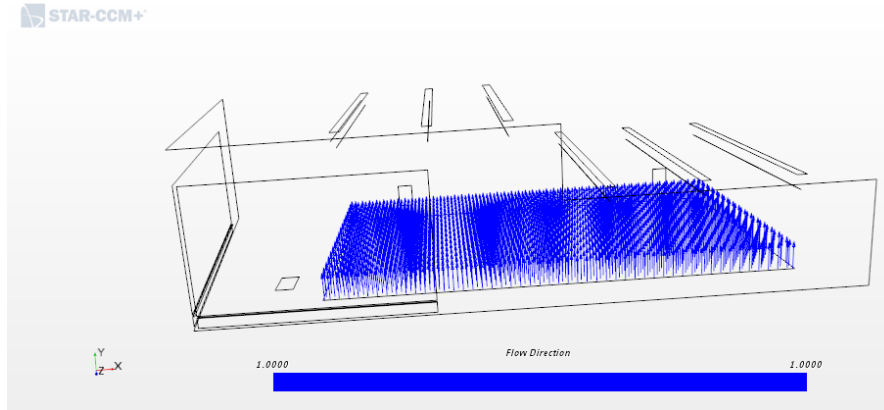


Figure 32: Evaporation

When it comes to define the boundary condition for the inlet air flow, it is defined as a **mass flow inlet**, but with diverse turbulence model conditions. The variety of supplied air flow from different ventilation cases and different inlet flows require basically defining the turbulent model at each inlet.

Table 9: Boundary condition

| Boundary | Boundary condition |
|---------------------------------|--|
| External window | Surface temperature of 22.9°C |
| External walls | Surface temperature of 26.9°C |
| Other walls | Adiabatic wall with no slip condition |
| Exhaust | Gradient pressure outlet |
| Water bath | Mass flow inlet, $T = 28^{\circ}\text{C}$, 99.9% H_2O and $1.0e^{-6}\% \text{Cl}_2$ |
| Inlet air flow | Mass flow inlet with with thermal temperature of 30°C |
| Turbulent specification | $k - \omega$ |
| Initial temperature of the hall | 28°C |

3.5.1 Mixing ventilation (MV) case:

The air flow in this case is supplied with a total air flow of $17500 \frac{\text{m}^3}{\text{h}}$ from six inlets of textile ducts mounted on the ceiling. These textile ducts are divided into three systems to maintain a good airflow supply. Furthermore, the textile duct features like holes and nozzles are designed as described in appendix [F].

The reason for using textile ducts in the swimming pool is its high initial energy in the form of velocity (momentum) through holes which ensures an effective air

change without dead zones. In addition, the textile duct usage in swimming pool have advantages such as, no condensation and no corrosion problems and also its flexibly and tailored design.



Figure 33: Textile duct illustrative picture

The first system consists of flow through three inlet ducts which are located at the lower height of the hall equal to 5 m (see figure 34). This system delivers an airflow of $8751 \frac{m^3}{h}$ with a temperature of $30^{\circ}C$ and it has generally a low turbulent intensity equal to 4%.

In order to define the boundary condition for the turbulent model $k - \omega$ at the inlets. Field functions for k and ω at each inlet location are assigned as shown in figures 35 and 36.

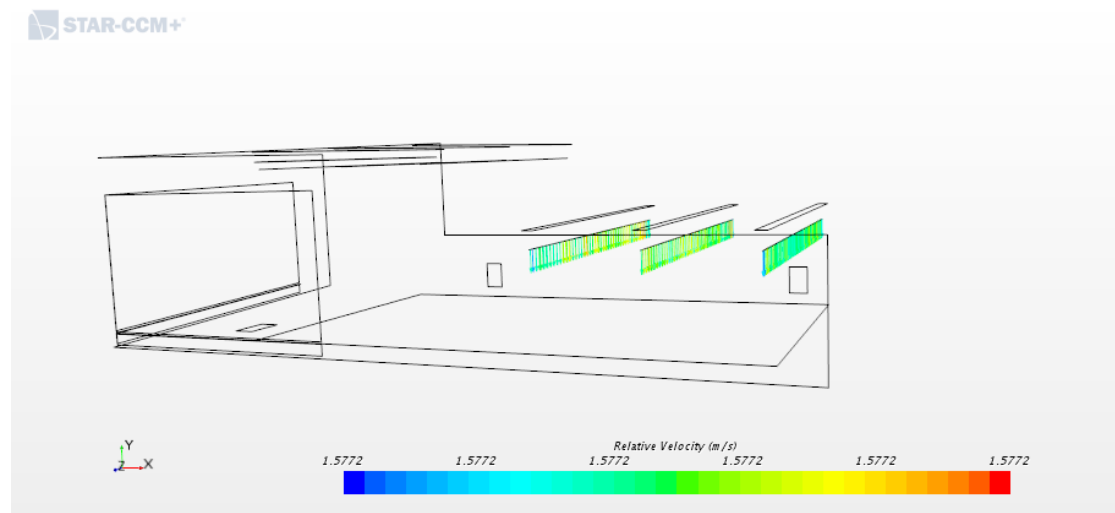


Figure 34: MV system 1.

```
TKE system 1 - Definition
1.5*${I system 1}*${I system 1}*${U inlet system1}*${U inlet system1}
```

Figure 35: The turbulent kinetic energy $k = \frac{3}{2}(Iv)^2$, turbulent intensity I and inlet air velocity U at MV system 1

```
omega1 - Definition
sqrt(${TKE system 1})/0.0023
```

Figure 36: The specific turbulent dissipation $\omega = \left[\frac{\sqrt{k}}{L\beta^{\frac{3}{4}}}\right]$ at MV system 1

The second system of the MV has two inlets and supplies a total air flow of $5824 \frac{m^3}{h}$ from a 8.5 m height (see figure 37). Its turbulence intensity is set to 5%. There is assigned a user defined turbulent kinetic energy k and specific turbulent dissipation ω at the two inlets figure

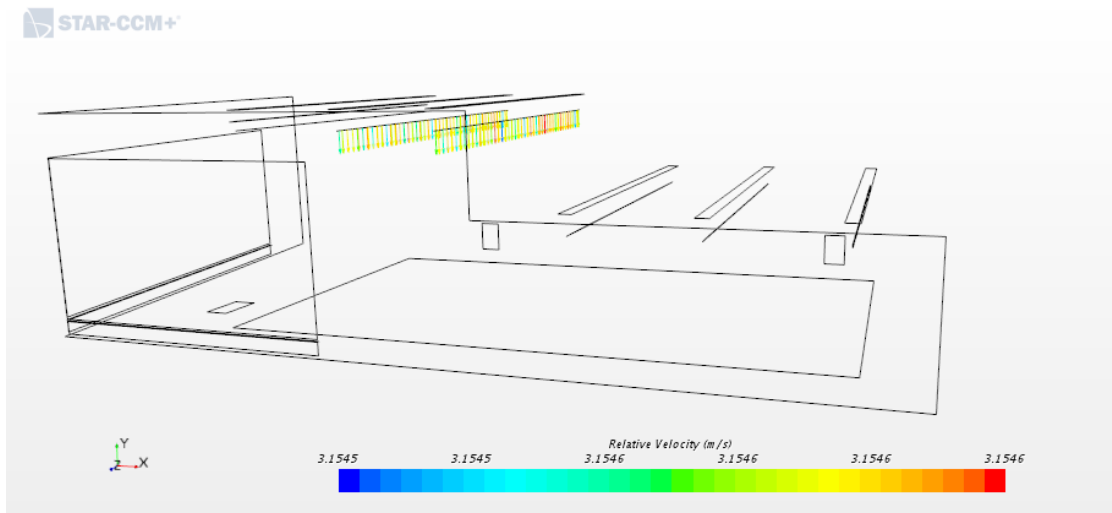


Figure 37: MV system 2.

```
TKE system 2 - Definition
1.5*${I system 2}*${I system 2}*${U inlet system 2}*${U inlet system 2}
```

Figure 38: The turbulent kinetic energy $k = \frac{3}{2}(Iv)^2$, turbulent intensity I and inlet air velocity U at MV system 2

```
omega2 - Definition
sqrt(${TKE system 2})/0.0011
```

Figure 39: The specific turbulent dissipation $\omega = [\frac{\sqrt{k}}{L\beta^{\frac{1}{4}}}]$ at MV system 2

The third system supplies air flow of $2917 \frac{m^3}{h}$ and has a turbulent intensity of 5%. This system has also an inlet air flow direction normal toward the west facade (see figure 40). Inlet k and ω are assigned as described before.

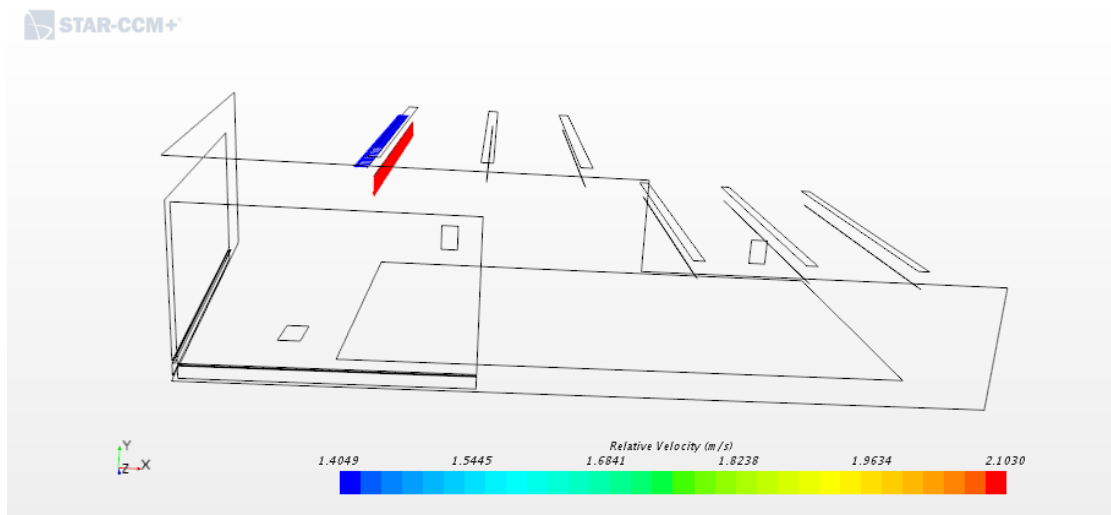


Figure 40: MV system 3

```
TKE system 3 - Definition
1.5*${I system 3}*${I system 3}*${U inlet system 3}*${U inlet system 3}
```

Figure 41: The turbulent kinetic energy $k = \frac{3}{2}(Iv)^2$, turbulent intensity I and inlet air velocity U at MV system 3

```
omega3 - Definition
sqrt(${TKE system3})/0.0011
```

Figure 42: The specific turbulent dissipation $\omega = \left[\frac{\sqrt{k}}{L\beta^{\frac{1}{4}}}\right]$ at MV system 3-90 degree

```
TKE system 3-90degree - Definition
1.5*${I system 3}*${I system 3}*${uinlet3 90 degree}*${uinlet3 90 degree}
```

Figure 43: The turbulent kinetic energy $k = \frac{3}{2}(Iv)^2$, turbulent intensity I and inlet air velocity U at MV system 3-90 degree

```
omega3-90 - Definition
sqrt(${TKE system 3-90 degree})/0.0011
```

Figure 44: The specific turbulent dissipation $\omega = \left[\frac{\sqrt{k}}{L\beta^{\frac{1}{4}}}\right]$ at MV system 3-90 degree

3.5.2 Mixing ventilation-displacement ventilation (MV-DV) case

This system includes both the previous MV system and a DV system that supply an additional air flow of $1000 \frac{m^3}{h}$ to compensate for heat lost in cold period with a turbulent intensity equal to 1. The system supplies a total airflow of $27500 \frac{m^3}{h}$. The air supply for this case from different air inlets are shown in figure 45.

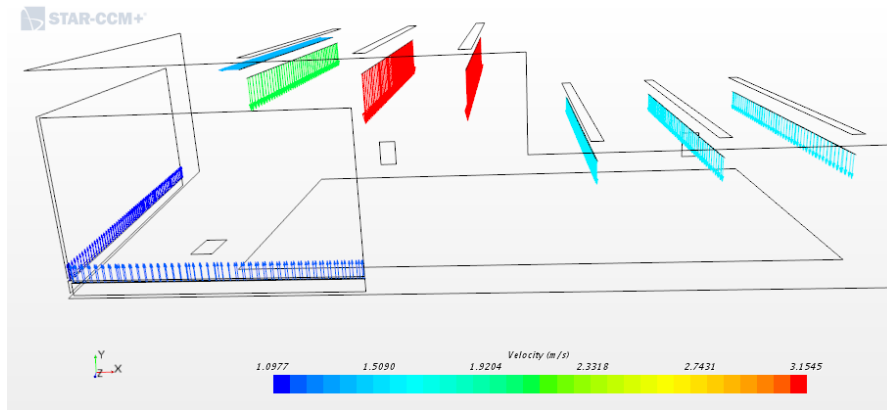


Figure 45: MV-DV system

```
TKE window - Definition
1.5*${I window}*${I window}*${Uinlet window}*${Uinlet window}
```

Figure 46: The turbulent kinetic energy $k = \frac{3}{2}(Iv)^2$, turbulent intensity I and inlet air velocity U at DV under windows

```
omega window - Definition
sqrt(${TKE window})/0.0111
```

Figure 47: The specific turbulent dissipation $\omega = \left[\frac{\sqrt{k}}{L\beta^{\frac{1}{4}}} \right]$ at DV under windows

3.5.3 Displacement ventilation (DV4, 5 and 7 ACH)

These are displacement ventilation that supply airflow of 20568, 25710 and 35994 $\frac{m^3}{h}$ respectively from inlet flow under the windows. k and ω are assigned for each inlets in this different cases, based on their different air flow and inlet air velocity.

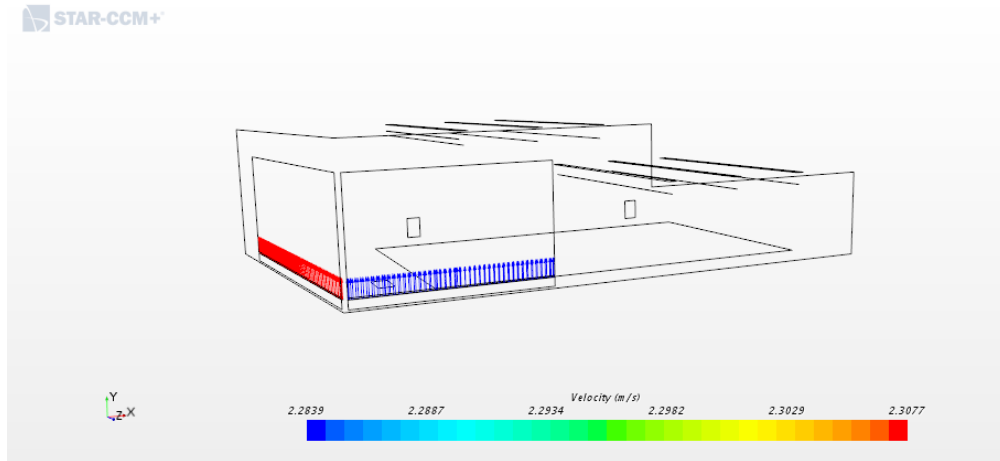


Figure 48: DV 7 ACH inlet flow

4 Results and discussion

Table 10 summarises the main features of the different cases studied in this work. This confirms that the MV system has 12% less chlorine concentration in the swimming breathing zone compared with DV7 ACH system. Furthermore the MV system has high air exchange efficiency ACE which can lead to increased energy efficiency with 50% compared to the DV7 ACH system. The data used to compare the chlorine concentration in the swimming breathing zone for the investigated ventilation cases is based on the surface average of molar concentration of chlorine in the swimming breathing zone (see appendix H). The presented data in the table about ACE is based on contour plots and xy-plots which is presented later in this section.

Table 10: Different test cases

| Investigated cases | ACE level on the swimming breathing zone | ACE level on people around | The surface average of molar concentration of chlorine in the swimming breathing zone $\frac{k.mol}{m^3}$ | The chlorine concentration reduction in procent (-) | Ventilation energy saving |
|--|--|----------------------------|---|---|---------------------------|
| MV (3.5 ACH) | 0.62-0.84 | 0.60-0.76 | 5.34×10^{-9} | - 12.0% | 50% |
| MV-DV (MV 3.5 ACH) + (DV 2 ACH) = (5.5 ACH) | 0.44-0.59 | 0.40-0.51 | 3.89×10^{-9} | - 36.0% | 21.0% |
| DV4 ACH | 0.64-0.85 | 0.54-0.77 | 6.05×10^{-9} | +1.0% | 42.0% |
| DV5 ACH | 0.49-0.65 | 0.42-0.60 | 6.08×10^{-9} | +0.5% | 28.5% |
| DV7 ACH | 0.35-0.46 | 0.30-0.42 | 6.09×10^{-9} | - | - |

The table shows also that the MV-DV system has the lowest chlorine concentration in the swimming breathing zone with 36% less in chlorine concentration compared with the DV7 ACH system. This system has intermediate air exchange efficiency ACE which can lead to increased energy efficiency with 21% compared with the DV7 ACH system. The ventilation energy saving is estimated by comparing the number of air change per hour ACH for the particular cases to the ACH of DV7 system.

On the other hand, it is noticed that insignificant increase in chlorine concentration when the inlet air flow in DV system decreases as shown in table 10. The DV5 ACH system and the DV4 ACH system have an increased chlorine concentration in the swimming breathing zone with 0.5% and 1% respectively.

The swimming breathing zone is defined to be 10 cm above the water surface, and the zone for people around is defined to be 1.6 m above floor. Relevant solution data is extracted of these defined plans. This is useful to provide the xy-plots with further data about the swimming breathing zone condition. The zones are shown in figure 49.

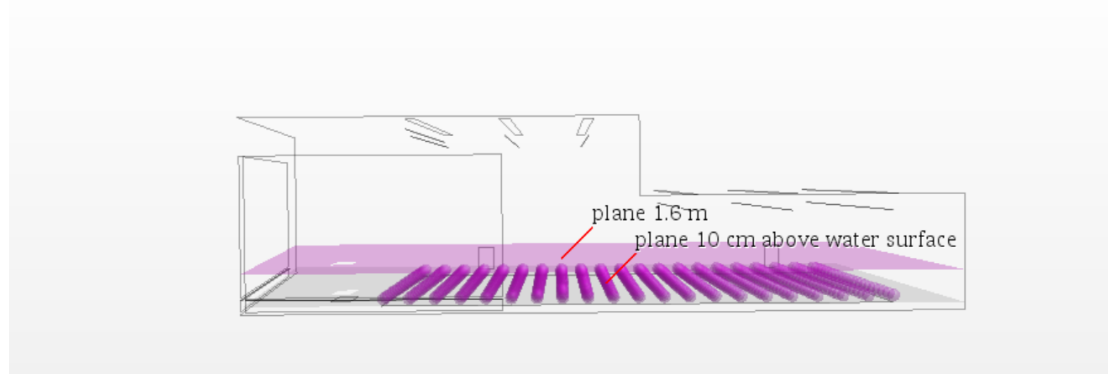


Figure 49: The swimming breathing zone and the zone for people around the swimming pool

This section presents further detailed results for the five investigated ventilation cases in Åfjord swimming pool. The results will be presented in two parts for each investigated case. The first part is for the swimming breathing zone and the second part is for the people around the swimming pool.

In this study contour plots for the LMA, ACE, the molar concentration of chlorine above the the water bath, the air temperature, the air velocity and the relative humidity are used for analysis. Relevant XY plots for LMA and molar chlorine concentration, ACE and molar chlorine concentration, LMA and ACE, ACE and air velocity and ACE and air temperature are discussed.

The residual for all five simulated cases in this study are presented in appendix F. Figure 50 shows a representative residual plot for the MV case.

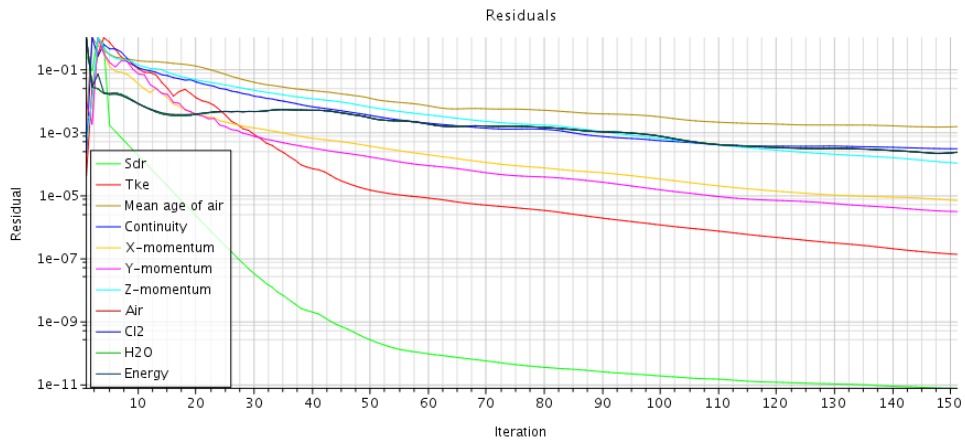


Figure 50: The MV case residual

4.1 Mixing ventilation (MV) case

4.1.1 Swimming breathing zone

Figure 51 shows the contour plot of LMA in representative XZ-plane in the breathing zone. The LMA value varies from 0.77 to 1.03. The lowest values are in the water bath area while the highest value around the east and west external walls and windows. Generally, The contour plot shows good LMA values for the swimming breathing zone.

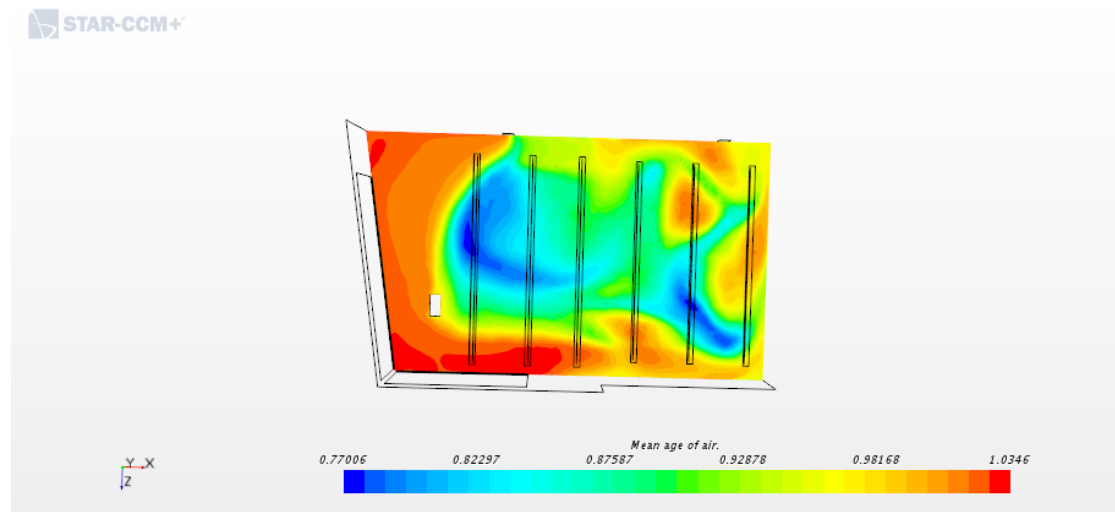


Figure 51: MV case: LMA on swimming breathing zone. The west external wall is along the $-Z$ direction and the south external walls is along the $+X$ direction

It can be seen from figure 52 that ACE value varies from 0.61 around the external walls and windows to 0.83 in the water bath area. The ACE values confirms a good ventilation mode nearly "piston ventilation" especially in the bath area. The high ACE values for this case would lead to a low energy usage due to the decrease in airflow supply.

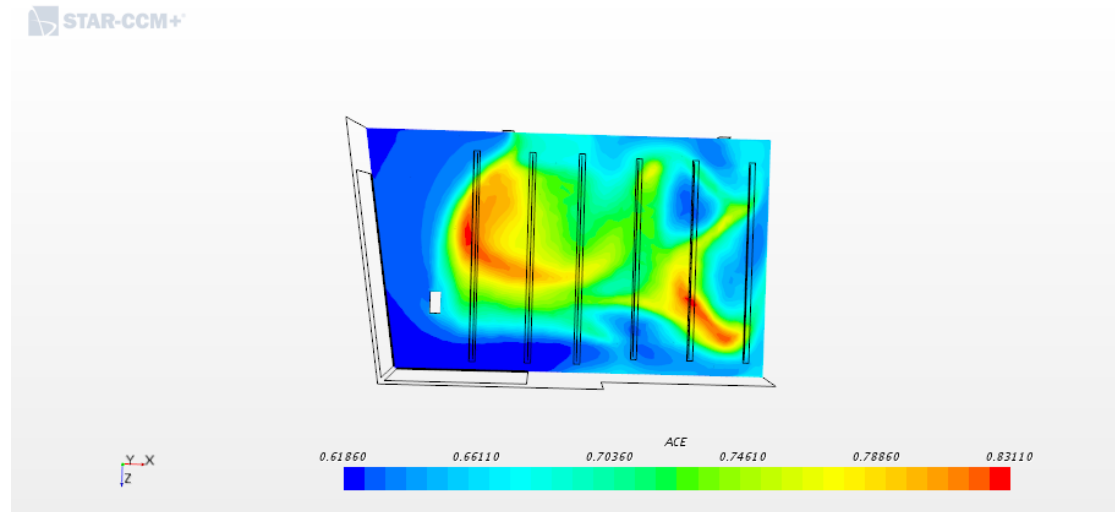


Figure 52: MV case: ACE on swimming breathing zone

Investigation of the chlorine concentration in swimming pool is of a big interest due to the effect and irritations caused by chlorine to the swimmers/human beings.

The molar concentration of chlorine is higher in the bath area with $9.34e^{-9}[\frac{kmol}{m^3}]$ and smaller around the external walls with a value of $3.20e^{-9}[\frac{kmol}{m^3}]$ (see figure 53). This is expected as the source of the chlorine evaporates from the water bath. The MV system shows good performance to reduce the chlorine concentration in the bath area.

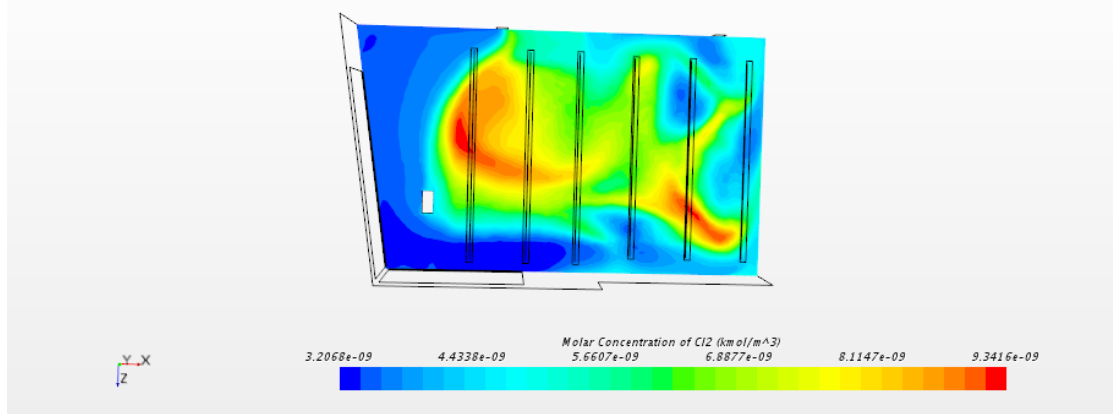


Figure 53: MV case: Molar concentration of chlorine on swimming breathing zone

The XY plot offers us more information than the contour plot can offer. The relationship between the LMA and molar concentration of chlorine as shown in figures 54 reveals that the chlorine concentration is smaller in area where the LMA are high around 1.

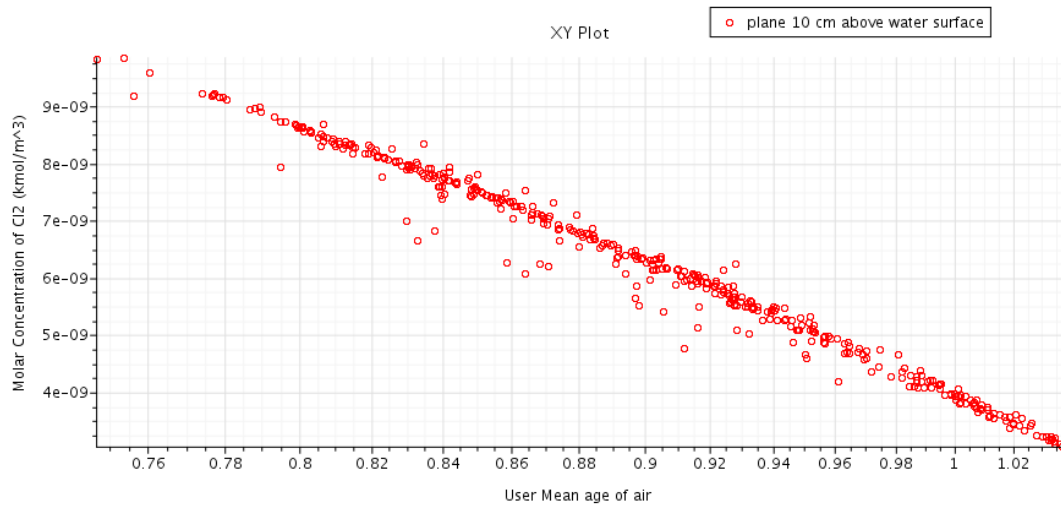


Figure 54: MV case: Relation of LMA and chlorine concentration on swimming breathing zone

Figure 55 also reveals high chlorine concentration in area where the ACE value is high around 0.85. However, the difference between the high and small chlorine concentration in the swimming pool area is small as shown in the graph.

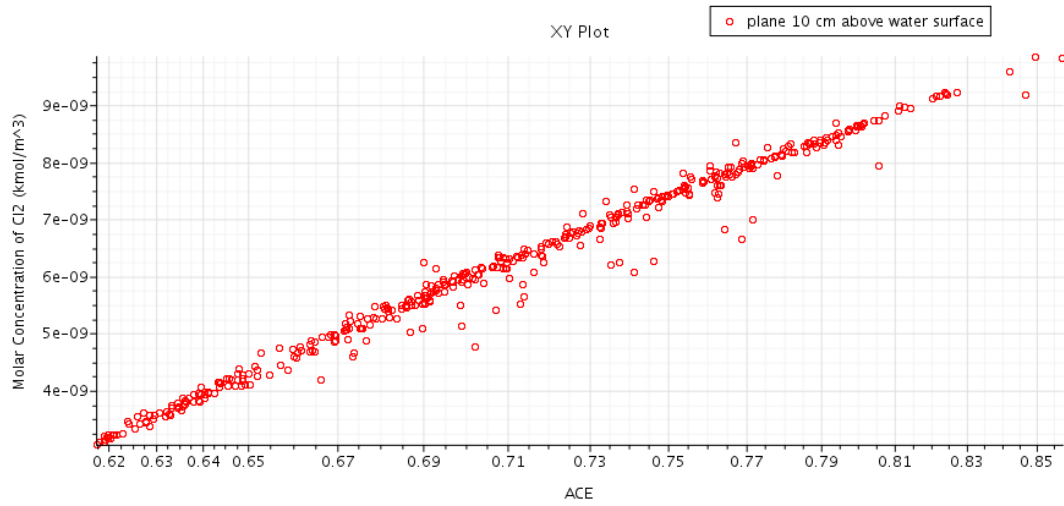


Figure 55: MV case: Relation of ACE and chlorine concentration on swimming breathing zone

The relationship between the ACE and LMA is shown in figure 56. Clearly higher ACE matches with lower LMA values.

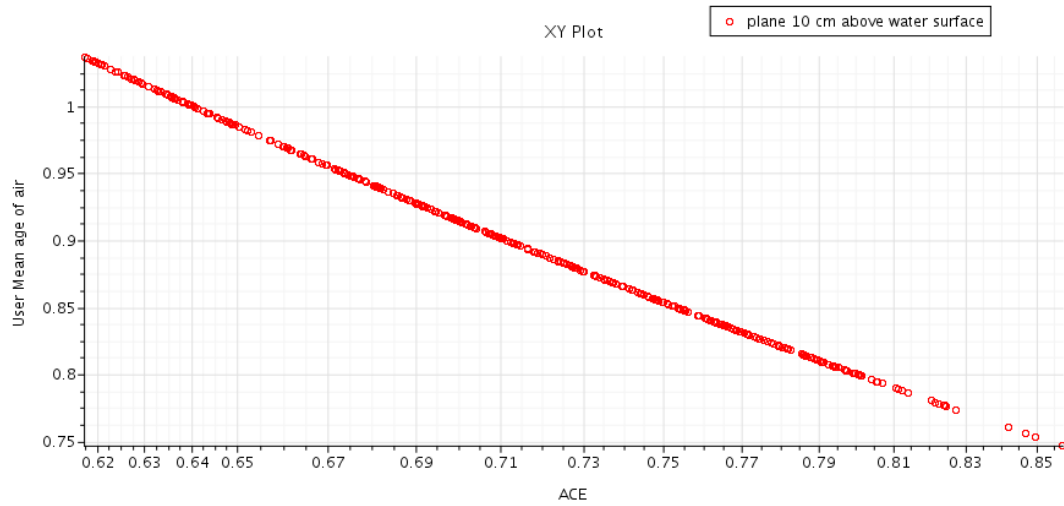


Figure 56: MV case: Relation between ACE and LMA on swimming breathing zone

4.1.2 People around

The result confirms good LMA values for the people around the water bath as shown in figure 57.

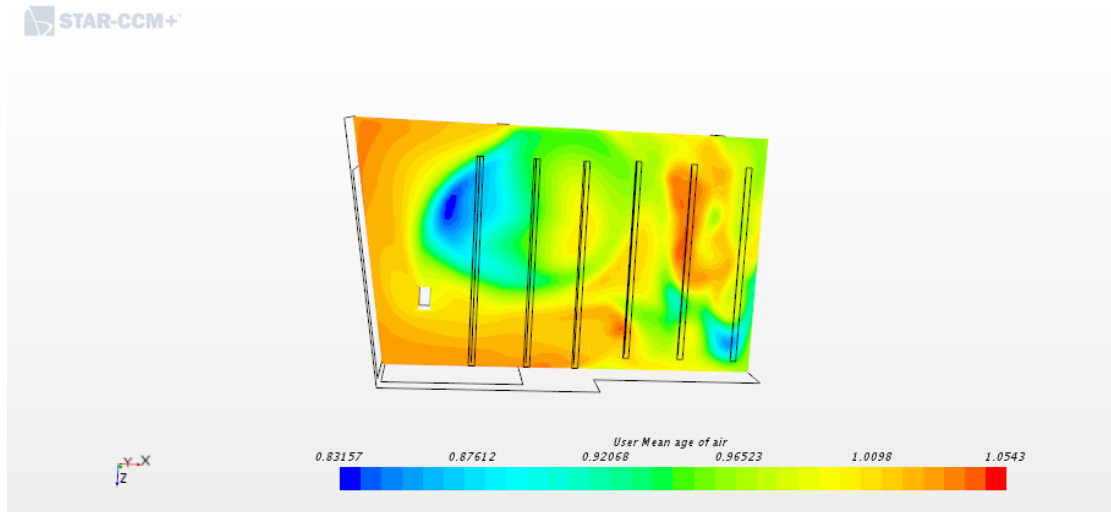


Figure 57: LMA on people around

This result also confirms good ACE for the people around the swimming pool, It shows a little more efficient ventilation than the mode of "mixing ventilation" as shown in figure. 58.

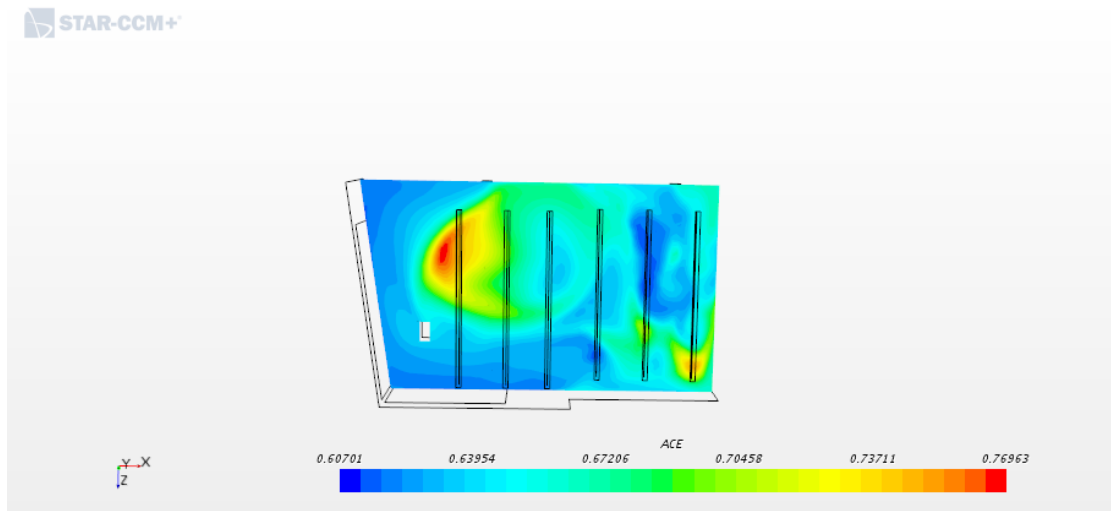


Figure 58: MV case: ACE on people around

The air temperature varies from 22.9 °C on the external windows to around 29.3 °C deeper inside the hall (see figure 59).

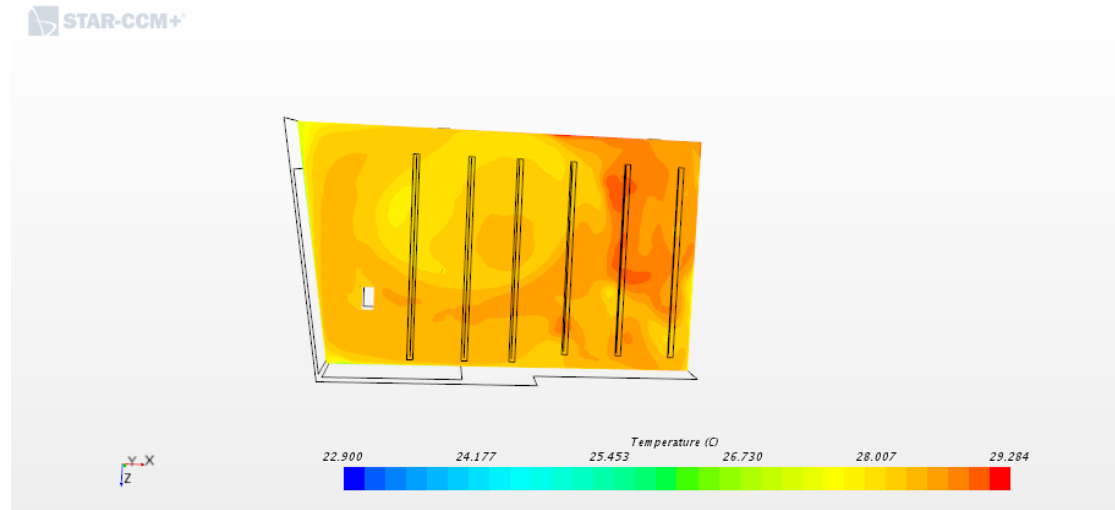


Figure 59: Air temperature on people around

The result in figure 60 shows high air velocity $\approx 0.4 \frac{m}{s}$ around external windows, moving towards the zone for the people around and continuing inside the water bath region. This is called draught risk. Often in winter time, cold, natural convective flows from glazed facade causes draught risk [31]. Air velocity higher than $0.2[\frac{m}{s}]$ can be considered as a thermal discomfort [32].

All simulated cases in this study were simulated when the outside temperature is assumed to be in a very cold winter day equal to -21.4°C . Normally in cold period, there will be additional airflow to compensate for the heating in swimming pool. The MV-DV hybrid system case represents the case of the MV system with additional airflow under windows which avoids this draught risk.

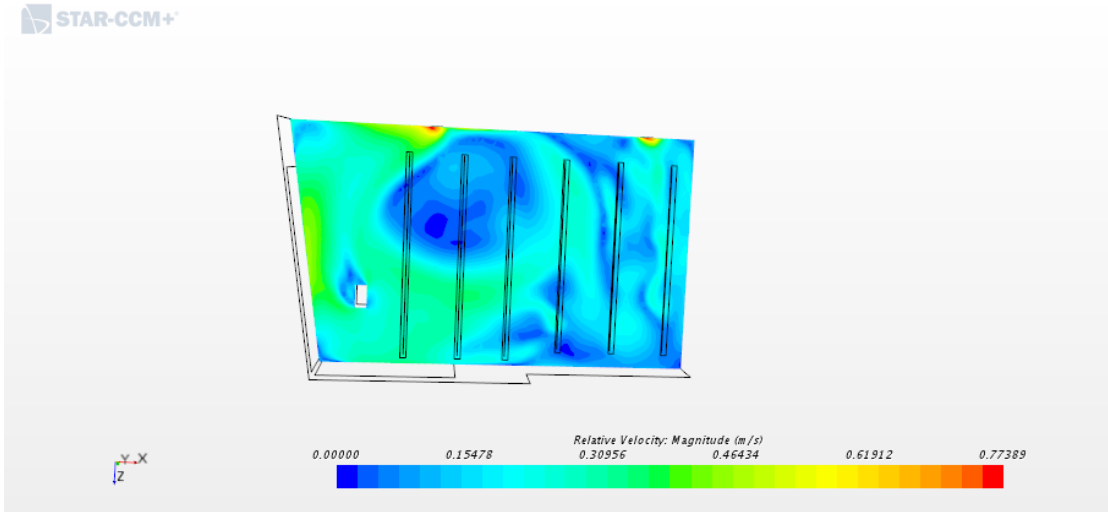


Figure 60: MV case: Air velocity on people around

The result confirms that the MV system maintains good air humidity level lying between RH= 54% and 63% (see figure 61).

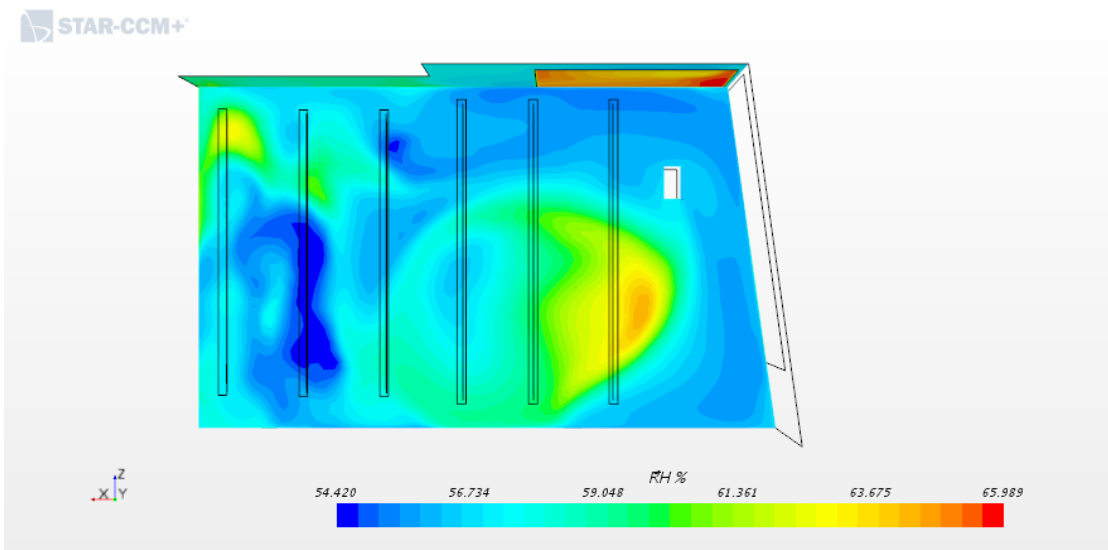


Figure 61: MV case: Relative air humidity on people around

Figure 62 shows that condensation problem on the external windows and facade could be avoided in passive house swimming pool. However, the result shows relative air humidity equal to 66% for this investigated case.

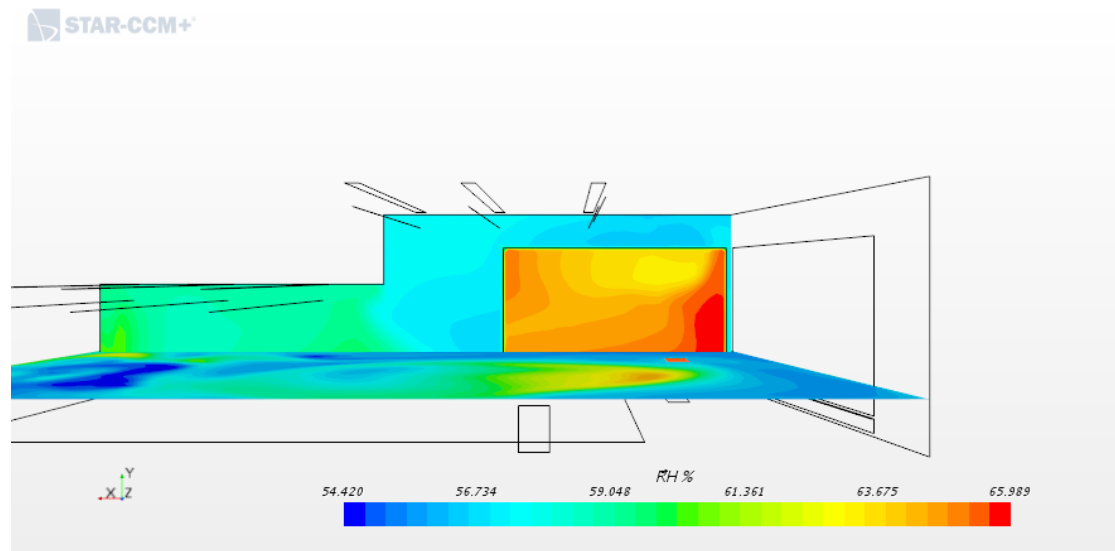


Figure 62: MV case: Air velocity on people around

The relationship between LMA and ACE as a result of the conducted test for the people around the swimming pool in this case is described in figure 63.

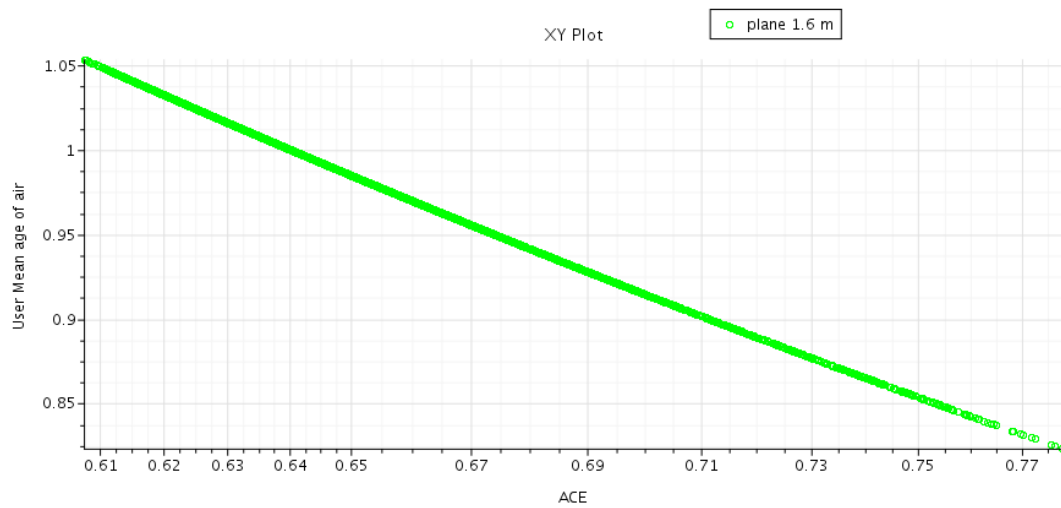


Figure 63: MV case: Relation of ACE and LMA on people around

It can be stated from the figure 64 that air exchange efficiency ACE increases with decreasing in the air velocity marginally. High air velocity caused by draught risk decreases both the thermal comfort and the ventilation air exchange efficiency ACE.

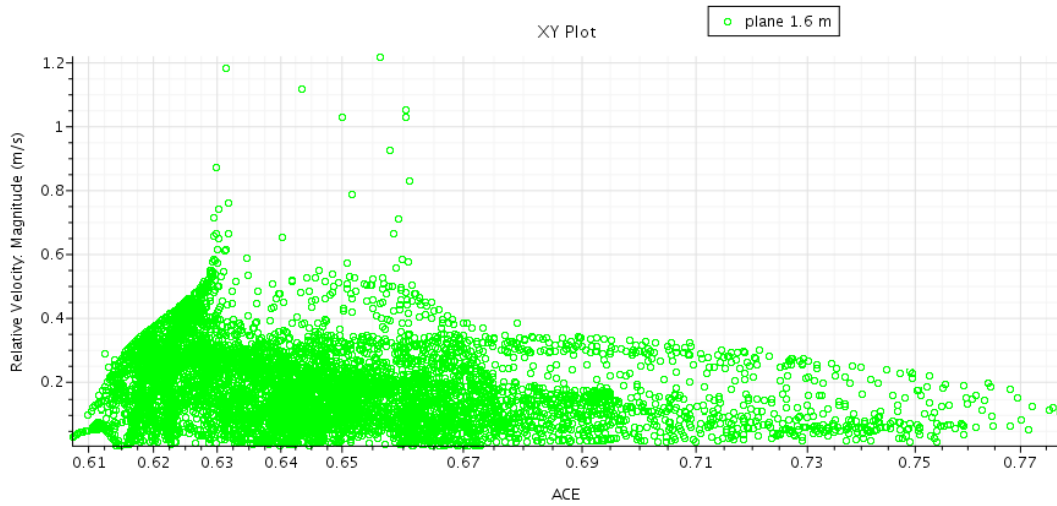


Figure 64: MV case: Relation of ACE and air velocity on people around

4.2 Mixing ventilation-displacement ventilation (MV-DV) case

4.2.1 Swimming breathing zone

LMA values varies from 0.80 to 1.08 as shown in figure 65. Areas with lower LMA are more presented here than the case for the MV system. Especially around the external walls and windows. The reason behind this is a higher inlet airflow in this case.

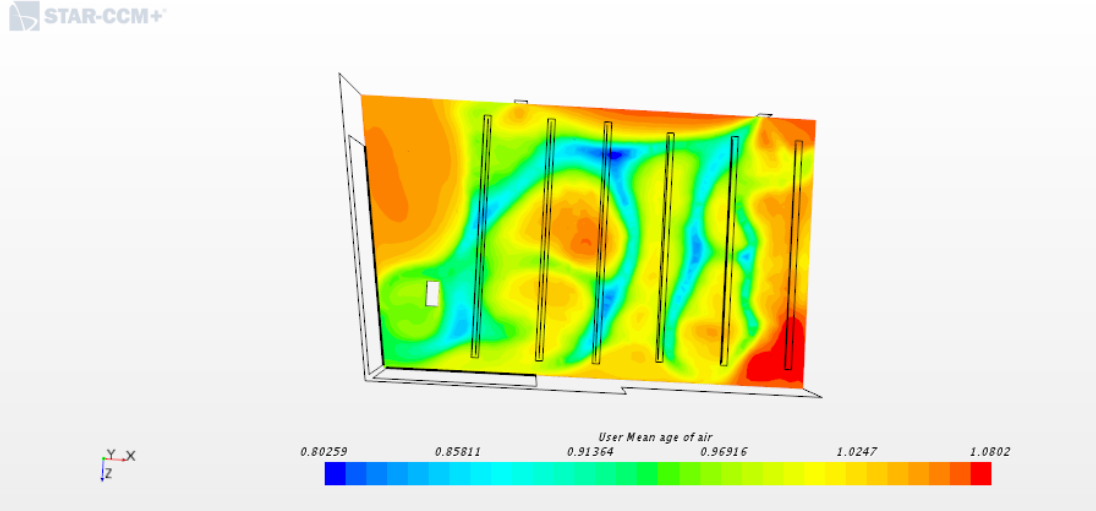


Figure 65: MV DV hybrid case: LMA on swimming breathing zone

The ACE values in this case confirms that the ventilation mode is nearly "full mixing ventilation" in the swimming breathing zone as shown in figure 66. The ACE value for this case shows that the energy usage is higher than the MV case.

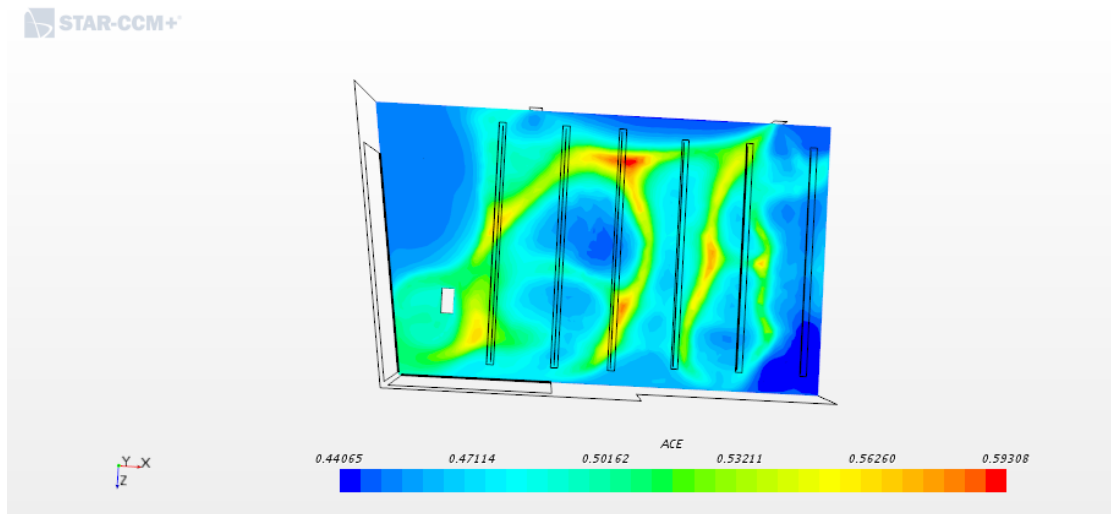


Figure 66: MV DV case: ACE on swimming breathing zone

The molar concentration of chlorine varies from the lowest value $2.0e^{-9} [\frac{kmol}{m^3}]$ to the highest chlorine concentration $8.55e^{-9} [\frac{kmol}{m^3}]$ in the water bath region (see figure

67). It is noticeable that the case for the MV DV system shows significant decrease in the chlorine concentration in the swimming zone than the MV system.

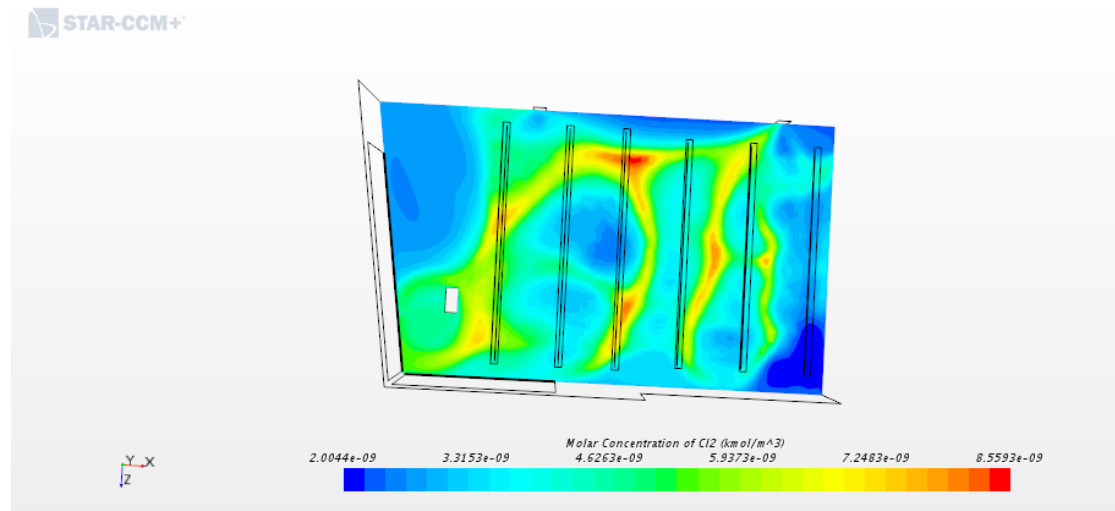


Figure 67: MV DV case: Molar concentration of chlorine on swimming breathing zone

Chlorine concentration is lower in region where the LMA is high (around 1) and higher in region where the LMA is low. The concentration points here have a better alignment with the graph than the case for the MV system. This reflects a stable and more chlorine concentration removing.

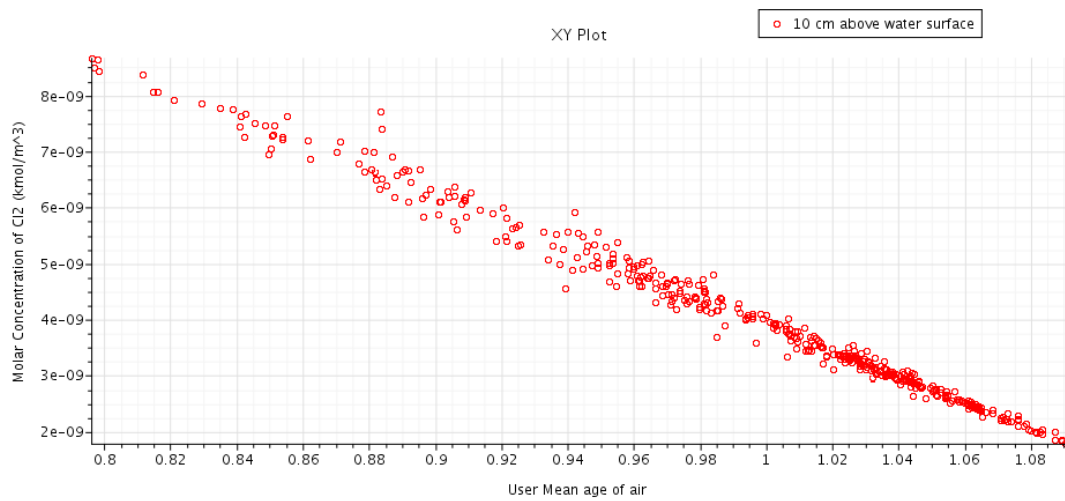


Figure 68: MV DV case: Relation of LMA and chlorine concentration on swimming breathing zone

The MV-DV system shows a lower chlorine concentration in region where the ACE is low. Figure 69 reveals that the higher ACE the higher the chlorine concentration.

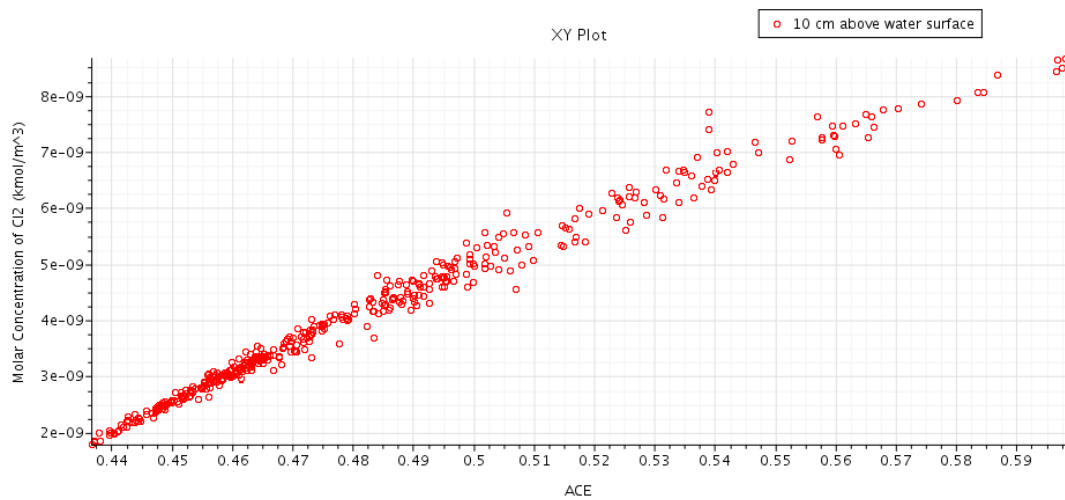


Figure 69: MV DV case: Relation of ACE and chlorine concentration on swimming breathing zone

Figure 70 describes the relationship between the LMA and ACE in the swimming breathing zone for the MV DV hybrid system case.

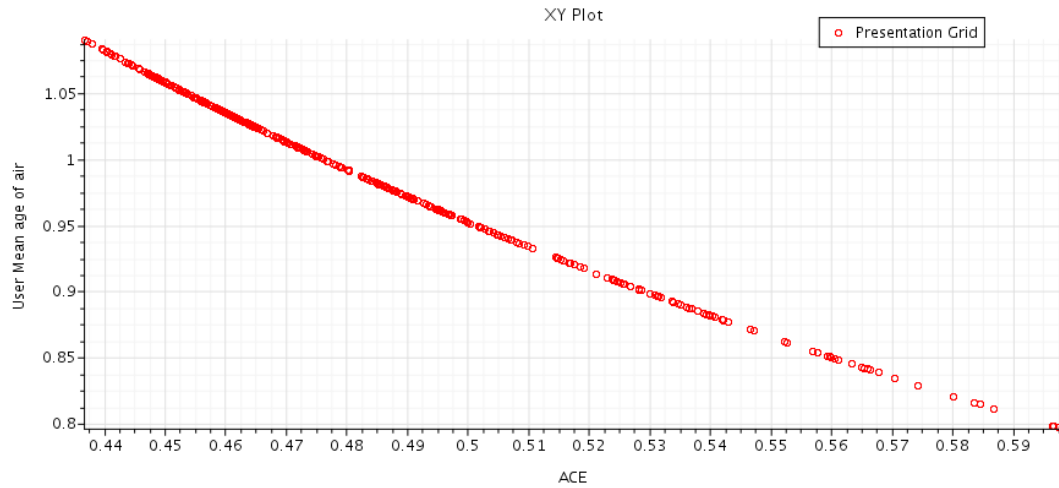


Figure 70: MV DV case: Relation of ACE and LMA on swimming breathing zone

4.2.2 People around

The result confirms good LMA value for the people around the swimming pool as shown in figure 71.

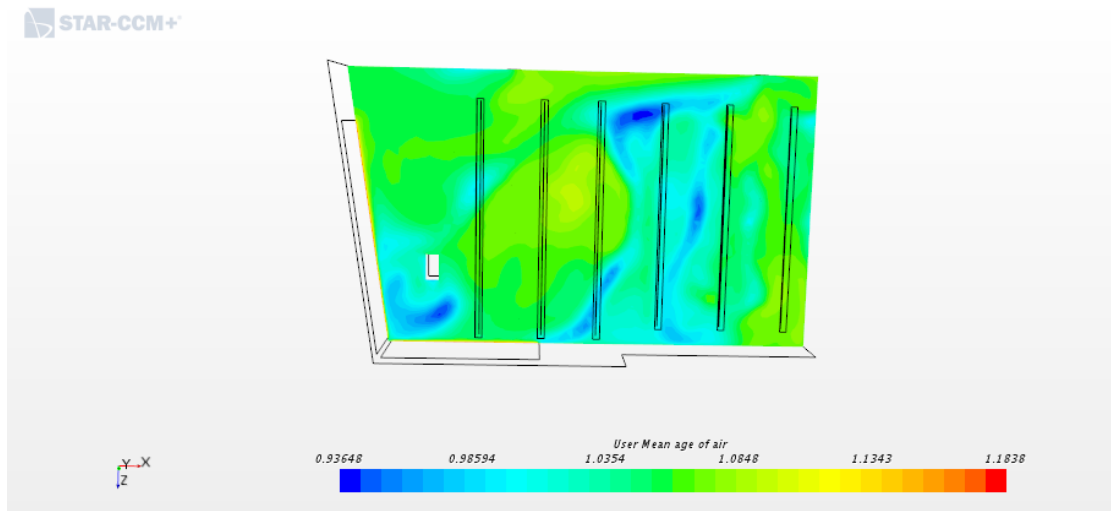


Figure 71: MV DV case: LMA on the people around

The result shows ACE values (around 0.45) which it is similar to "fully mixing ventilation" mode for the people around the swimming pool as shown in figure 72. Generally the result for the MV DV system confirms the mode of fully mixing ventilation for the swimmers and for the people around around the swimming pool.

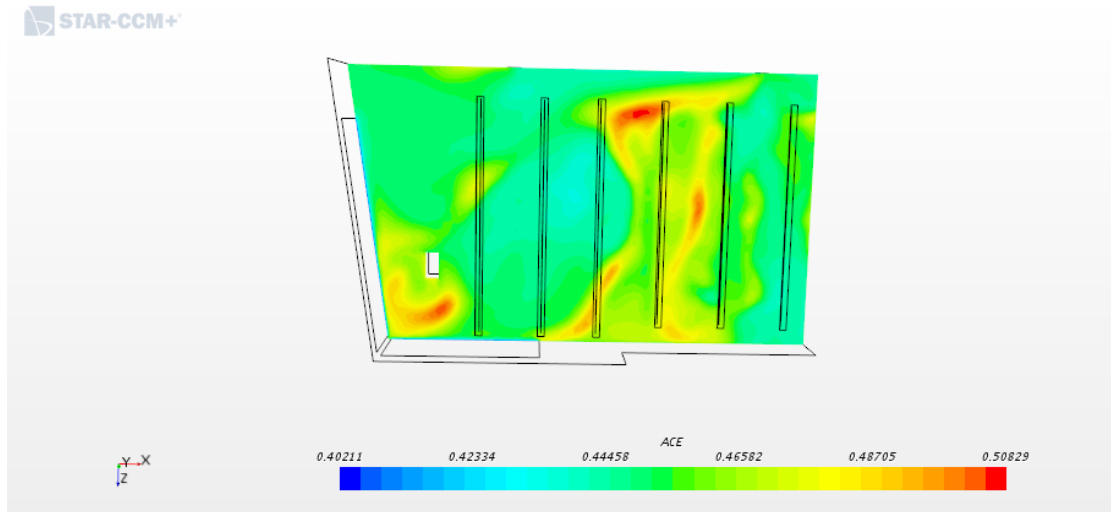


Figure 72: ACE on the people around

The MV DV hybrid system shows more stable air temperature than the MV system due to its higher air flow (see figure figure 73).

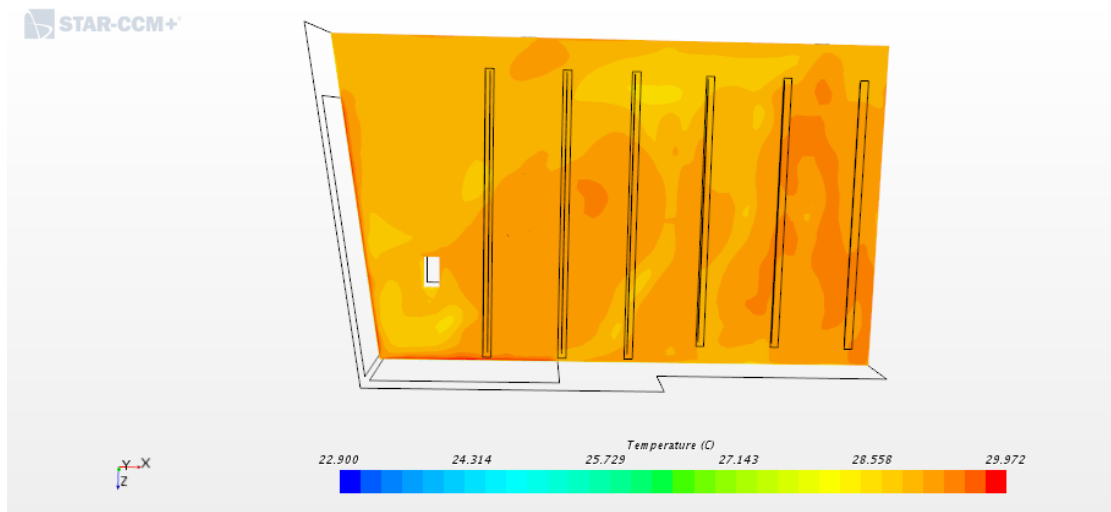


Figure 73: MV DV cas: Air temperature on the people around

Figure 74 below confirms that the detected draught risk in the case of MV system is avoided. The air velocity is around $2\frac{m}{s}$ which contribute for a good thermal comfort.

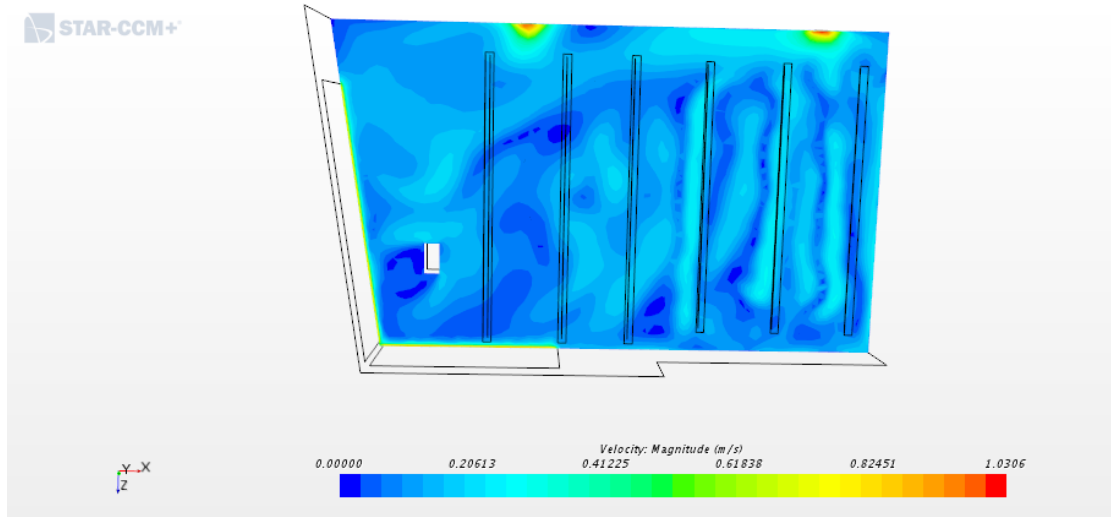


Figure 74: MV DV case: Air velocity on the people around

It can be seen from figure 76 that the external windows have a low relative humidity as a result from having the inlet air flow under the external windows.

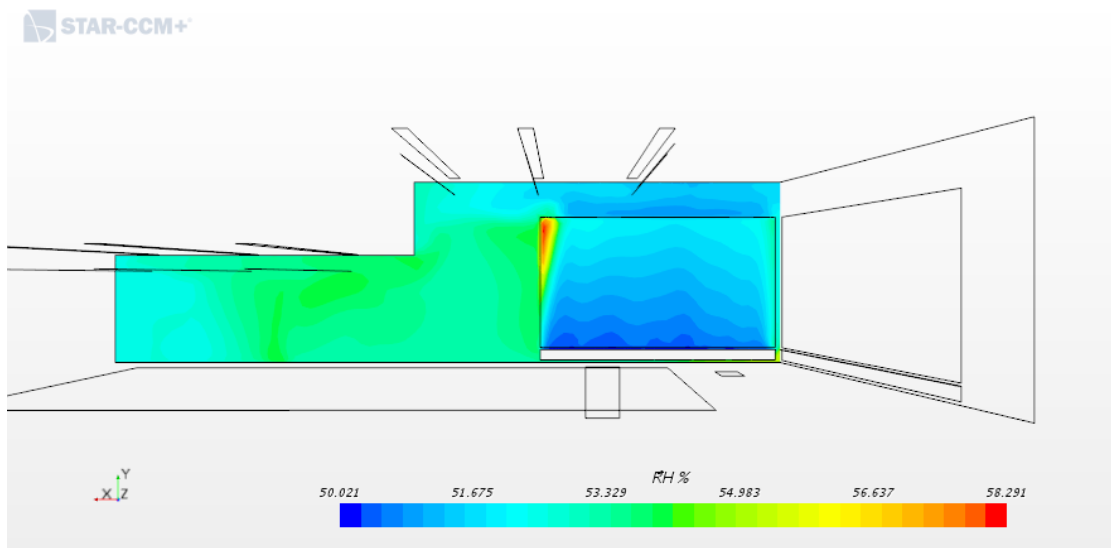


Figure 75: MV DV case: Air humidity on the external window

The relative humidity is considered good and lying between 50% and 58% for the people around the swimming pool as shown in figure76. It is noticed that The MV DV system has a lower relative humidity than the MV system.

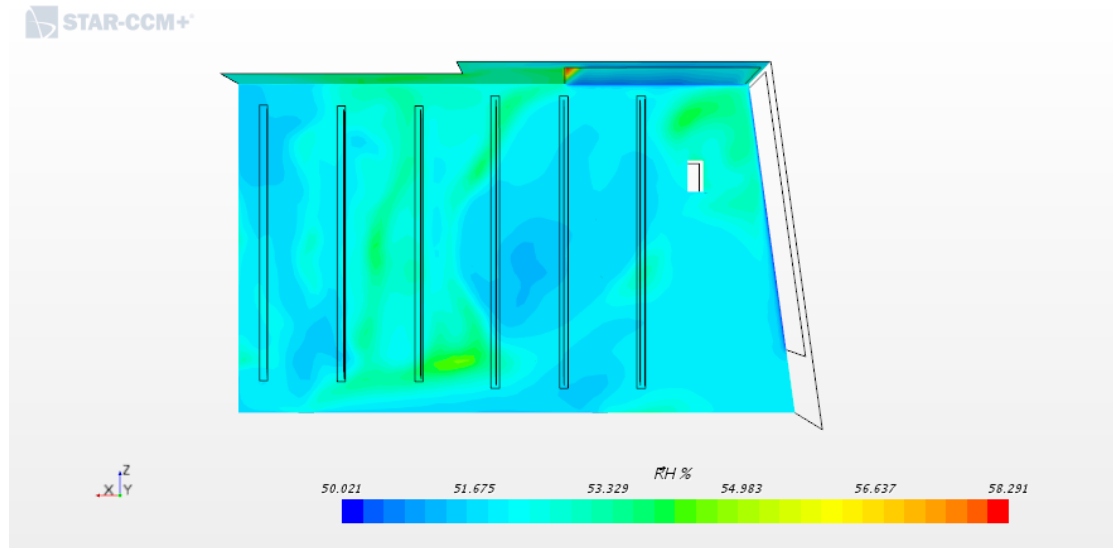


Figure 76: MV DV case: Relative humidity on the people around

The relationship between LMA and ACE as a result of the conducted test for the people around in this case is described in figure 77.

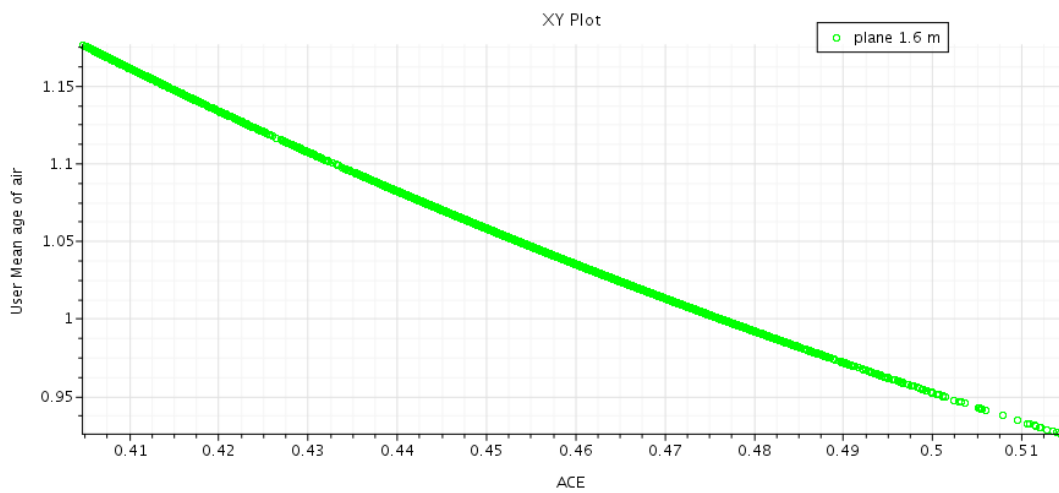


Figure 77: MV DV case: Relation between ACE and LMA on the people around

4.3 Displacement ventilation (DV4 ACH) case

4.3.1 Swimming breathing zone

The contour plots in the result section shows that the DV4, 5 and 7 ACH systems have the same air flow pattern. They all have the position of the inlet airflow under the external windows.

The LMA values varies from 0.76 to 1.0. The low LMA values are widely presented in the swimming breathing zone and outside the swimming breathing zone (see figure 78).

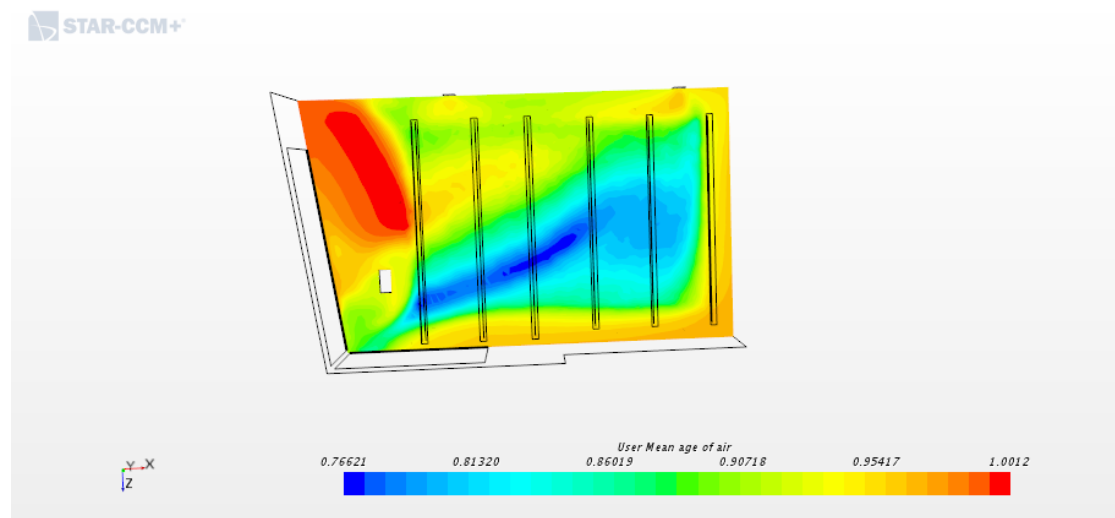


Figure 78: MV DV case: LMA on swimming breathing zone

The ACE values varies from 0.63 to 0.83 as shown in figure 79. The high ACE values are widely presented in swimming breathing zone. The high ACE values for this case indicate a nearly "fully piston ventilation".

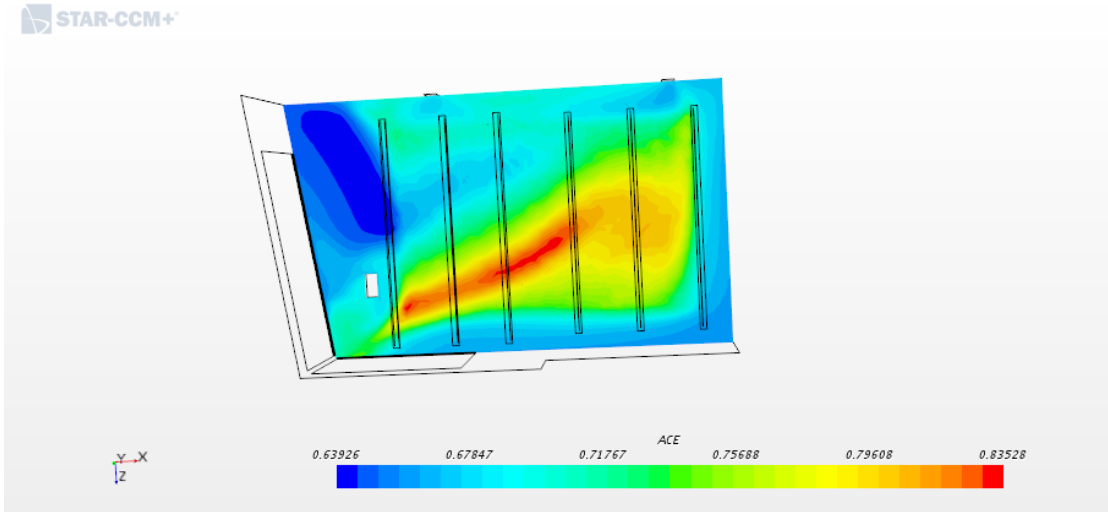


Figure 79: DV4 ACH case: ACE on the swimming breathing zone

The DV 4 ACH system case shows less performance in in order to remove the chlorine concentration in the swimming breathing zone compared with the MV case as shown in figure 80.

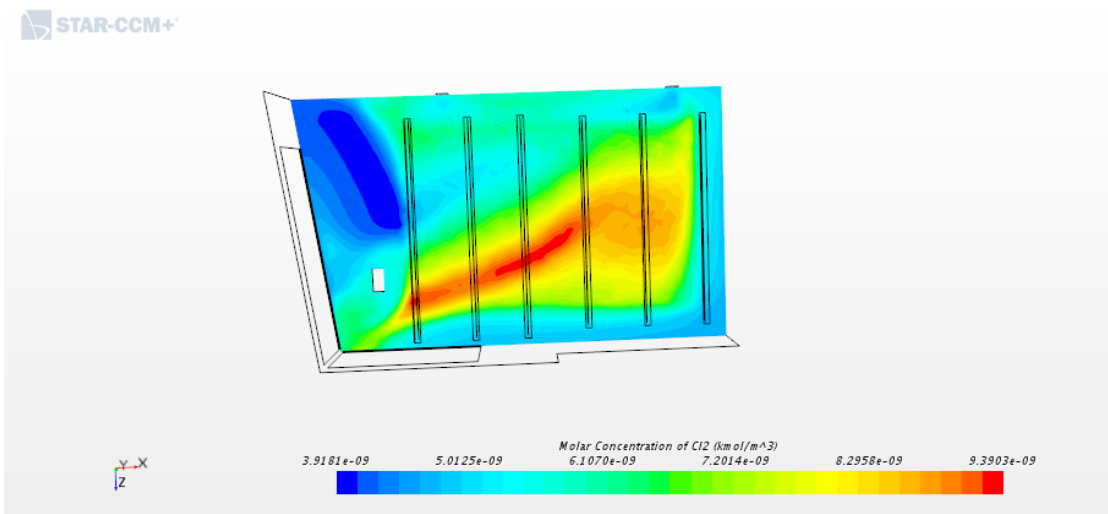


Figure 80: DV4 ACH: Molar concentration of chlorine on the swimming breathing zone

Figure 81 shows the relationship between LMA and chlorine concentration as a result of the conducted test for this case. The chlorine concentration is low when

the age of air LMA is high (around 1).

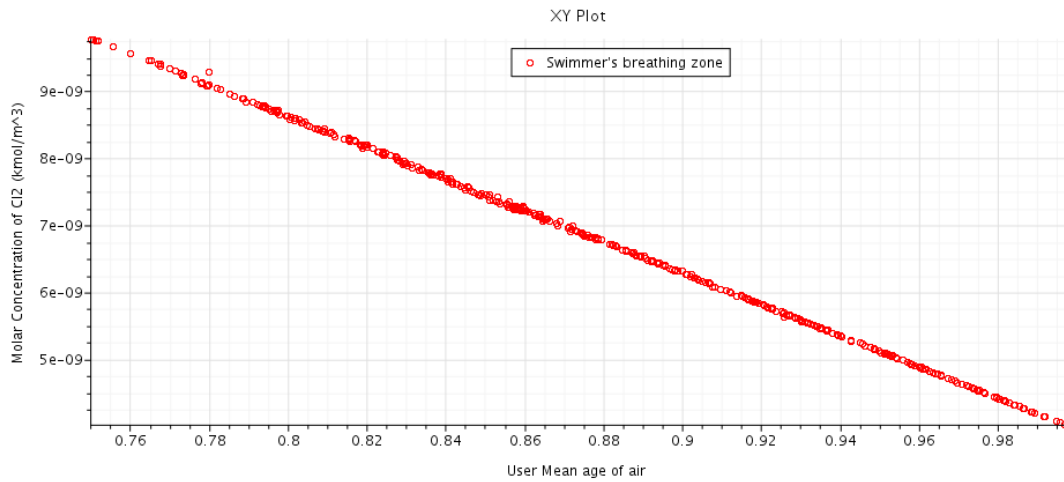


Figure 81: DV4 ACH case: Relation of LMA and chlorine concentration on swimming breathing zone

As the previous investigated cases in this section, it is clearly that high ACE values leads to high chlorine concentration.. Figure 82 shows stable and smooth relation between the graph and chlorine concentration points.

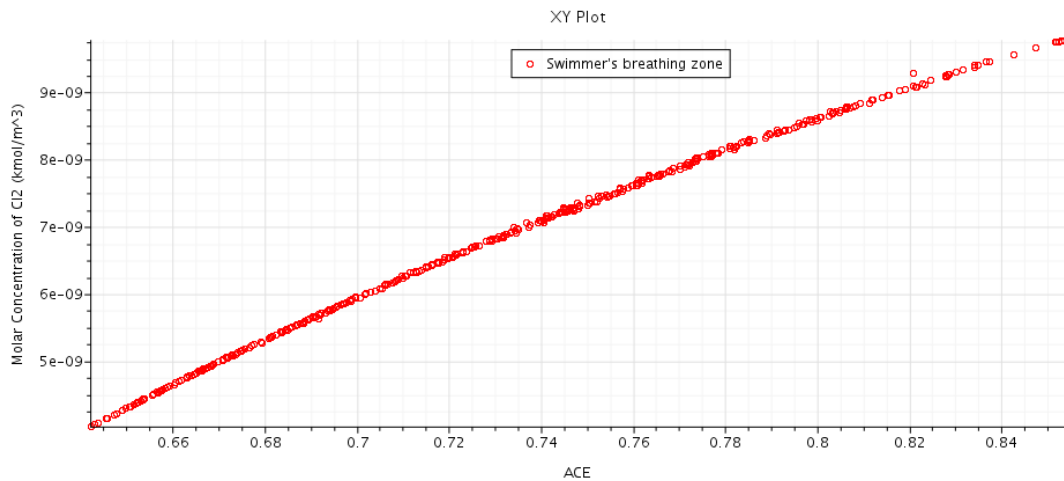


Figure 82: DV4 ACH: Relation of ACE and chlorine concentration on the swimming breathing zone

Figure 83 describes the relationship between the LMA and ACE in the swimming breathing zone for the DV4 ACH system case.

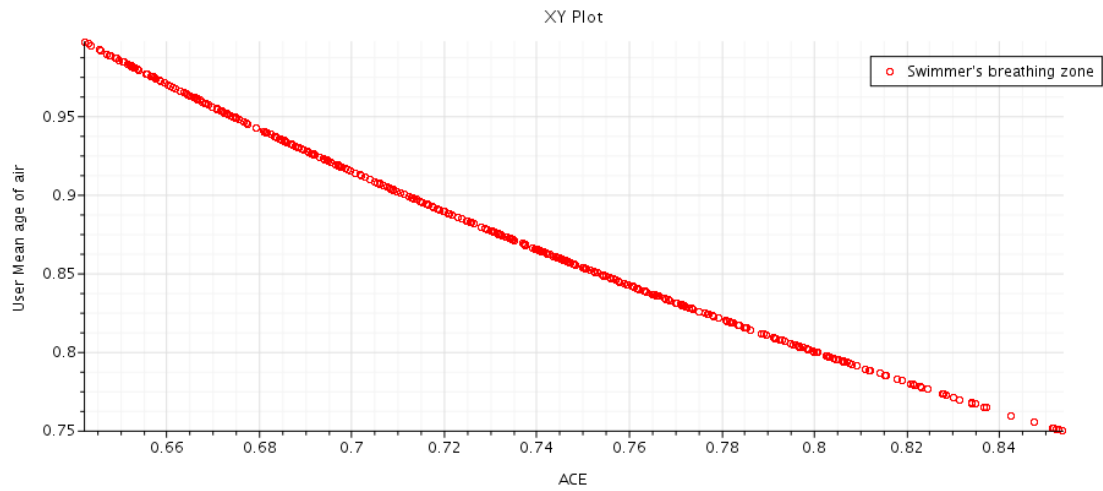


Figure 83: Relation of ACE and LMA on swimming breathing zone

4.3.2 People around

The result shows good LMA values for the DV4 system for the people around the swimming zone (see figure 84).

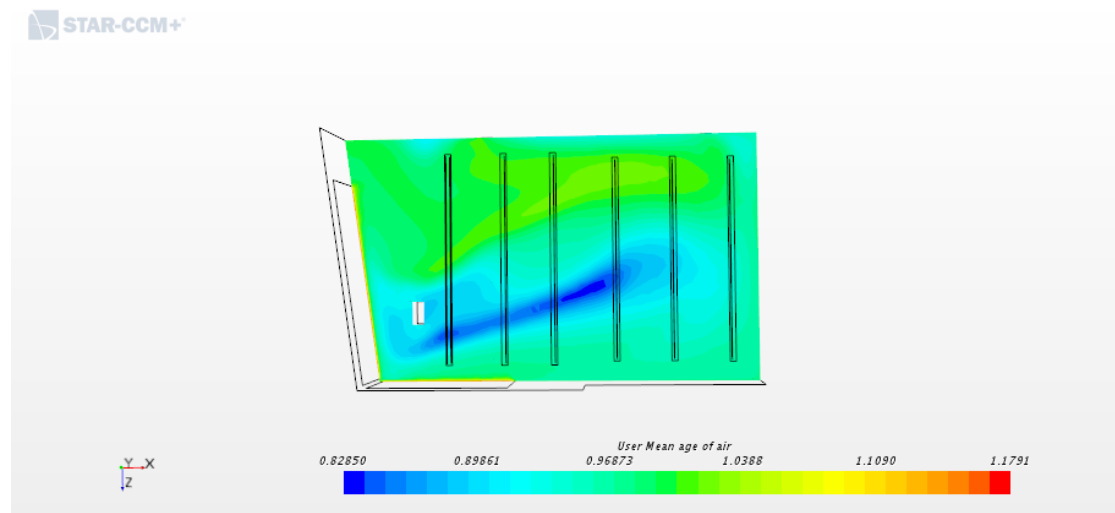


Figure 84: DV4 ACH: LMA on people around

Figure 85 shows that the DV4 ACH system has almost the same ACE values level as the investigated MV case for the people around the swimming pool.

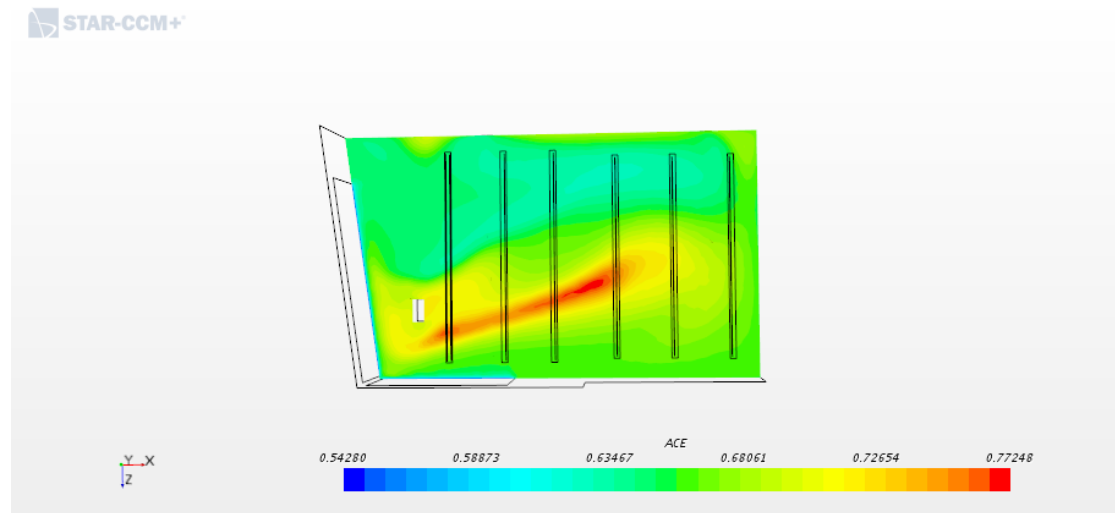


Figure 85: DV4 ACH: ACE on people around

It can be seen from figure 86 that the air temperature is stable for the people around the swimming pool. And relatively stable temperature around the external windows and facades where the inlet air flow is located.

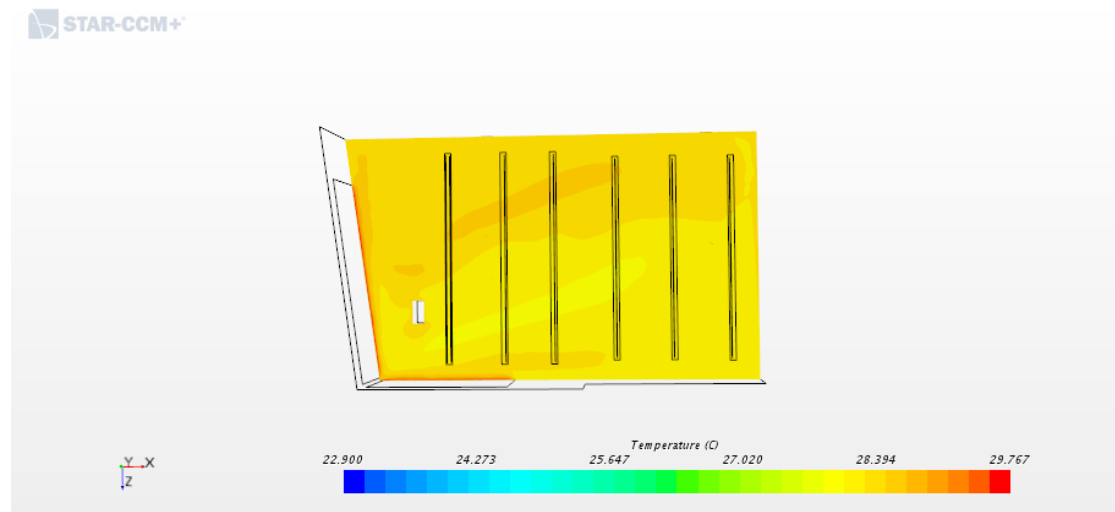


Figure 86: DV4 ACH: Air temperature on people around

The results shows stable air velocity around the external windows in the DV4 ACH case as shown in figure 87.

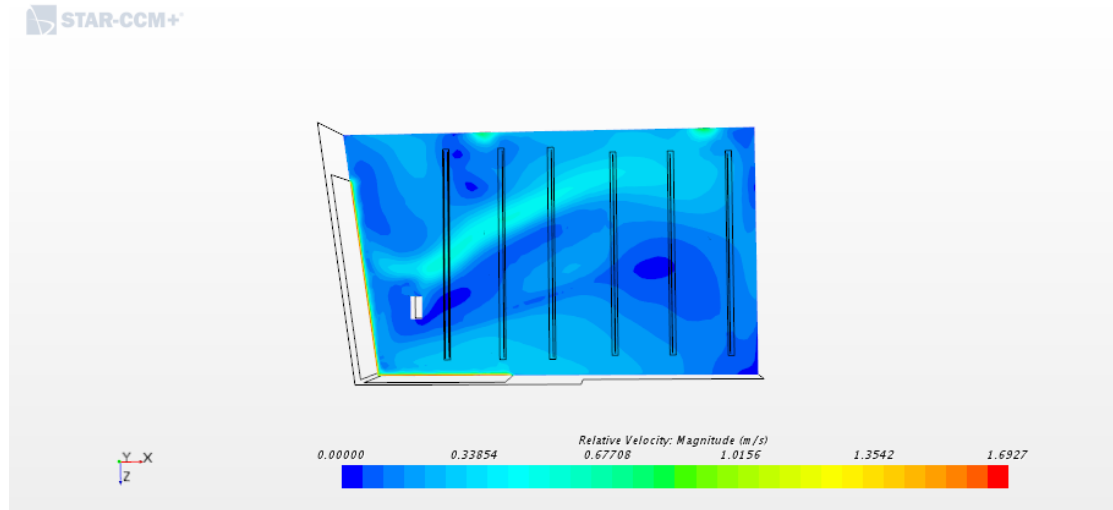


Figure 87: DV4 ACH: Air velocity on people around

The relationship between LMA and ACE as a result of the conducted test for the people around is described in figure 88.

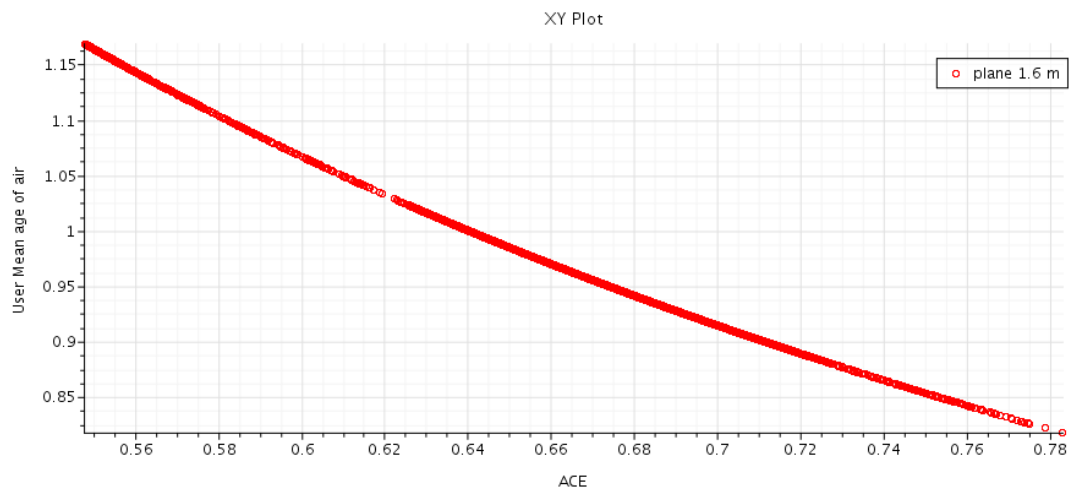


Figure 88: DV4 ACH: Relation between ACE and LMA on people around

4.4 Displacement ventilation (DV5 ACH) case

4.4.1 Swimming breathing zone

The previous results for the investigated case DV4 ACH system show good stable air temperature and air velocity. Normally high air flow contributes for good thermal comfort in swimming pools. The DV5 and DV7 ACH systems supply high inlet air flow. Therefore, the investigation for these cases is focused on ACE and on the air quality in the breathing zones.

The results confirms a lower LMA values than the DV4 ACH system in the swimming breathing zone as shown in figure 89. The reason for lower LMA, is the higher supplied air flow in this case.

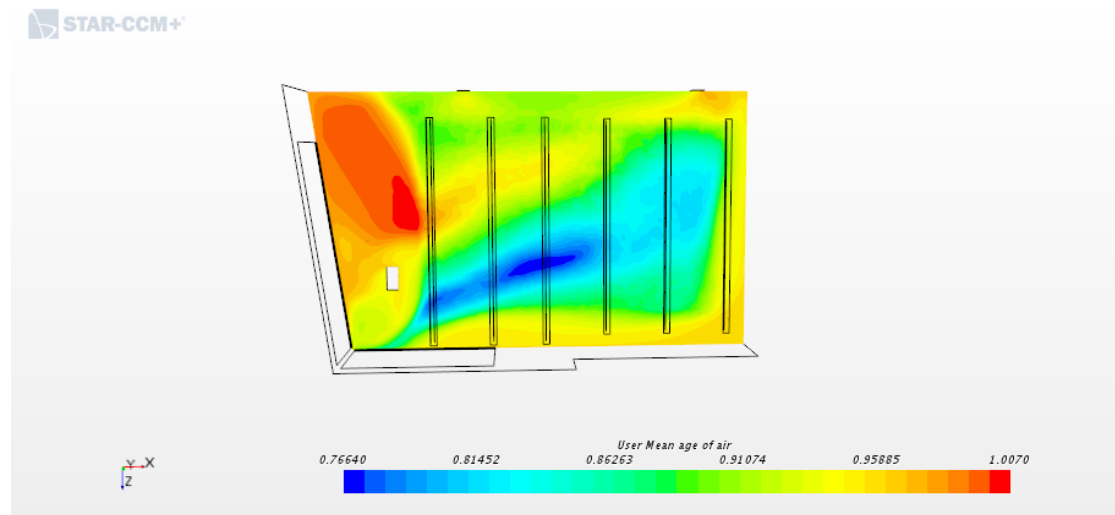


Figure 89: DV5 ACH: LMA on swimming breathing zone

The result confirms fully "mixing ventilation" mode for the case of the DV5 system (see figure 90). ACE values are around 0.5 and lead to higher energy usage compared to the DV4 ACH system.

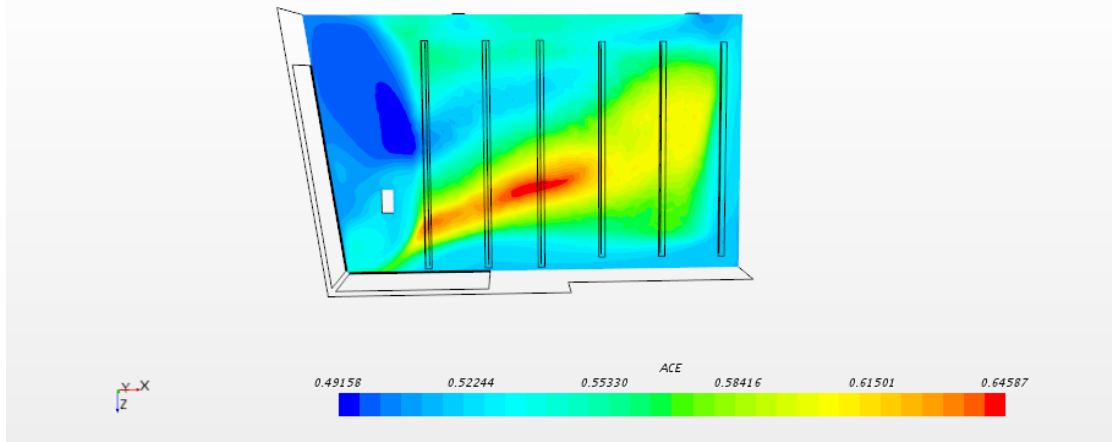


Figure 90: DV5 ACH: ACE on swimming breathing zone

Figure 91 shows insignificant reduction in chlorine concentration compared with the DV4 ACH system. Increasing airflow above 4 ACH in swimming pool should be considered due to cover the heat lost and not to reduce chlorine contaminant.

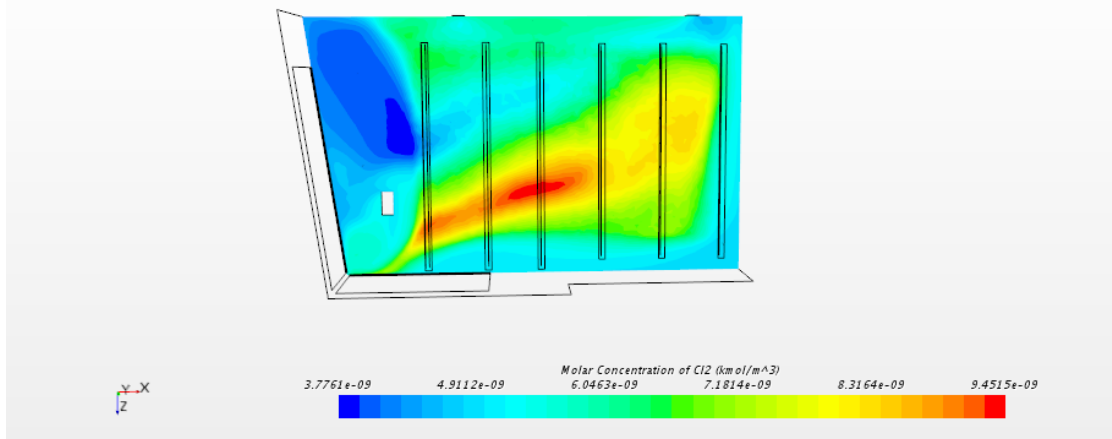


Figure 91: DV5 ACH: Molar concentration of chlorine on swimming breathing zone

The relationship between the LMA and chlorine concentration in the swimming breathing zone is shown in figure 92. Low LMA values have higher chlorine concentration. It is clearly from all previous investigated cases in this study that

the LMA with a value very close to one is very effective to reduce the chlorine concentration.

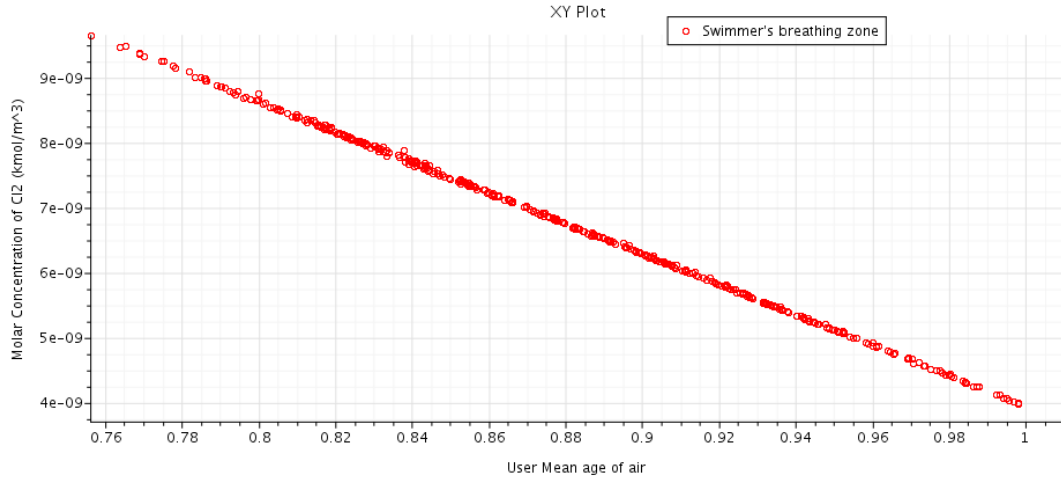


Figure 92: DV5 ACH: Relation of LMA and chlorine concentration on swimming breathing zone

The DV5 system has ACE values vary from 0.45 to 0.65 which confirms less energy efficiency than the DV4 system figure 93. DV5 ACH system is good choice to cover heat lost in the winter time.

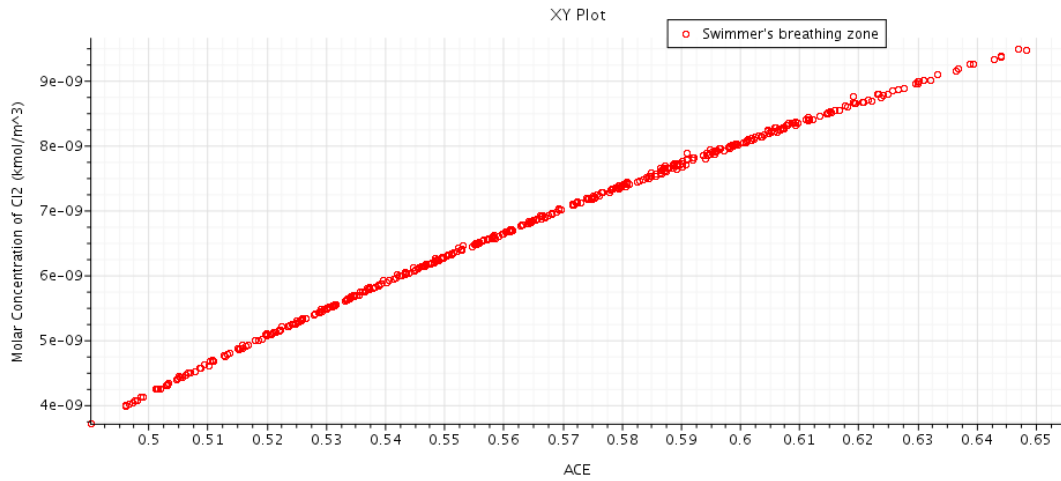


Figure 93: Relation of ACE and chlorine concentration on swimming breathing zone

Figure 94 describes the relationship between the LMA and ACE in the swimming breathing zone for the DV5 ACH system case. The more ACE, the less the LMA.

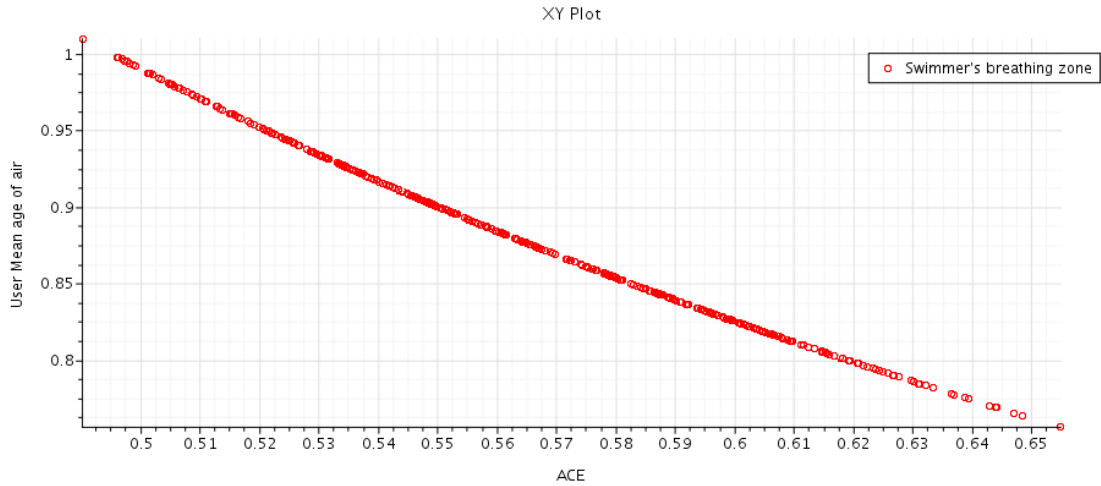


Figure 94: DV5 ACH: Relation of ACE and LMA on swimming breathing zone

4.4.2 People around

The DV5 ACH system has a lower LMA values than the DV4 ACH system due to its higher air flow (see figure 95)

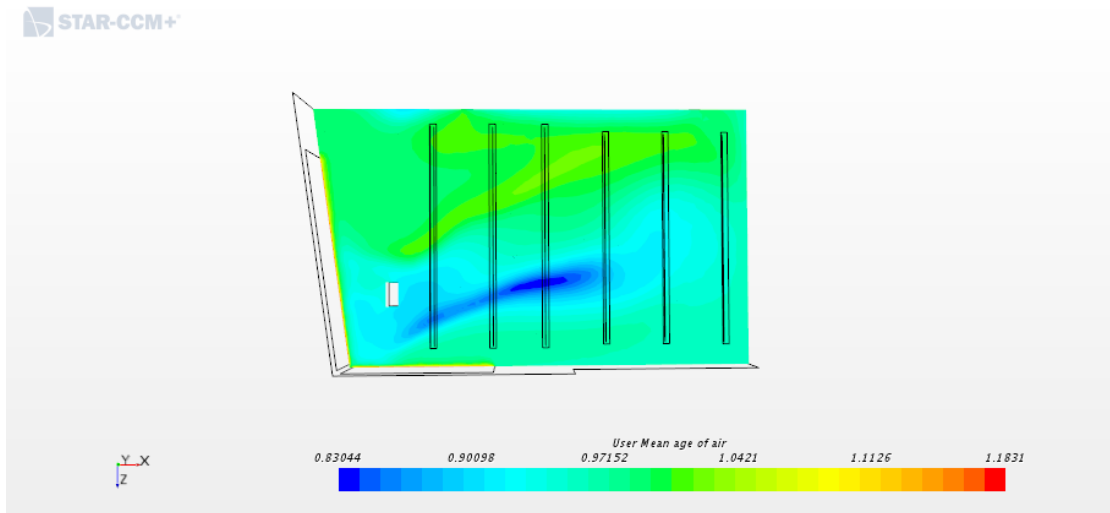


Figure 95: DV5 ACH: LMA on people around

The result confirms nearly "fully mixing ventilation" mode for the people around the swimming zone in the case of the DV5 system (see figure 96).

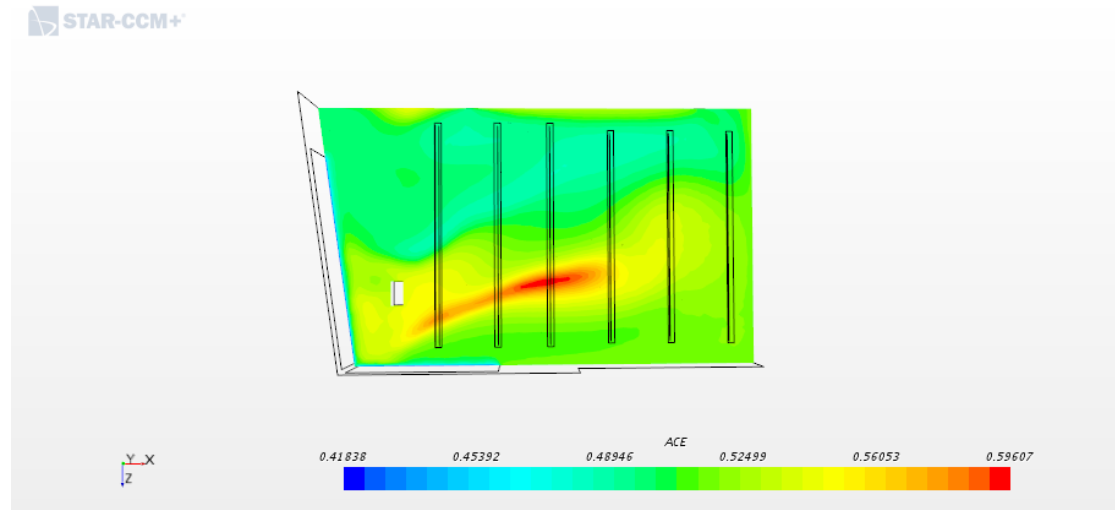


Figure 96: DV5 ACH: ACE on people around

The relationship between LMA and ACE as a result of the conducted test for the people around is described in figure 97

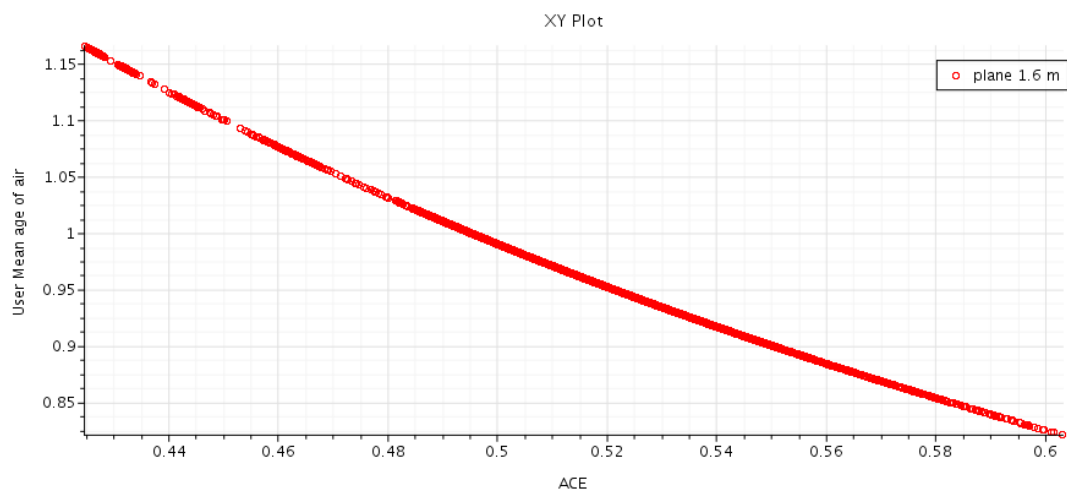


Figure 97: DV5 ACH: Relation of ACE and LMA on people around

4.5 Displacement ventilation (DV7 ACH) case

4.5.1 Swimming breathing zone

The DV7 ACH system has a lower LMA than all investigated cases due to its high inlet air flow equal to $36000 \frac{m^3}{h}$ (see figure 98).

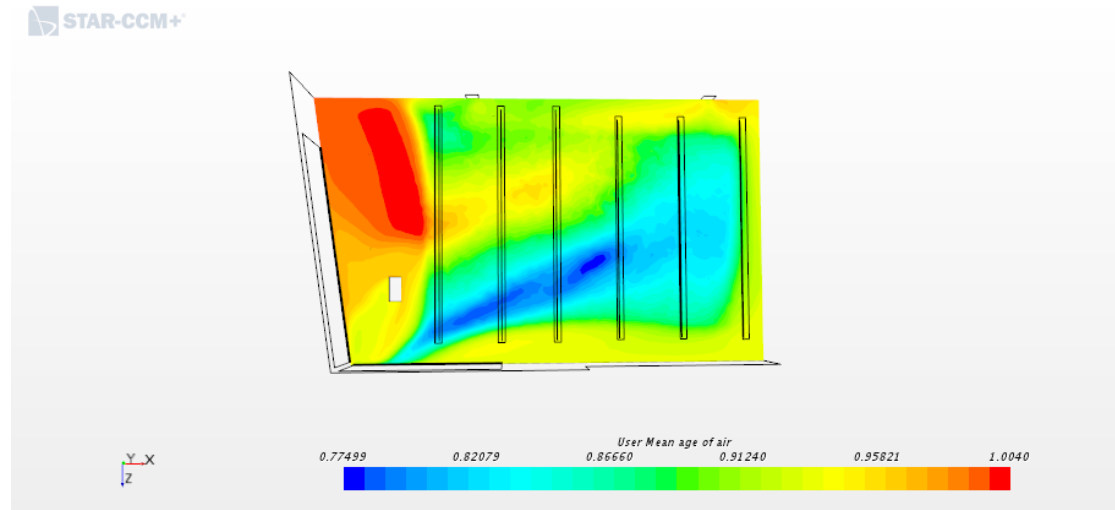


Figure 98: DV7 ACH: LMA on swimming breathing zone

The result confirms totally inefficient energy ventilation mode for the the DV7 ACH system. ACE low vaules are widely presented as shown in figure 99.

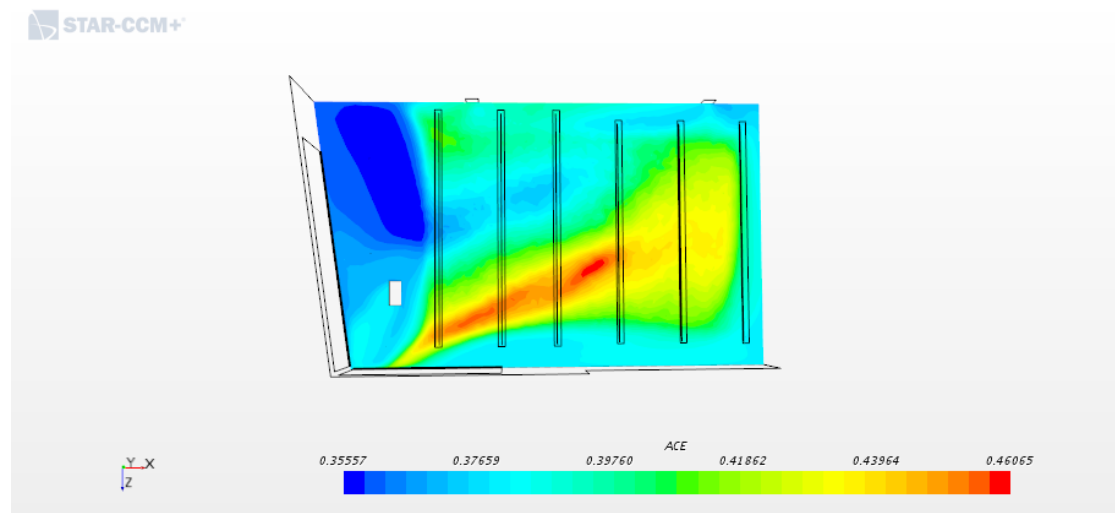


Figure 99: DV7 ACH: ACE on swimming breathing zone

Figure 100 confirms insignificant reduction in chlorine concentration compared with the DV5 ACH system. Increase the airflow to 7 ACH in the swimming pool is not convenient to reduce chlorine concentration.

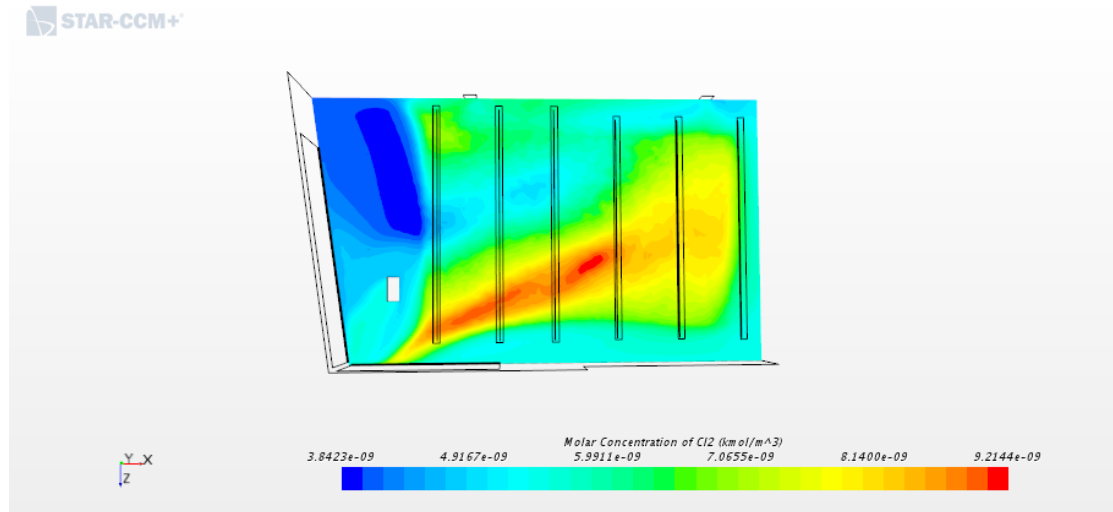


Figure 100: DV7 ACH: Molar concentration of chlorine on swimming breathing zone

The relationship between LMA and molar chlorine concentration is described in figure 101.

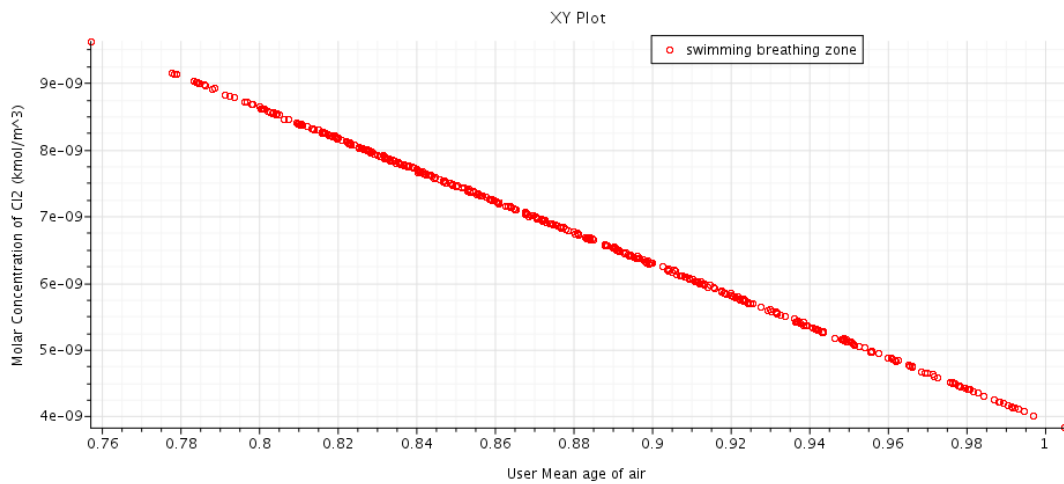


Figure 101: DV7 ACH: Relation of LMA and chlorine concentration on the swimming breathing zone

Figure 102 shows the relationship between the ACE and the chlorine concentration in the swimming breathing zone. The ACE values for this system are very low and inefficient.

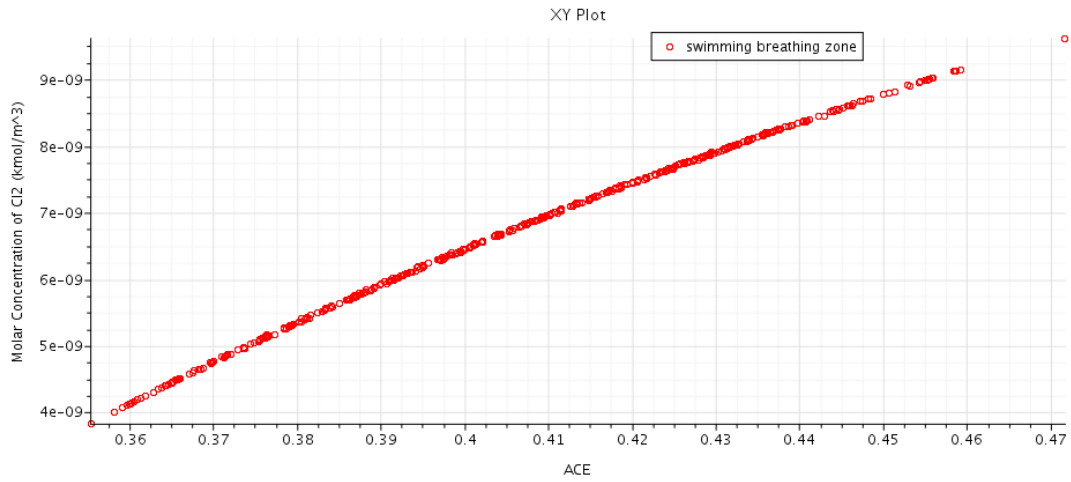


Figure 102: DV7 ACH: Relation of ACE and chlorine concentration on swimming breathing zone

Figure 103 describes the relationship between the LMA and ACE in the swimming breathing zone for the DV7 ACH system case.

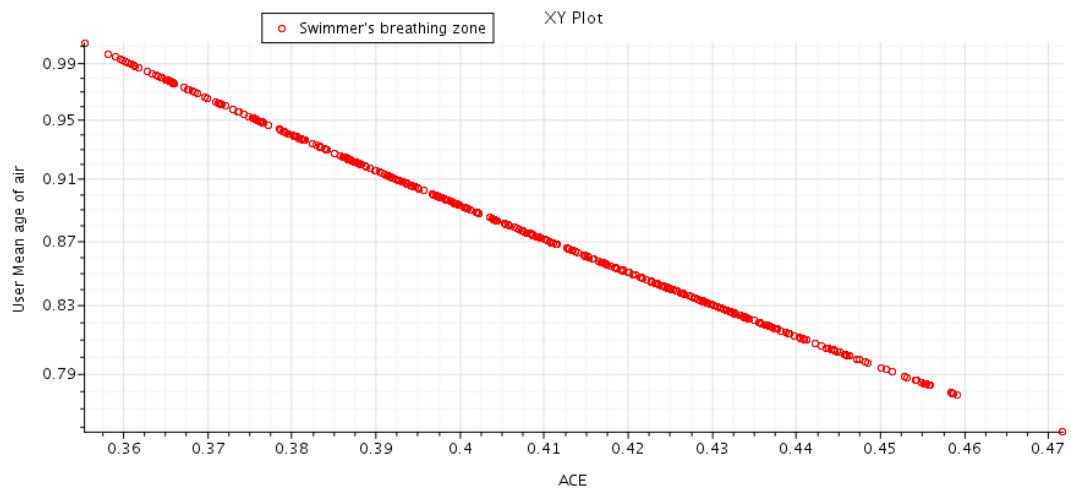


Figure 103: DV7 ACH: Relation of ACE and LMA on swimmer's breathing zone

4.5.2 People around

The DV7 ACH system shows a lower LMA values than all investigated cases (see figure 104).

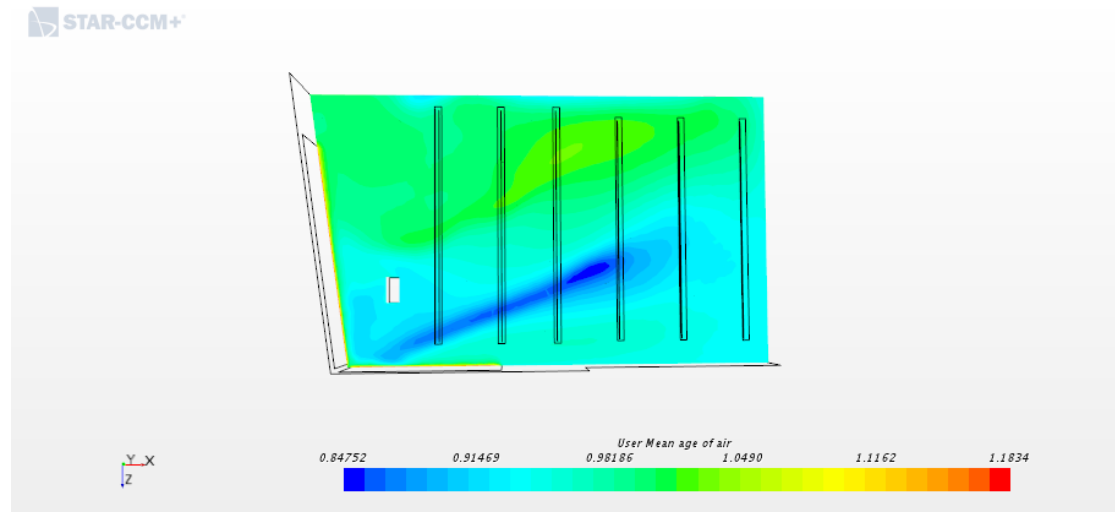


Figure 104: DV7 ACH: LMA on people around

The result confirms inefficient energy ventilation for the people around the swimming pool. The ACE values are between 0.3 and 0.42 system (see figure105).

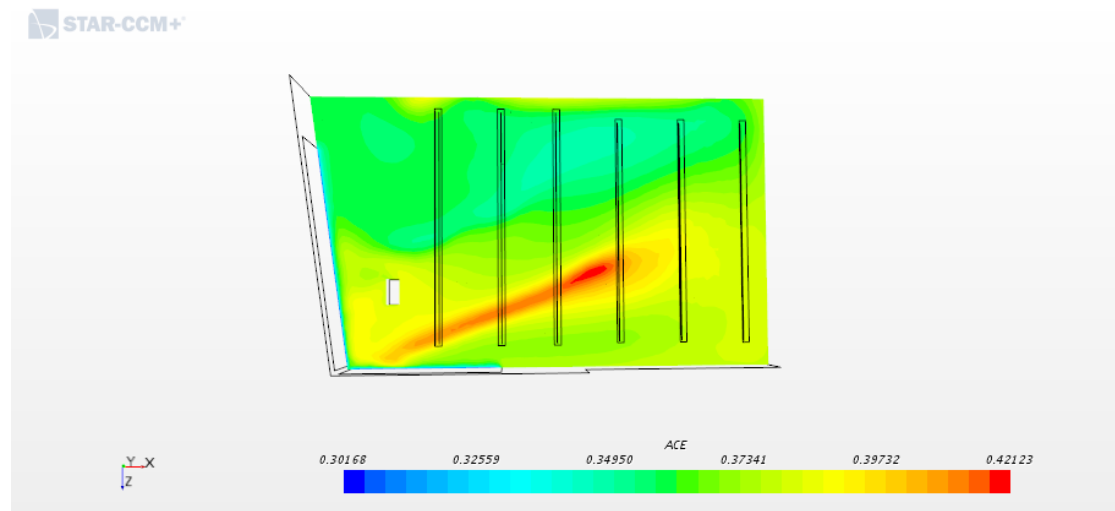


Figure 105: DV7 ACH: ACE on people around

The relationship between LMA and ACE as result of the conducted test for the people around in this case is described in figure 106.

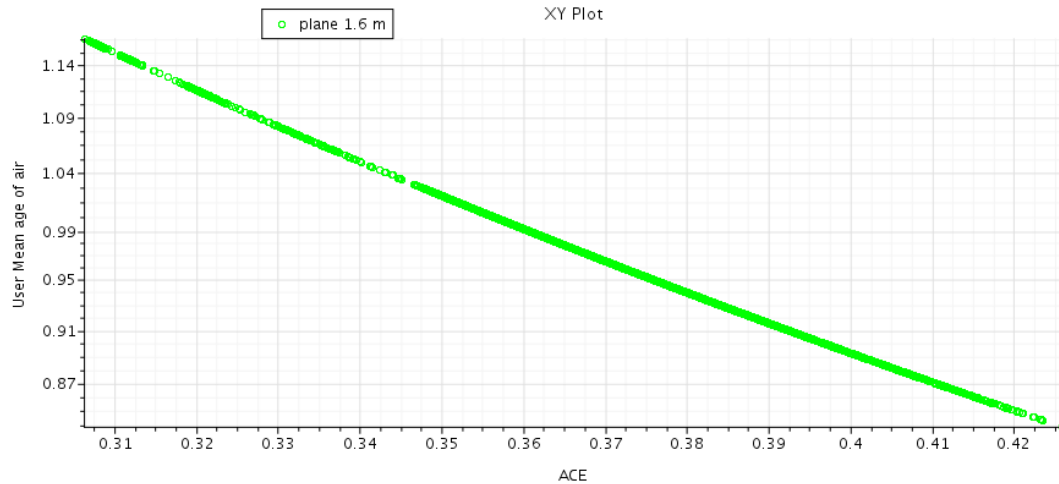


Figure 106: DV7 ACH: Relation of ACE and LMA on people around

5 Conclusion

It is apparent in this study that (MV) case is a highly recommended ventilation option to use in Åfjord swimming pool. The air distribution strategy (textile ducts installed above the water bath) combined with exhaust outlet, positioned on the floor level is an operational ventilation system in the investigated swimming pool. Due to the measure indicator for air quality with local mean age of air LMA there are no stagnant air flow regions. Also, due to the air exchange efficiency indicator ACE, the system exchanges the air efficiency similar to "piston mode" ventilation. Worthy reduction in operation expenses is strongly expected for this system.

Furthermore the investigated (MV) case confirms improved air quality in the swimming breathing zone with at least 12% reduction in chlorine concentration compared to the rule of thumb system DV7 ACH which operate with more than two times airflow of the (MV) case. There is no sign observed for condensation risk on the external window, and the thermal comfort due to the measured air temperature, relative humidity and air velocity are also considered to be accepted.

It is also apparent in this study that the (MV-DV) case is a highly recommended option to use in Åfjord swimming pool specially during winter time when the heat demand increases or in special cases (very crowded visiting situation) when the the need for more air supply is considered as necessary. The combination of MV system with DV (additional air flow supply under the external window), makes the system robust to reduce the chlorine concentration in the swimming breathing zone up to 36% compared to the rule of thumb system DV7 ACH. This system exchange the air with intermediate efficiency simliar to "fully mixing" ventilation due to the ACE measurements. The energy saving in ventilation operation for this system is expected to become around 21%. This system provides good thermal comfort due to the measured stable air temperature, low air velocity and lower humidity level than the MV case.

Furthermore, it is also recommended for Åfjord swimming pool not to operate with just displacement ventilation inlet air flow under windows. This system provides good thermal comfort in general but poor air quality in form of high chlorine concentration in the swimming breathing zone.

5.1 Future work

In future detailed analysis with the apparent relationship between the chlorine concentration in the swimming pool and the air quality indicator local mean age of air LMA and air exchange efficiency ACE can be performed. All investigated cases show low chlorine concentration in the swimming breathing zone when the LMA is equal to 1 or very close to one. Recommendation to increase the supply air flow to decrease the chlorine contaminant in swimming pool is not sufficient as higher airflow leads to decrease the LMA while the chlorine concentration increases. On the other hand the chlorine concentration in the swimming breathing zone increases when the the air exchange efficiency ACE increases. However this study presents two situations where they have almost the same ACE level (see table 10) but with different chlorine concentration in the swimming pool. The (MV-DV) case and the (DV5 ACH) case both have almost the the same ACE level on the investigated zone but the result confirms different chlorine concentration in the swimming breathing zone for the two investigated cases. The (MV DV) case has 36.5% decreased chlorine concentration in relation to the (DV5 ACH) case . The other situation is, the (MV) case and the (DV4 ACH) case both have almost the same ACE level but they have different chlorine concentration in the swimming breathing zone. The study shows also decreasing in the air exchange efficiency ACE when the air temperature or the air velocity increases.

This study confirms that the best way to improve the air quality is to investigate the ventilation strategy in the swimming pool. Examination the hall with varying the positions of inlet air flow and exhaust will contribute for a better understanding of the air quality in swimming pool.

6 References

References

- [1] NORGES SVØMMEFORBUND, editor. Svømmeidrett og svømmeanlegg i Norge;. Available from: <https://svomming.no/nsf-eldre-web/svommeidrett-og-svommeanlegg-i-norge/> [cited 14.12.2018].
- [2] Enova, editor. Enovas byggstatistikk 2017, Rapporten presenterer analyser og statistikk om energibruk fordelt etter bygningstyper, samt variasjoner avhengig av alder, størrelse og oppvarmingsssystem;. Available from: https://www.enova.no/download?objectPath=upload_images/5C6245BC2AD74248BB629BFA95145AA3.pdf&filename=Enovas%20byggstatistikk%202017.pdf [cited 2018-03-20].
- [3] Kampel W, Aas B, Bruland A. Characteristics of energy-efficient swimming facilities A case study. *Energy*. 2014;75:508 – 512. Available from: <http://www.sciencedirect.com/science/article/pii/S0360544214009438>.
- [4] Rojas G, Grove-Smith J. Improving Ventilation Efficiency for a Highly Energy Efficient Indoor Swimming Pool Using CFD Simulations. *Fluids*. 2018;3(4). Available from: <http://www.mdpi.com/2311-5521/3/4/92>.
- [5] Weng S, A Weaver W, Zare Afifi M, Blatchley T, S Cramer J, Chen J, et al. Dynamics of gasphase trichloramine (NCl₃) in chlorinated, indoor swimming pool facilities. *Indoor Air*. 2011 10;21:391 – 399.
- [6] Bougault V, Turmel J, Levesque B, Boulet LP. The Respiratory Health of Swimmers. *Sports medicine (Auckland, NZ)*. 2009 02;39:295–312.
- [7] Limane A, Fellouah H, Galanis N. Three-dimensional OpenFOAM simulation to evaluate the thermal comfort of occupants, indoor air quality and heat losses inside an indoor swimming pool. *Energy and Buildings*. 2018;167:49 – 68. Available from: <http://www.sciencedirect.com/science/article/pii/S0378778817325938>.
- [8] Limane A, Fellouah H, Galanis N. Simulation of airflow with heat and mass transfer in an indoor swimming pool by OpenFOAM. *International Journal of Heat and Mass Transfer*. 2017;109:862 – 878. Available from: <http://www.sciencedirect.com/science/article/pii/S0017931016324541>.
- [9] Koper P, Lipska B, Michnol W. Assessment of thermal comfort in an indoor swimming pool making use of the numerical prediction CFD. *Architecture Civil Engineering Environment*. 2010;3(3):95–104.

- [10] Li Z. CFD Simulations for Water Evaporation and Airflow Movement in Swimming Baths. *Ventinet*. 2005;(14):10–11.
- [11] Shah MM. Improved method for calculating evaporation from indoor water pools. *Energy and Buildings*. 2012;49:306 – 309. Available from: <http://www.sciencedirect.com/science/article/pii/S0378778812001041>.
- [12] Shah MM. Prediction of evaporation from occupied indoor swimming pools. *Energy and Buildings*. 2003;35(7):707 – 713. Available from: <http://www.sciencedirect.com/science/article/pii/S0378778802002116>.
- [13] Shah MM. Improved model for calculation of evaporation from water pools. *Science and Technology for the Built Environment*. 2018;24(10):1064–1074. Cited By 0. Available from: <https://www.scopus.com/inward/record.uri?eid=2-s2.0-85056143246&doi=10.1080%2f23744731.2018.1483157&partnerID=40&md5=3ab3af1e4dcb7078fb5e0e4624bf7f82>.
- [14] Srebric J, Chen Q. Simplified Numerical Models for Complex Air Supply Diffusers. *HVAC&R Research*. 2002;8(3):277–294. Available from: <https://www.tandfonline.com/doi/abs/10.1080/10789669.2002.10391442>.
- [15] Li Y, Nielsen PV. CFD and ventilation research. *Indoor Air*. 2011;21(6):442–453. Available from: <https://onlinelibrary.wiley.com/doi/abs/10.1111/j.1600-0668.2011.00723.x>.
- [16] Åfjord kommune, editor. Åfjordbad og kulturhus;. Available from: https://www.afjord.kommune.no/_f/p1/if037b835-c25e-4b29-9f48-e5b3e2613632/kult-a-bad_plansjercompressed.pdf [cited 2018-03-20].
- [17] Byggforsk, editor. 552.315 Ventilasjon og avfukting i svømmehaller og rom med svømmebasseng;. Available from: https://www.byggforsk.no/dokument/534/ventilasjon_og_avfukting_i_svoemnehaller_og_rom_med_svoemnebasseng# [cited 2018-03-03].
- [18] CIBSE, editor. Understanding Swimming Pool Ventilation;. Available from: <https://www.cibse.org/getmedia/96df56ce-1cd2-4dbe-8412-a91ce1b2bf3b/Pool-CPD-Mar-17-no-Intpool.pdf.aspx> [cited 2018-03-03].
- [19] Versteeg HK, Malalasekera W. An Introduction to Computational Fluid Dynamics. 2nd ed. the Finite Volume Method; 2007.

- [20] National Aeronautics and Space Administration NASA, editor. Navier- Stokes Equations;. Available from: <https://www.grc.nasa.gov/www/BGH/nseqs.html> [cited 14.03.2019].
- [21] Engineeringtoolbox, editor. Prandtl Number;. Available from: https://www.engineeringtoolbox.com/prandtl-number-d_1068.html [cited 2018-03-20].
- [22] NORGES SVØMMEFORBUND, editor. Svømmeidrett og svømmeanlegg i Norge;. Available from: <https://svomming.no/wp-content/uploads/2006/03/Spesifikasjon-svømmeanlegg.pdf> [cited 27.02.2018].
- [23] Paul Tymkow MKHJ Savvas Tassou. Building Services Design for Energy Efficient Buildings. 1st ed. Energy efficient ventilation; 2013. Available from: [https://books.google.no/books?id=yp8y3UZr89UC&pg=PA126&lpg=PA126&dq=Liddament+\(1993\)+mean+age+of+air&source=bl&ots=TE2AzFMky5&sig=ACfU3U0gGt89mD7-HydeWFSV6Sc0r74xfQ&hl=no&sa=X&ved=2ahUKEwiSibT-94TiAhVCAxAIHclLCWoQ6AEwAXoECAgQAQ#v=onepage&q=Liddament%20\(1993\)%20mean%20age%20of%20air&f=false](https://books.google.no/books?id=yp8y3UZr89UC&pg=PA126&lpg=PA126&dq=Liddament+(1993)+mean+age+of+air&source=bl&ots=TE2AzFMky5&sig=ACfU3U0gGt89mD7-HydeWFSV6Sc0r74xfQ&hl=no&sa=X&ved=2ahUKEwiSibT-94TiAhVCAxAIHclLCWoQ6AEwAXoECAgQAQ#v=onepage&q=Liddament%20(1993)%20mean%20age%20of%20air&f=false).
- [24] Bartak M, Cermak M, A Clarke J, Denev J, Drkal F, Lain M, et al. Experimental and numerical study of local mean age of air; 2001. .
- [25] Novoselac A, Srebric J. Comparison of Air Exchange Efficiency and Contaminant Removal Effectiveness as IAQ Indices. ASHRAE Transactions. 2003 01;.
- [26] Roulet CA. Ventilation and Airflow in Buildings: Methods for Diagnosis and Evaluation. 1st ed. Age of Air and Ventilation Efficiency; 2012. Available from: <https://books.google.no/books?id=QVaMUp8oMmMC&pg=PA41&lpg=PA41&dq=Ventilation+modes+with+typical+airflow+patterns+and+air+change+efficiencies+Roulet,+2004&source=bl&ots=vIThqkmR8f&sig=ACfU3U0PFdDQYuXK4aMgcsxKFlqwhvOvtA&hl=no&sa=X&ved=2ahUKEwjSuezww4niAhU06KYKHRa9DIoQ6AEwC3oECAgQAQ#v=onepage&q=Ventilation%20modes%20with%20typical%20airflow%20patterns%20and%20air%20change%20efficiencies%20Roulet%2C%202004&f=false>.
- [27] Byggforsk, editor. 473.010 Generelt om passivhus. Valg og konsekvenser;. Available from: https://www.byggforsk.no/dokument/4108/generelt_om_passivhus_valg_og_konsekvenser [cited 2018-03-20].
- [28] Byggforsk, editor. 451.021 Klimadata for termisk dimensjonering og frostsikring;. Available from: <https://www.byggforsk.no/dokument/>

204/klimadata_for_termisk_dimensjonering_og_frostsikring [cited 2018-03-20].

[29] Byggforsk, editor. 471.111 Beregningsmetode for å unngå kondens eller muggvekst på innvendige overflater;. Available from: https://www.byggforsk.no/dokument/534/ventilasjon_og_avfukting_i_svoemnehaller_og_rom_med_svoemnebasseng# [cited 2018-03-20].

[30] Stina Odelros, editor. How gases present in the environment affect OBA mirror surfaces at indoor swimming pool facilities;. Available from: <https://senseair.com/media/1861/eqc-how-gases-present-in-the-environment-affect-oba-mirror-surfaces-at-indoor-pdf> [cited 2018-04-20].

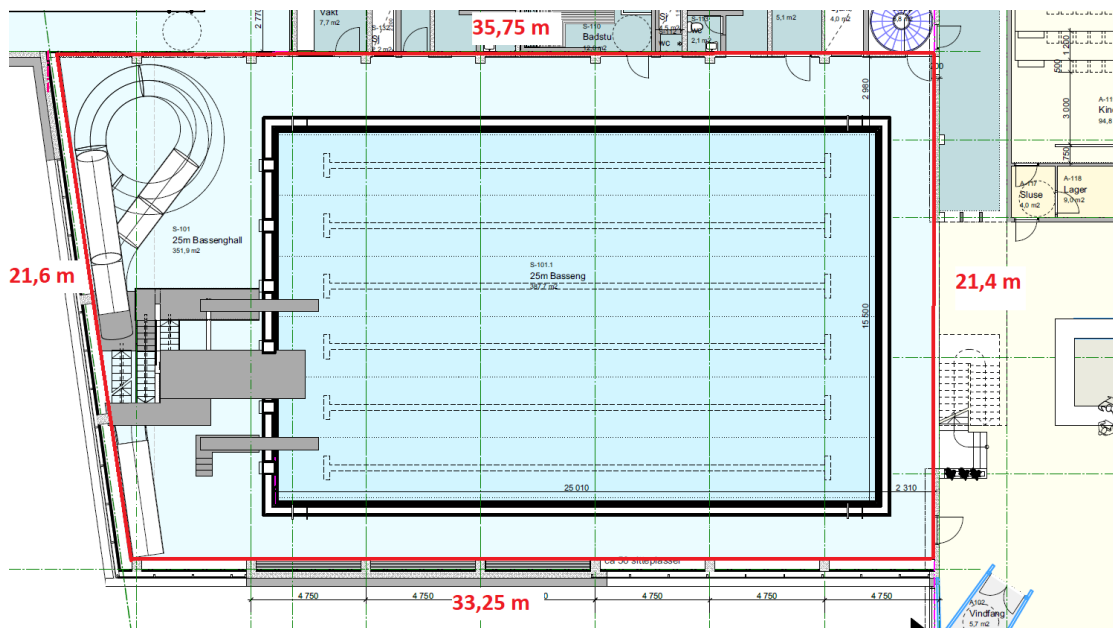
[31] Heiselberg P. Draught risk from cold vertical surfaces. Building and Environment. 1994;29(3):297 – 301. Special Issue Papers from Indoor Air '93. Available from: <http://www.sciencedirect.com/science/article/pii/0360132394900264>.

[32] Byggforsk, editor. 421.501 Termisk inneklima. Betingelser, tilrettelegging og målinger;. Available from: https://www.byggforsk.no/dokument/4108/generelt_om_passivhus_valg_og_konsekvenser [cited 2018-03-20].

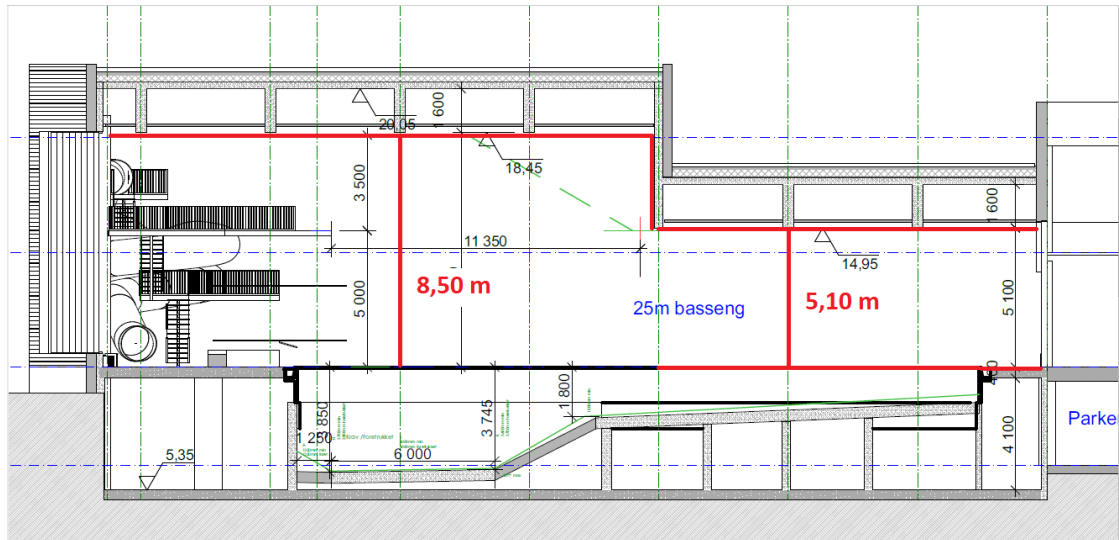
A ASHRAE Shah's density difference table

| Water Temp., °C | Density Difference $\rho_r - \rho_w$, kg/m ³ Space Air Temperature and Relative Humidity | | | | | | | | | | | |
|-----------------|--|--------|--------|--------|--------|--------|--------|--------|--------|--------|--------|--------|
| | 25°C | | 26°C | | 27°C | | 28°C | | 29°C | | 30°C | |
| | 50% | 60% | 50% | 60% | 50% | 60% | 50% | 60% | 50% | 60% | 50% | 60% |
| 25 | 0.0185 | 0.0148 | 0.0135 | 0.0096 | 0.0084 | 0.0043 | 0.0034 | 0 | 0 | 0 | 0 | 0 |
| 26 | 0.0246 | 0.0209 | 0.0196 | 0.0157 | 0.0145 | 0.0104 | 0.0095 | 0.0051 | 0.0044 | 0 | 0 | 0 |
| 27 | 0.0308 | 0.0271 | 0.0258 | 0.0218 | 0.0207 | 0.0166 | 0.0156 | 0.0113 | 0.0105 | 0.0059 | 0.0054 | 0.0005 |
| 28 | 0.0370 | 0.0333 | 0.0320 | 0.0281 | 0.0270 | 0.0228 | 0.0219 | 0.0175 | 0.0168 | 0.0122 | 0.0116 | 0.0068 |
| 29 | 0.0434 | 0.0397 | 0.0384 | 0.0344 | 0.0333 | 0.0292 | 0.0282 | 0.0238 | 0.0231 | 0.0185 | 0.0180 | 0.0131 |
| 30 | 0.0498 | 0.0461 | 0.0448 | 0.0409 | 0.0397 | 0.0356 | 0.0347 | 0.0303 | 0.0295 | 0.0249 | 0.0244 | 0.0195 |

B Plan view



C Section view



D Facades

Fasade Nord

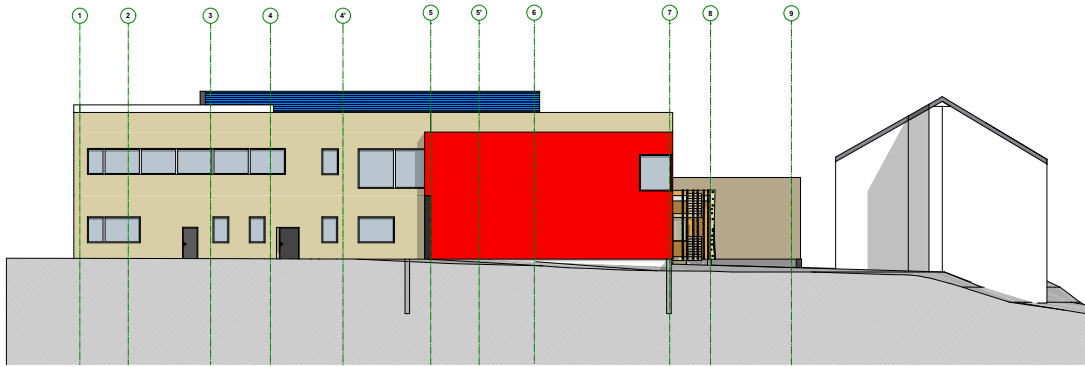
Fasade Vest

FORELØP/IG07.12.2018

| | |
|---|-----------------------------|
| Kont: P1.2 AS, NHHK-arkitektur AS | |
| LØS: P1.2.0286.05 | |
| SIS: - | |
| SIS: - | |
| SIS: - | |
| SIS: - | |
| SIS: - | |
| SIS: - | |
| SIS: - | |
| Kartgrunnlag: | Datum: Eurof - X18 side: XX |
| Høydesystem: NN XXXX | |
| P1.2 AS Hoffmannsveien 7 • 2014 Trondheim +47 73 38 42 50 hofmann@p1.no www.p1.no | |
| NHHK-arkitektur AS Alneshøgata 12 • 0172 Oslo • 22 01 40 20 hofmann@nhhk.no | |
| Opphavrett: Tegninger kan ikke benyttes utenfor dette eller i annen sammenheng uten forbehold eller skriftlig samtykke. Kun tegninger merket "Arbeidsdrøging" kan benyttes som prosjektdokumenter. PDF-filer garanteres ikke å være i samsvar med de utvalgte arkiverte filene. Ved stikk i eller med sikringsdrøgingen må kontrollert ut på stedet. | |
| KULT Å BAD | |
| Prosjekt: SKISSEPROSJEKT | |
| Titelblad: | |
| Ajord kommune | |
| Prosjekt nr: 2018019 | Tegnet av: NN NN |
| Dato: 05.11.2018 | Målestokk: 1:250(A3) |
| Tegning: Fasade Nord og Vest | |
| Figur nr: A40-1 | Rev: |



Fasade Sør



Fasade Øst

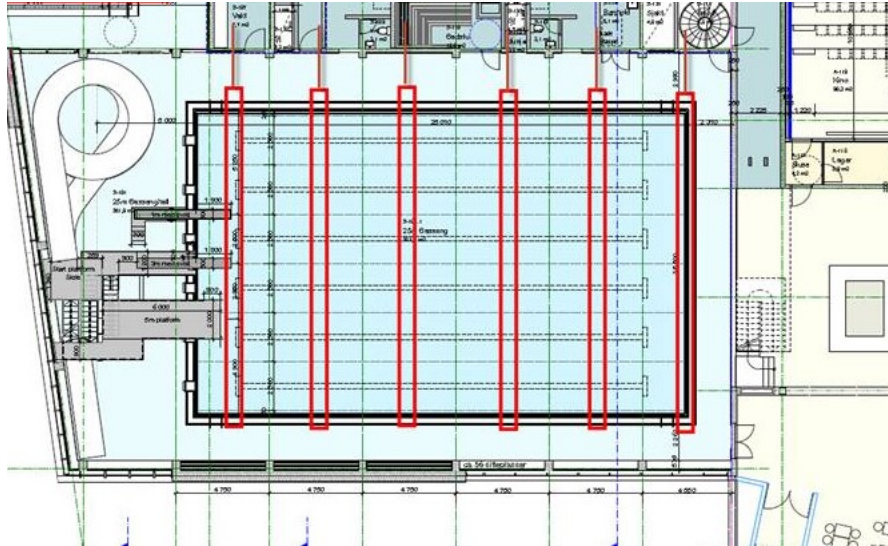
FORELØP/IG07.12.2018

| | |
|---|-----------------------------|
| Prosjekt: Skisseprosjekt Tiltaksnavn: Ajford kommune | |
| Prosjekt nr: | Tegnet av: NN NN |
| 2018019 | NN NN |
| Dato: | Målestokk: 1:250(A3) |
| 05.11.2018 | |
| Tegning: Fasade Sør og Øst | |
| Tegning av: A40-2 | Rev: |

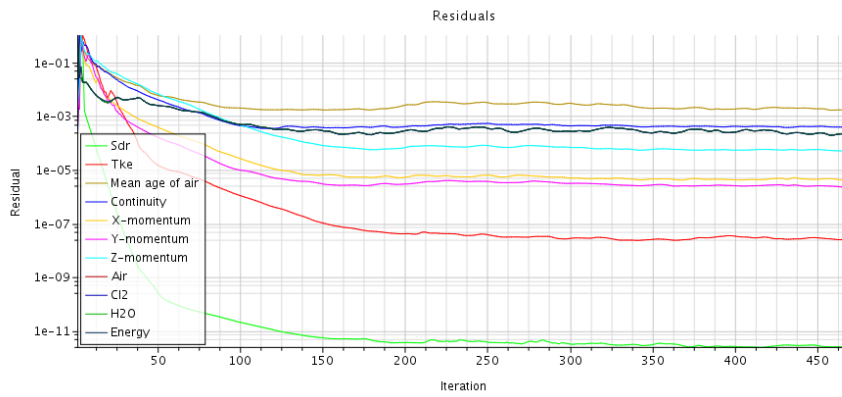
Opphavrett:
 Tegninger kan bli benyttet annerledes eller i annen sammenheng enn fortløst eller skiltlig samtykke. Kun tegninger merket "Arbeidsdrøfting" kan benyttes som produksjonsdrøfting. PDF-filer garanteres ikke å være i samsvar med originalen på grunn av digitale feil. Ved stikk i eller med eksisterende bygningssystem, må kontrollert bli på plass.

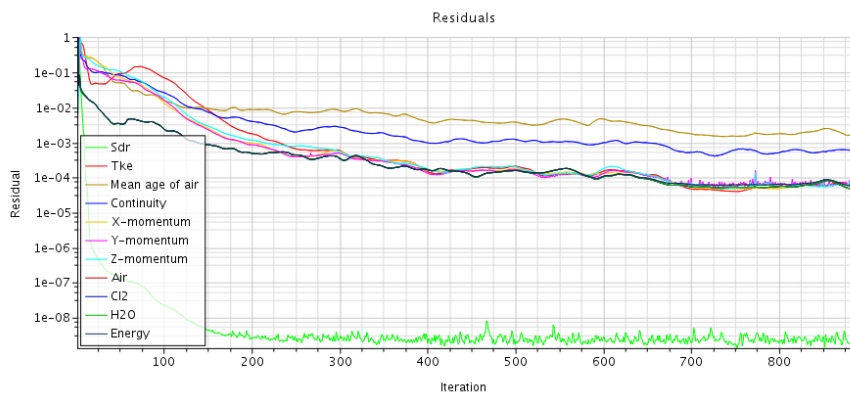
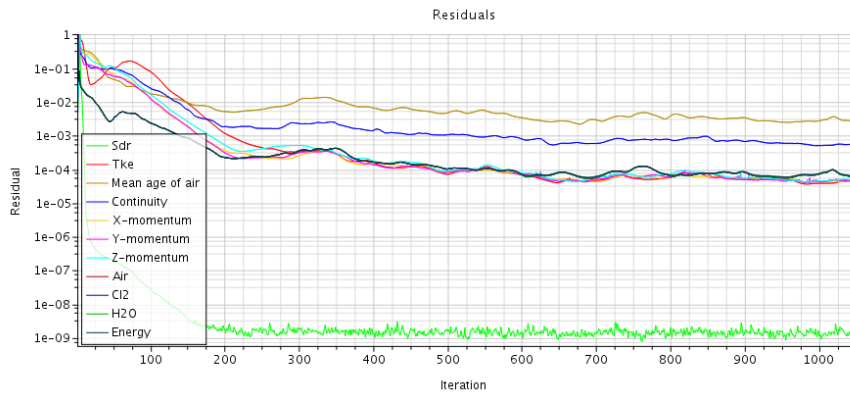
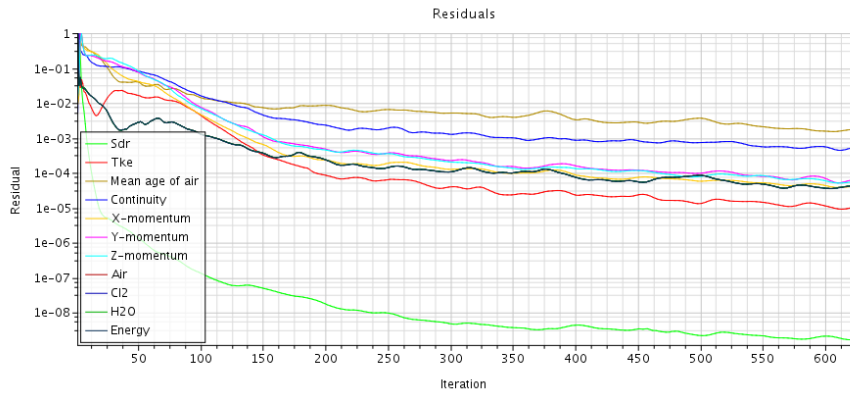
KULT Å BAD
 P.R. I.I. AS
 Industriparken 7 • 2014 Trondheim
 +47 73 88 42 82 | kontakt@prid.no
 www.prid.no
 NUNO
 NUNO AS
 Alneshøgata 12 • 0172 Oslo • 22 01 40 20
 kontakt@nunoarkitektur.no

E Ventilation pipes and exhaust plan



F Residual plots





G Textile duct specification

COWI AS

KE FIBERTEC

AIR THE WAY YOU WANT

TILBUD

Tilbudsnummer:

Versjon:

Prosjekt:

Åfjord kommune revidert 2702

Dato:

27.02.2019

Side:

3 av 9

| Pos. nr. | Produkt |
|-----------------------------------|--|
| Svømmebasseng : System # 1 | |
| 1-1/1.1 (10) 3 Stk. | KE-Inject System #Åfjord kommune revidert 2702 #Svømmebasseng Dimensjon: Ø500 mm, L=17000 mm Materiale: MultiWeave Farve: Hvit (Pantone 11-0601-TP) Opheng: 1 row SafeVulst, L=15 mm Lynlås etter: 100, 5100, 10100, 15100 Med 12 rows LV Inject ved 180° |
| 1-1M (20) | KE-Montagesett, Safetrack #Åfjord kommune revidert 2702 #Svømmebasseng SafeGevind Rustfri |
| Svømmebasseng : System # 2 | |
| 1-2/1.1 (30) 2 Stk. | KE-DireJet System #Åfjord kommune revidert 2702 #Svømmebasseng Dimensjon: Ø500 mm, L=17000 mm Materiale: MultiWeave Farve: Hvit (Pantone 11-0601-TP) Opheng: 1 row SafeVulst, L=15 mm Lynlås etter: 100, 5100, 10100, 15100 Med 1 row 18 mm Dyse Med 7 Stk./m ved 165° Med 1 row 18 mm Dyse Med 7 Stk./m ved -165° |
| 1-2M (40) | KE-Montagesæt, Safetrack #Åfjord kommune revidert 2702 #Svømmebasseng SafeGevind Rustfri |

AIR THE WAY YOU WANT



97

KE Fibertec Norge AS
Teglverksveien 83
N-3057 Solbergelva

Tlf. +47 97 57 59 45
jorn@ke-fibertec.no

TILBUD

Tilbudsnummer:

Versjon:

Prosjekt:

Åfjord kommune revidert 2702

Dato:

27.02.2019

Side:

4 av 9

| Pos. nr. | Produkt |
|-----------------------------------|---|
| Svømmebasseng : System # 3 | |
| 1-3/1.1 (50) 1 Stk. | KE-DireJet System #Åfjord kommune revidert 2702 #Svømmebasseng Dimensjon: Ø500 mm, L=17000 mm Materiale: MultiWeave Farve: Hvit (Pantone 11-0601-TP) Opheng: 1 row SafeVulst, L=15 mm Lynlås etter: 100, 5100, 10100, 15100 Med 1 row 18 mm Dyse Med 3 Stk./m ved 90° Med 1 row 18 mm Dyse Med 6 Stk./m ved 165° Med 1 row 18 mm Dyse Med 6 Stk./m ved -165° |
| 1-3M (60) | KE-Montagesæt, Safetrack #Åfjord kommune revidert 2702 #Svømmebasseng SafeGevind Rustfri |



H The surface average of molar chlorine concentration in the swimming breathing zone

This appendix shows the surface average of molar chlorine concentration in the swimming breathing zone for the systems MV, MV-DV, DV4, DV5 and DV7 ACH respectively.

Surface Average of Molar Concentration of Cl2 on Volume Mesh

| Part | Value (kmol/m ³) |
|---------------------------------|------------------------------|
| ----- | ----- |
| Plane 10 cm above water surface | 5.342445e-09 |
| ----- | ----- |
| Total: | 5.342445e-09 |

Surface Average of Molar Concentration of Cl2 on Volume Mesh

| Part | Value (kmol/m ³) |
|---------------------------------|------------------------------|
| ----- | ----- |
| Plane 10 cm above water surface | 3.888233e-09 |
| ----- | ----- |
| Total: | 3.888233e-09 |

Surface Average of Molar Concentration of Cl2 on Volume Mesh

| Part | Value (kmol/m ³) |
|---------------------------------|------------------------------|
| ----- | ----- |
| Plane 10 cm above water surface | 6.087161e-09 |
| ----- | ----- |
| Total: | 6.087161e-09 |

Surface Average of Molar Concentration of Cl2 on Volume Mesh

| Part | Value (kmol/m ³) |
|---------------------------------|------------------------------|
| ----- | ----- |
| Plane 10 cm above water surface | 6.078443e-09 |
| ----- | ----- |
| Total: | 6.078443e-09 |

Surface Average of Molar Concentration of Cl2 on Volume Mesh

| Part | Value (kmol/m ³) |
|---------------------------------|------------------------------|
| ----- | ----- |
| Plane 10 cm above water surface | 6.048896e-09 |
| ----- | ----- |
| Total: | 6.048896e-09 |